Performance Simulation of Single- and Double-Effect Absorption Refrigeration Systems Used for Solar Cooling Applications

محاكاة أداء أنظمة التبريد بالامتصاص المفرد والمزدوج التأثير المستخدم في تطبيقات التبريد الشمسي

By:

Noor Sameer Ali Al Kaab

Dissertation submitted in partial fulfilment of requirements for the Degree of MSc Intelligent Building Design and Automation

Faculty of Engineering & IT

Dissertation Supervisors

Dr. Alaa Abdul-Ameer

&

Prof. Bassam Abu-Hijleh

November – 2012

DISSERTATION RELEASE FORM

Student Name	Student ID	Programme	Date
Noor Sameer Ali Al Kaab	100047	MSc Intelligent Building Design and Automation	14 / 11 /2012

Title

Title Performance Simulation of Single- and Double-Effect Absorption Refrigeration Systems Used for Solar Cooling Applications

I warrant that the content of this dissertation is the direct result of my own work and that any use made in it of published or unpublished copyright material falls within the limits permitted by international copyright conventions.

I understand that one copy of my dissertation will be deposited in the University Library for permanent retention.

I hereby agree that the material mentioned above for which I am author and copyright holder may be copied and distributed by The British University in Dubai for the purposes of research, private study or education and that The British University in Dubai may recover from purchasers the costs incurred in such copying and distribution, where appropriate.

I understand that The British University in Dubai may make that copy available in digital format if appropriate.

I understand that I may apply to the University to retain the right to withhold or to restrict access to my dissertation for a period which shall not normally exceed four calendar years from the congregation at which the degree is conferred, the length of the period to be specified in the application, together with the precise reasons for making that application.

Signature

Abstract

Cooling is very essential for the various aspects of modern life. One of the important applications is the air conditioning field. With increasing oil prices, alternative ways are needed to ensure energy conservation. One of the promising ways is the solar energy use for cooling. The absorption refrigeration system (ARS), which uses thermal energy, is market available but researches on improving their performance are still needed.

In this study, simulation of two design configurations of ARS is performed. These configurations are single- and double-effect ARS. In order to compare the performance predictions of these configurations, similar assumptions are used. Condenser and absorber temperatures are assumed 40°C. Evaporator temperature is varied as 4, 5, 6 and 7°C and the generator temperature is varied as 100, 110, 120, 130, 140, and 150°C.

The results for the single-effect ARS show enhanced COP with generator temperature, at any evaporator temperature. The COP of single-effect ARS was highest of 0.693, at generator temperature of 120°C and evaporator temperature of 7°C. Moreover, the performance degraded with lower evaporator temperature. The simulation study for the double-effect ARS shows that the increase of generator-I temperature from 100 to 150°C decreases generator-I thermal energy by 7.52%. Moreover, the increase of generator-I temperature increases the COP, at any evaporator temperature to reach maximum of 1.164 at temperature of 130°C and evaporator temperature of 7°C. The comparison show that the double-effect ARS has higher COP compared with single-effect, at any evaporator temperature. The percentage increase of COP varies from 49.5% (at generator temperature of 100°C and evaporator temperature of 4°C) to 68.6% (at generator temperature of 150°C and evaporator temperature of 7°C).

The energy storage tank response is studied based on night and daytime operation. For the night operation, electric heat is used whereas for the daytime operation, the heat is supplied to the tank through solar panels. Simulink models are used to investigate the open loop and closed loop responses of the tank. Moreover, appropriate controller is used. The simulation results showed improved performance with closed system but generally the response of the system is slow.

Based on the outcomes of the study, it is recommended to consider other designs of absorption system for simulation. Also, simulation at other absorber and condenser temperatures can be performed.

خلاصة البحث

التبريد هو ضروري جدا لمختلف جوانب الحياة العصرية. وأحد التطبيقات الهامة للتبريد هو في مجال تكييف الهواء. ومع زيادة أسعار النفط ، هناك حاجة ماسة لإيجاد وسائل بديلة لضمان الحفاظ على الطاقة .إحدى الطرق الواعدة هو استخدام الطاقة الشمسية لأغراض التبريد. حاليا نظام التبريد بالامتصاص والذي يستخدم الطاقة الحرارية في تشغيله هو متاح في السوق ولكن لا تزال هناك حاجة لمزيد من الأبحاث على تحسين أدائها.

في هذه الدراسة ، تم عمل محاكاة لتصميمين مختلفين من تصاميم نظام التبريد بالامتصاص وهي التصميم ذو التأثير المفرد وذو التأثير المزدوج. ومن أجل المقارنة بين توقعات الأداء من هذه التصاميم تم استخدام افتراضات متماثلة. درجات الحرارة فرضت 40 درجة في المكثف والممتص وفعالية المبادل الحراري فرضت عند 0.7. عند محاكاة هذه التصاميم تم استخدام درجات حرارة في المبخر متغيرة إلى 4، 5، 6، وكذلك 7 درجات مئوية. كذلك تم استخدام درجات حرارة في المولد متغيرة إلى 100، 110، 120، 130، 140، كذلك 150 درجة مئوية.

نتائج محاكاة التصميم ذو التأثير المفرد أظهرت تحسن معامل أداء النظام مع درجة حرارة المولد عند أي درجة حرارة في المبخر. معامل أداء النظام للتصميم ذو التأثير المفرد وصل لأعلى قيمة له (0.963) عند درجة حرارة المولد 120 درجة وعند درجة حرارة المبخر 7 درجات. وعلاوة على ذلك ، فإن أداء النظام تدهور مع خفض درجة حرارة المبخر. كذلك فإن نتائج محاكاة التصميم ذو التأثير المزدوج أظهرت تحسن معامل أداء النظام مع درجة حرارة المولد الأول عند أي درجة حرارة في المبخر. ارتفاع درجة الحرارة المولد الأول من 100 إلى 150 درجة مئوية يقلل من الطاقة الحرارية اللازمة في المولد الأول بمقدار 7.52% تحسن معامل أداء النظام مع درجة حرارة المولد الأول لتصل إلى 1.164 عند درجة حرارة المولد الأول 130 درجة وعند درجة حرارة المبخر 7 درجات. المقارنة بين التصاميم دلت على أن معامل أداء النظام للتصميم ذو التأثير المزدوج أعلى منه في التصميم ذو التأثير المفرد. نسبة الزيادة في معامل أداء النظام تراوحت بين 49.5% (عند درجة حرارة المولد 100 درجة وعند درجة حرارة المبخر 4 درجات) وبين 68.6% (عند درجة حرارة المولد 150 درجة وعند درجة حرارة المبخر 7 درجات) في هذه الدراسة تم عمل محاكاة لاستجابة الخزان الحراري باستخدام برنامج السيمولينك لدراسة أداء منظومة التحكم ذات الدورة المفتوحة والمغلقة وأظهرت النتائج بطء زمن الاستجابة للمنظومة. تم خلال المحاكاة شحن الخزان الحراري من سخان كهربي (أداء ليلي) ومن منظومة شمسية (أداء نهاري) . تمت حسابات شدة الإشعاع الشمسي الكلي لمدينة دبي خلال ذروتي الصيف والشتاء.

واستنادا إلى نتائج هذه الدراسة ، فمن المستحسن أن تنظر تصاميم أخرى للمحاكاة من تصاميم نظام التبريد بالامتصاص . وكذلك يمكن تنفيذ المحاكاة عند درجات حرارة أخرى في الممتص والمكثف.

Acknowledgements

First and foremost my immense gratitude goes to my country Kuwait.

I am greatly indebted to my supervisor Prof. Bassam Abu-Hijleh, Dean and Atkins Chair, Head of Sustainable Design of the Built Environment Program, for his continuous help and support.

I also would like to thank Dr. Alaa Ameer, Associate Professor and Admission Tutor, who offered me his precious time, guidance, advice and expertise throughout the course of this dissertation from the formative stages until the final draft.

I share the credit of my work with my Uncle Dr. Mohamed Abdellatif, who has been so supportive in the entire process of my dissertation.

My sincere appreciation and thanks also go to Mr. Marzouk Nasser AL–Kharafi, President of AL-Kharafi Group, who supported me and granted permission to access their premises, sites and companies and facilitated my tasks during projects assignments and study cases time.

My deepest thanks extended to Eng. Hossam Fawzi, Eng. Shafea AL-Ali, Eng. Khaled AL-Manzalawy, and all engineering team who willingly shared their knowledge and offered me their expertise at Kharafi National Company. I consider it an honour to work with them.

I would be remiss without mentioning my tutors Prof Robert Whalley and Dr. Fadeyi Moshood Olawale, whose outstanding generosity will be remembered always.

I am also very grateful to the Government of the United Arab Emiratis, and the British University in Dubai for granting me a scholarship and opportunity to achieve my Master Degree.

Finally, a special thanks to my grandmother, my parents, my sister Sarah, and all family members for their prayers, love, support, encouragement and faith in me.

To each of the above, I will always appreciate all they have done to me.

Dedication

This dissertation dedicated, with love and immense gratitude to my country Kuwait, to my grandmother Mrs. Om Taleb Dehrab and to my mother Mrs. Najwa Dahrab, who have been the source of encouragement and inspiration throughout my life.

Table of Contents

Contents	Page

Contents	Page

Contents	Page

List of Figures

List of Tables

List of Notations

a_H	Ability of collector to capture and convert solar radiation
a_o	Threshold effects of pump
A	Constant, area of solar panel
A_n	Coefficient
B	Constant
B_n	Coefficient
C	Constant
C_n	Coefficient
C_N	Constant = 1
h	Enthalpy, solar hour angle
H	Daily total solar radiation
$I(t)$	Total solar radiation
I_{ND}	Normal direct beam radiation
l	Latitude angle
m	Mass flow rate of flow branch
$\dot{m}$	Mass flow rate at a point
mc	Mass control
m_c	Cold stream mass flow rate
m_h	Hot stream mass flow rate
n	Constant
Q	Heat
R_{gi}	Refrigerant mass generated in generator-I
R_{gii}	Refrigerant mass generated in generator-II
R_{is}	Intermediate solution mass ratio
R_{ss}	Strong solution mass ratio
R_{ws}	Weak solution mass ratio

S	Laplace operator
T	Temperature
T_a	Daytime average ambient temperature; Absorber temperature
Tc	Temperature control
T_c	Cold water temperature; Condenser temperature
T_e	Evaporator temperature
TF	Transfer Function
T_g	Generator temperature
T_h	Hot temperature
$T_{sat)p}$	Saturation temperature at solution pressure
T_{sol}	Solution temperature
x	Solution concentration
α	Surface tilt angle
β	Solar altitude angle
δ	Solar declination angle
ε	Heat exchanger effectiveness
ϕ	Solar azimuth angle
γ	Surface azimuth angle
η	Solar panel efficiency
θ	Solar incidence angle
τ	Residence time parameter

List of Terminologies

AI	Artificial Intelligence
ARS	Absorption Refrigeration System
ASHRAE	American Society of Heating, Refrigerating and Air Conditioning Engineers
BIPV	Building-integrated photovoltaic
COP	Coefficient of Performance
DHW	Domestic Hot Water
EC	Electrochromic
EV	Expansion Valve
GHG	Greenhouse Gas
HE	Heat Exchanger
H_2O	Water
HTD	High Temperature Desorber
HVAC	Heating, Ventilation and Air Conditioning
IEA	International Energy Agency
LCD	Liquid Crystal Display
LiBr	Lithium Bromide
LTD	Low Temperature Desorber
MPC	Model Predictive Control
NH_3	Ammonia
PCM	Phase Change Materials
PCT	Phase Change Temperature
PDLC	Polymer Dispersed Liquid Crystals
PV	Photovoltaic
SHGC	Solar Heat Gain Coefficient
SHX	Solution Heat Exchanger
SP	Solution Pump
SPD	Suspended Particle Devices
TABS	Thermally Activated Building System
TCM	Thermo-chemical Materials

TES	Thermal energy storage
TOU	Time-of-use
TR	Ton of Refrigeration
TSWH	Thermosiphon Solar Water Heaters
WWR	Window to Wall Ratio

Chapter I

Introduction

1.1 Research Background

A dramatic increase in the price of energy as a result of the 1973 oil embargo demand has forced people to think about energy conservation. As a result of this situation, energy conservation in the sense of energy efficiency and the use of renewable energy is vital. It has been estimated that considerable amount of the national annual consumption of primary energy is used for building sectors. Energy consumption and the efficiency of energy use in buildings depend on design and the conservation strategies that have been taken to save energy (Kieider and Rabl, 1994; Beggs, 2009).

Components such as building materials, orientation, and shape, percentage of glazing area, HVAC system, ventilation, and lighting density are highly dependent on the design of the building. These components play an important role in building energy use. In general, three basic systems determine the efficiency of energy use in buildings (Chiogioji and Oura, 1982; Waters, 2003; Seem, 2007):

- Energised systems, such as those required for heating, coding, lighting, ventilation, business equipment operation, etc.
- Non-energised systems such as walls, roofs, floors and windows
- Human systems, such as maintenance, operation, and energy management.

Each of these systems con be modified for significant savings of energy. However, modifications must be analysed in terms of comfort of occupants, cost-effectiveness and pollution control.

Before designing energy strategies for commercial buildings, a clear picture of the most significant component of energy utilisation should be developed based on annual energy use patterns. Methods of conservation should then be applied to get desired energy saving. For hot climate regions, coding is the largest annual energy consumption component followed by ventilation, lighting, and heating (Stein and Reyndds, 1992). In

terms of annual energy use, electricity is the major energy cost for buildings, especially for the countries of relatively low cost of natural gas (Puthawala *et al.*, 2011).

One of the ways to improve the energy performance of buildings is to employ solar systems that can reduce fossil fuel requirements. Generally, the earth receives solar energy at a rate of 5.6×10^{24} Joules/year which is equivalent to about 30,000 times the energy used at the present time (Dixon and Leslie, 1978, Waters, 2003). Utilisation of this huge amount of renewable energy requires knowledge of the nature of solar insulation, the factors that influence its intensity and systems that utilise such energy.

1.1.1 Sustainability and Sustainable Buildings

Since the world energy crisis in the early 1970s, scientists have paid more attention to improve energy use, exploit renewable energy resources and reduce impacts of energy use on the environment. More and more evidences shows that the global climate change is mainly caused by greenhouse gas (GHG) emissions, which are directly related to the combustion of fossil fuels. In recent decades, the concept of sustainability has entered the engineering world, and it appears to be connected with every aspect of engineer's profession. In building industry, "building sustainability is a means to provide a safe, healthy, comfortable indoor environment while simultaneously limiting the impact on the Earth's natural resources" (ASHRAE, 2002).

Sustainable development in the building industry is concerned with a quite range of issues including building materials, construction sites, integrated systems, energy consumption and indoor environment. The concept of green building design applied to the Heating, Ventilating and Air Conditioning (HVAC) industry requires that design engineers regard not only the reduction of the energy use by HVAC systems but also the mitigation of the related environmental impacts. While every building seems like to be connected with sustainability, the environmental impacts of buildings continue to increase (McQuiston *et al.*, 2005). In commercial building sector all over the globe, the end-use energy consumption of HVAC systems accounts for considerably higher percentage of the total end-use energy consumption. Therefore, the effectiveness of energy use for space heating and cooling is increasingly important and essential for the application of sustainable development in the building industry, which is one of the motivations of this study (Underwood, 1999; Stene, 2005).

Over the past few decades, many advanced technologies have been developed and used in the field of HVAC industry. Accordingly, the efficiency of major energy consumed components of HVAC systems, such as chillers, boilers, fans, pumps, and heat exchangers, have been dramatically raised. Some optimal control strategies have been promoted to make the operations of HVAC systems more effective (Underwood, 1999).

1.1.2 Energy Crisis and Solar Applications

The current energy crisis and the economic constraint make it impossible to believe that any government must consider the possible means to fulfil the growing energy demand in the near future. Against this back-drop, the only alternative is to pursue a demand-side strategy to reduce the energy consumption, as stated earlier, in conjunction with the exploitation of alternative energy sources. A strategic means of accomplishing this is to:

- Promote energy efficient devices,
- Begin a transition towards renewable energy sources,
- Promote national self-reliance,
- Decentralise the energy supply,
- Incorporate energy auditing within the framework of people's daily lives,
- Ensure compatibility of energy strategies to other global problems.

Solar energy as generally defined includes energy derived directly from sunlight as well as indirectly in the form of wind, waves, tides, ocean thermal gradients, or as fuel from biomass and other photo-chemical reaction products. Over the past few decades there has been an explosive growth in solar energy research and development. Solar energy is an energy source that can be tapped in many different ways, and is not restricted by conventional transmission or distribution constraints. Exciting opportunities exist in the application of solar energy conversion techniques from passive solar applications to the use of photovoltaics. Photovoltaic (PV) technology has received a great deal of attention due to many technical advantages for a wide range of end-uses. PV technology requires little repair and maintenance. Since the late seventies, PV devices have been introduced in several countries all over the world but on a limited scale due to high capital costs and custom duties. However, there has already been a sufficient improvement in the technology with successful results which warrants us to look more closely with a view of providing useful information to policy makers and potential users. It is also important to realise that solar energy is only a component of an integrated energy system planning,

and must be viewed and treated in this context. For solar energy to succeed and become viable, each keen government must undertake institutional reforms and pass favourable legislation (Tonkoski *et al*, 2011).

1.1.3 Building Energy Consumption Components and Solar Homes

1.1.3.1 Energy consumption components

a) Building envelope

An architect's ability to properly develop the functional and esthetical features of a building is very important in controlling heating end coding equipments, as well as corresponding initial and operating costs. Geographic location, variation of outside temperature and wind and solar intensities are influential factors in building envelope design. The ultimate choice of the building configuration should be determined based on both design and energy issues (Stein and Reyndds, 1992, Puthawala *et al.*, 2011).

Heat loss to and from the envelope depends on many factors, other than climate conditions. These include structure, window to wall ratio (WWR), U-value (of the wall, roof, floor, and window), geometrical shape, orientation, and others. Out of these characteristics, WWR is one of the most significant factors affecting energy demand. Hence, it should be determined through economic analysis for the specified geographic location (Johnson and Besant, 1994; Hunn *et al.*, 1993).

b) Ventilation

The ventilation rate is one of the basic factors mat affects annual energy use, equipment sizing and first cost of HVAC systems. For office buildings, the old ASHRAE Standard 62-81 recommended ventilation rates of 2.3 l/s for each person in the areas designated for non-smoking and 9.4 l/s for each person for the areas designated for smoking (ASHRAE, 1981). ASHRAE Standard 62-89 does not distinguish the presence of smoking and simply recommends a minimum of 9.4 l/s per person (ASHRAE, 1989). This modified standard for outside air rate, based on indoor air quality, remains a subject of debate. The outdoor ventilation air requirements specified by ASHRAE exceed rate to meet oxygen replacement requirements and control carbon dioxide concentrations which, for normal activities, are about 0.6 and 1.8 l/s per person, respectively (Puthawala *et al.*, 2011).

According to Eto and Meyer (1988), the changes in the ventilation rate from the former standard would increase chiller and boiler size up to 20 and 10 percent, respectively. The largest increase in the boiler capacity occurs in colder climates and the smallest in milder ones. Meanwhile, the largest increases in chiller capacity are found in climates with the greatest cooling requirement. The annual energy use for heating would increase by about 8 percent and the annual energy use for cooling by about 14 percent.

One way to reduce the ventilation cost or life cycle cost of HVAC system is through heat recovery devices. Waste heat recovery devices such as run-round heat exchangers, heat pipes, and rotary air-to-air regenerative heat exchangers (heat wheels) are widely used in HVAC systems.

c) Lighting

Lighting systems are designed to create safe and pleasing visual working environments. Lighting systems use a large portion of a building's energy. Lighting may represent 23 percent or more of the total energy consumption in commercial buildings and it has an impact on the energy consumption of the HVAC system (Chiogioji and Oura, 1982). The lighting system has a greater impact on the annual cooling energy used in warm climates than in cold climates. Efficient lighting systems not only decrease electrical energy waste but also decrease the operating cost of air-conditioning in hot climates by decreasing the amount of cooling load. For example, according to Shavit and Richard (1993) an individual dimmable electronic ballast system could save 64, 5, and 12 percent for the lighting, fan and chiller systems, respectively.

d) HVAC systems and equipment

HVAC systems differ according to the precise location of the heating and cooling coil in the air stream and according to the manner in which systems meet varying space loads in each zone. Energy conservation standards are particularly difficult to develop for HVAC systems. The factors that affect the energy performance of HVAC system are difficult to describe. Some of the general recommendations for HVAC systems for heating dominated climates are (ASHRAE/IES, 1989):

- the elimination of simultaneous heating and coding of supply air for a single conditioned space (a major objective of efforts to improve the efficiency of HVAC systems)
- use of automatic off-hour control (time clock)

- large central systems should have options to isolate zones or small groups of zones during unoccupied periods
- optimal insulation thickness
- minimum leakage of air distribution system to avoid energy lasses
- use of systems with an economiser cycle
- use of heat recovery systems
- use of direct digital control systems for better energy management
- use of variable speed pumping system (can save considerable pumping energy, especially in large distribution systems)
- use of renewable energy sources if economically justified

In studying the influence of these on energy consumption, computer modelling of buildings can help greatly. In addition, simulation makes it possible to individually evaluate the impact of each parameter on energy use.

1.1.3.2 Solar homes

One of the interesting applications of solar energy technologies can be found in what is called solar house. First, it is important to explain the concept of "optimally designed solar house" (Wong *et al.,* 2005). Although it is difficult to give a formal definition of this term, optimally designed solar house share some common features (Underwood and Yik, 2004):

- Use of multiple solar-based technologies and design techniques (e.g., passive solar design, PV panels, solar thermal collectors).
- Incorporation of solar energy as an essential design principle from an early phase, not as an afterthought or addition without major impact. For example, a conventional house with a "token" 100 W of PV panels would not qualify.
- Integrated design so that a coherent plan for the interaction of the different systems should exist. Systems may have more than one function.
- Controlled operation so that control strategies should be an essential part of the system's design from the early stages.

1.1.4 Simulation Studies

The dynamic simulations are very essential in order to evaluate the performance of the renewable energy systems and the effect of control strategies, especially in the HVAC

field of application. MATLAB/Simulink has been increasingly used in recent years in building simulation because of the flexibility that it provides in prototyping control strategies (Hudson and Underwood, 1999; Kummert *et al.*, 2001; Riederer, 2005; van Schijndel and Hensen, 2005; Yu and Dexter, 2009).

MATLAB/Simulink is the tool chosen for this research. Selecting the right tool was an essential decision. Some of the advantages of MATLAB/Simulink that are taken into consideration are its general programming capabilities, the relative ease of implementation of new renewable energy technologies, and its focus on controls (not necessarily building controls) with "toolboxes" for system identification, model predictive control, signal processing, etc.

1.1.5 Solar Technology Applications

This part considers the applications of solar-thermal energy and photovoltaics (PV). The Gulf area is located in the "solar belt" where, by and large PV power is less intermittent i.e. solar energy is available almost all throughout the year. PV systems require a high initial investment to construct, however they have low operating costs and relatively low maintenance if well-constructed. For most applications using up to about 3 kW, PV power generation is one of the most economical means of electrical power supply (Yvette, 1988). Commercial adoption and widespread dissemination of this technology in the Gulf area and other developing countries has been limited so far, by high initial capital costs. The supply of solar energy from a collector is time dependent, and collector area is considerable for appreciable quantities of energy to be collected. Loads to be met by an energy system are also time dependent. The hourly load patterns, processes involved, in addition to the supply of solar energy determine the dynamics of a solar energy system (Kalogirou, 2004).

1.1.5.1 Solar water heating

Solar water heating has had a long and varied history. Considerable quantities of hot water are required for industrial processes, laundries, and domestic purposes. Most solar water heaters have some sort of collector-storage arrangement, and there are wide varieties of them in use today. They include (Kalogirou, 2004):

a) Thermosiphon systems or passive systems: circulation is by natural convection whenever solar energy heats up the water and establishes a density difference,
b) Pumped-direct systems

c) Pumped-indirect systems

In thermosiphon systems, no pumps or controllers are required. In the morning as the sun heats the collectors, hot water inside the solar collector rises by natural convection and the colder storage tank water flows into the collector by gravity. Thus the circulation loop is automatically established whenever there is enough sunshine, and circulation stops during periods of low solar flux when the upward buoyancy force is unable to overcome the pipe fictional losses. The minimum distance of tank elevation above the top of the collector array is 25 cm (Jansen, 1985). To prevent reverse circulation, the tank should be located above the collector. A typical thermosiphon water system is as show in Figure 1.1.

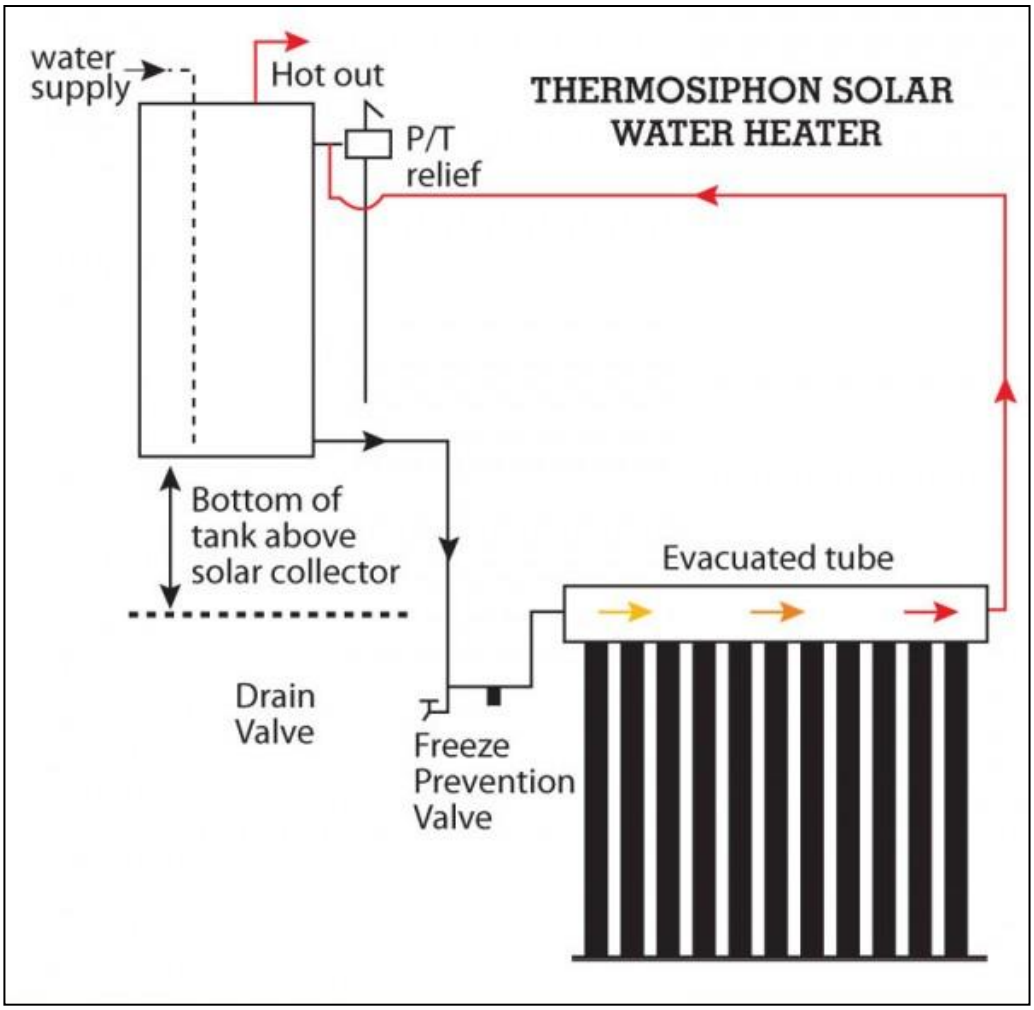

Figure 1.1 Typical thermosiphon water heater systems

(http://www.wncgreenbuilding.com/images/uploads/Thermosiphon-solar-water-heater-66.jpg)

Pumped or forced-circulation systems are, more than not controlled by a differential thermostat, turns the pump ON when the temperature gradient of the tank is sufficient to ensure control stability (Duffie and Beckman, 1991). The pump can also be driven by a photovoltaic module (Wenham *et al.*, 2006). A check valve may be needed to prevent reverse circulation and resultant night-time thermal losses from the collector, as shown in Figure 1.2. Auxiliary energy can also be added to improve system performance and for instances of low solar flux.

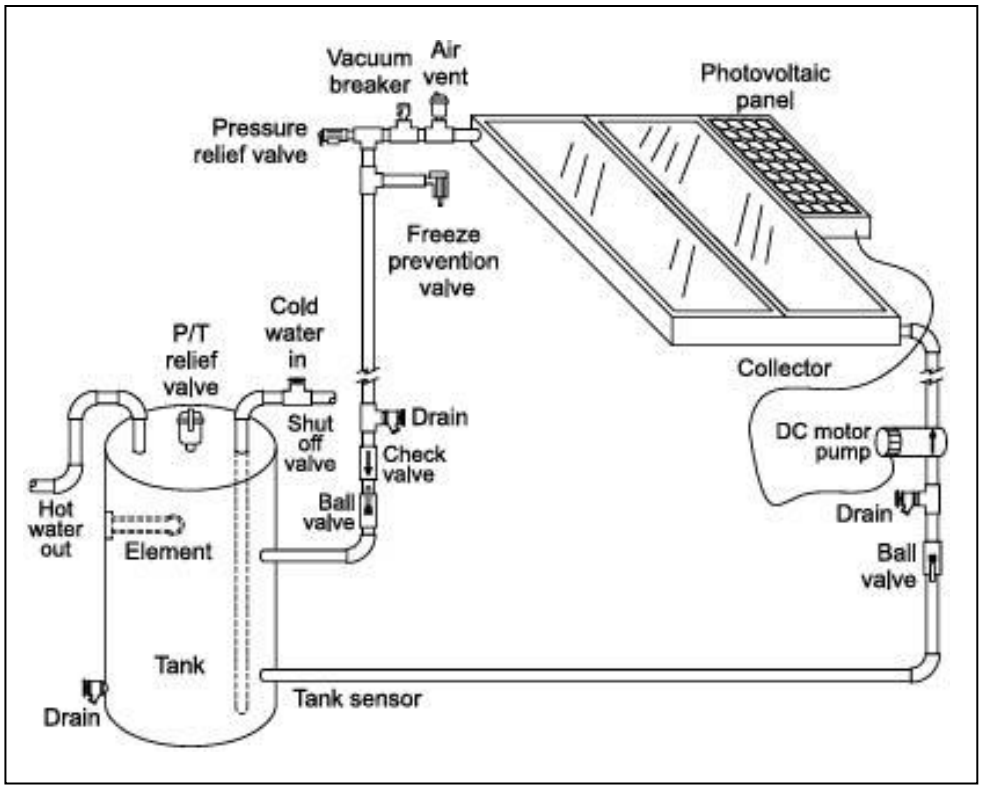

Figure 1.2 Pumped or forced-circulation water heater systems

(http://www.hopesun-solar.com/en/tec%20pic/detail2.jpg)

The design of hot water systems is based on the hot water delivery temperature, average daily hot water usage, available insolation and a host of other factors. Usually solar water heaters have annual efficiencies in the region of 30 to 50% for a well-designed system (Kalogirou, 2004). Solar water heaters are manufactured mostly in developed countries such as the United States, Canada, and Japan etc.

The potential demand for an economical solar water heater for use in households, hospitals and hotels makes it a viable solar energy application. The current mode of using electric water heaters for water heating is an expense which most home owners

cannot afford because of the (1) high cost of electricity, (2) shortage of electricity, and (3) cost of fuel for generator owners. The simplicity, reliability and low cost of thermosiphon solar water heaters (TSWH) for domestic water heating in comparison to forced circulation systems, accounts for their widespread use. Furthermore, performance study of Papakostas *et al.* (1995) showed that TSWH systems are comparable or even better than forced circulation systems

Very few studies have been conducted concerning hot water consumption patterns in Gulf, so initial designs of domestic hot water (DHW) systems will have to be based on studies conducted elsewhere. DHW consumption is dependent upon the lifestyle, climate, average family site, age of family members and the required temperature at the point of use of every country (Papakostas *et al.*, 1995). Therefore, some monitoring has to be done to analyse the influence of all these factors to incorporate them in the design criteria of DHW systems. Other factors to be considered are (1) the fuel for auxiliary heating of DHW systems, and (2) heat storage. The long-term performance of DHW solar systems can be approximated by a simple linear input-output mode1 relating the heat Q (in MJ) added to the tank during the day to three variables (Belessiotis and Haralabopolos, 1993).

$$Q = a_H\ H + a_T\ (T_a - T_c) + a_o \tag{1.1}$$

where,

H = daily total solar radiation (MJ/m^2) on collector,

T_a = the daytime average ambient temperature (°C),

T_c = the cold water supply temperature at the start of the day (°C),

a_H = the ability of collector to capture and convert solar radiation,

a_o = threshold effects of a pump if *DHW* system has one.

The market potential for solar hot water heating systems in Gulf area is high because there are few alternatives available such as electric water heaters or fuel stoves. Experimental and economic investigations prove that the technology is viable for both domestic and large-scale water heating. The cheapest and simplest means of domestic water heating recommended is a passive/thermosiphon system. However if cost is not an issue, PV pumped solar domestic hot water systems offers several advantages over conventional solar DHW systems (Belessiotis and Haralabopolos, 1993).

1.1.5.2 Solar cooling

Solar cooling of buildings is an attractive idea in hot climates such as the weather in the Gulf area. Cooling loads and the availability of solar radiation are approximately in phase especially in commercial buildings where night air-conditioning is not required. In several applications, cooling is provided to small individual spaces within a structure using room air-conditioners. There are several methods being used in solar air-conditioning today: (1) solar absorption cooling, (2) solar-mechanical systems, and (3) solar-related systems. The two main systems that are currently used for this purpose are absorption and desiccant cycles. Within these classes there are many variations in the way they operate due to different control strategies, temperature ranges, and cyclical characteristics. Solar cooling is an expensive option and cooling loads should be carefully estimated to minimise costs (Beggs, 2009).

Over the past few decades, considerable research has been devoted towards developing a low cost, high performance solar air-conditioning system. Several methods have been proposed to attain this objective: 1) low cost absorbents (e.g. lithium-zinc chloride) for open-cycle absorption cooling (Ameel *et al.*, 1995), and 2) desiccant (e.g. silica-gel and alumina) solar air-conditioning (Dupont *et al.*, 1994a).

A complete report on desiccant cooling presented by Pesaran *et al.* (1992) presents conclusive evidence that desiccant cooling and air dehumidification is a good alternative for air-conditioning (Dupont *et al.*, 1994b). Absorption machines are available on a commercial basis but are usually custom-made with specialised components, which make maintenance a specialised task. Desiccant systems, which are applicable in arid areas only, are not available commercially and may be expensive. A third alternative is the solar ejector air conditioner (Sokolov and Hershgal, 1993). One of the major economical drawbacks of solar heating or cooling lies in the fact that initial investments, are too high to justify seasonal utilisation only. The proposed system can be used for both heating and cooling using the same hardware, or a year-round space air-conditioning system. Although the utilisation of the proposed system requires very little mechanical energy, it suffers from poor thermal efficiency, requires a large collector area as well as large amounts of heat circulating throughout the system (Sokolov and Hershgal, 1993).

Solar air-conditioning technology is still at the development stage, and the technology available at this point can be expensive to be feasible in Gulf area. Passive cooling can be achieved by architectural features such as overhangs to provide shading, double roofs with space between for air circulation, ventilation to take advantage of prevailing winds, glass with high transmittance for the visible spectrum etc. (Duffie and Beckman, 1991).

1.2 Aims and Objectives

1.2.1 Aims of the Research

The aim of this study is to investigate the use of solar energy technologies in controlling the HVAC system energy needs employed in sustainable buildings.

1.2.2 Objectives of the Research

This research will focus on solar technology/absorption. Its objectives are including:

- identify and assess the potential of solar energy applications,
- investigate predictive control development and design strategies for solar home i.e. green house
- considering the benefits of using solar energy as an energy source for the operation of an absorption refrigeration system (ARS) used for HVAC applications
- evaluating the performance of single-effect ARS and double-effect ARS by means of system simulation
- use Matlab/Simulink to model the thermal energy charging to the storage tank
- analyse and discuss the simulation results

1.3 Organisation of the Dissertation

This dissertation comprised five chapters in addition to the references and appendixes. Chapter one is the introduction chapter. It includes background of the research, the aim and objectives of the study and the layout of the dissertation.

Chapter two is used to review the literature. It will be used to explain the idea behind the solar home or house and its control strategies. In this chapter, literature and technology review are presented on the traditional and advanced control strategies used for buildings and overview of the suitable technologies for solar homes. This chapter also will be used to review the solar energy use for HVAC applications and to present

analysis of absorption system components. It will include discussion of the main types of absorption systems that can be used for HVAC applications.

Chapter three will be devoted to describe the simulation procedures of the absorption refrigeration system (ARS) as the integral part of the solar cooling system. Simulation of the performance of the single-effect and double-effect ARS will be described. Also, this chapter will include simple Matlab/Simulink model to simulate the charging of the storage tank with thermal energy during night and daytime operation.

Chapter four will be used to present and discuss the results of the simulation.

Chapter five is devoted to present the conclusions and the different recommendations for future research. The references and appendixes will follow this chapter.

Chapter II

Literature Review

2.1 Introduction

The energy cost depends on large extent on the political conditions more than on the natural events. It is one of the most important characteristics of every economy. The prices of energy have gone through severe fluctuations since the oil crisis of 1970s. Usually, the energy price fluctuation has recognised consequences on the economy all over the globe because it affects the prices of nearly all product and service needed for the daily life.

It is important to consider the fact that the resources of the fossil fuels are very limited because of the extensive energy use over the last decades and these resources will finish very soon. Accordingly, it is very essential to look for or create other energy sources such as the making of new fuels. However, this alternative needs time, research efforts and money. The quick and fast solution is to make use of the available solar energy and to develop new technologies to make use of most of it, especially in the sector of building. This puts spotlight on the importance of thinking about the intelligent buildings, especially the buildings that rely on the solar energy for its operations, which can be widely termed as the solar homes.

This chapter is devoted to review the concepts of the solar homes and to explain the different ideas with which the solar energy can be used in the typical building aiming at decreasing the dependence on the other types of energy, which will be more beneficial for both the energy sector and for the economy as well. The control strategies that can be used for these buildings will be discussed and the possible means of energy storage will be explained and discussed as well. The new designs and the effects of the construction materials will be analysed to explore their role in using the energy more effectively for the applications of the solar homes. Also solar cooling concepts and designs will be reviewed.

2.2 Solar Buildings

2.2.1 Concepts of Solar Buildings

It is nearly well known to everybody that Earth receives from the sun, in single hour, an amount of radiative energy more than the requirements of humanity for the whole year. This is the main reason to consider the solar energy and the other renewable energy sources as the most promising alternative energy sources to replace the fossil fuels. The serious environmental damages (of which climate change is the most important) (IPCC, 2007), the unstoppable reduction of petroleum and other fossil fuels resources (IEA, 2010; Owen *et al.*, 2010), and the consequent economic and geopolitical pressures (Hirsch *et al.*, 2005; Hirsch, 2008), immediately require the use of the huge solar resource to replace the non-renewable energy sources.

Fortunately, enhanced design techniques and new technologies ease a more effective use of solar energy to satisfy the requirements of the buildings' occupants, and could finally have a large effect if their use becomes more widespread. Some of the most relevant trends are:

- Passive solar design (Athienitis and Santamouris, 2002)
- Increasingly accurate, informative and longer-term weather forecasts (Poulin *et al.*, 2006)
- Promising technologies, such as low emissivity coatings, argon-filled windows and triple-glazed windows
- Making main face of building with controllable blinds (Tzempelikos and Athienitis, 2005) and active windows (Assimakopoulos *et al.*, 2004), such as electrochromic, thermochromic and gasochromic technologies, that may be used for the control of solar heat gains and day-lighting
- Active thermal storage systems (Dincer, 2002).
- Building-integrated photovoltaic (BIPV) or BIPV/Thermal (BIPV/T) installations (Østergaard, 2003)
- Solar collectors (Duffie and Beckman, 2006)
- Ground source heat pumps (Biaou *et al.*, 2004)

The above mentioned design techniques and technologies allow new possibilities for the best employment of solar energy technologies in building sector. Although the amount of solar energy is huge, such as the case of most of the renewable energy sources, it is

exceedingly variable. Consequently, storage and management of this energy are necessary for the success of any solar house design. Accordingly, strategies needed to properly plan the solar energy collection, storage and then deliveries are essential.

Electric or thermal energy obtained from the applications of solar energy can be stored in different ways. Batteries can be used to allow some limited electric energy storage capacity, especially in off-grid systems or as a backup system that can be used for the cases of emergency. Grid-tied installations can eliminate the needs for electric energy storage because the grid has no specific capacity of electric energy storage. Therefore, if the electricity generated at a given time through the use of photovoltaic (PV) panels exceeds the requirements of the building, the excess electric energy can be delivered to the local grid. On the other hand, if the power generated by the PV panels is insufficient for the requirements of the building, then the grid will supply the building with the difference. Accordingly, the grid-tied installations can replace the batteries. Although electric grids can presently handle domestic grid-tied installations quite easily, higher PV penetration rates will demonstrate more challenging.

In a building, passive and active thermal energy storage (TES) system can be effectively employed. Passive thermal energy storage means the ability of the building materials to receive and steadily release energy to the indoor space of the building. It is well known that the materials of relatively high density and specific heat (such as concrete, stone or masonry) can store considerable amounts of heat. When these materials (which usually cover the internal surfaces of the building) are exposed to the solar gains entering the space through windows and transparent components of the building envelope, they can store a significant portion of this energy. Thus, the release of the thermal energy is delayed. This phenomenon allows the collected heat to be used during the night and cloudy intervals, and helps ease the indoor temperature fluctuations which can affect thermal comfort. Currently, the advanced technologies such as phase change materials (PCMs) can effectively increase the thermal mass of the building.

Active (or isolated) thermal energy storage system deals with the different devices such as hot or cold water reservoirs, ice storage devices, thermo-chemical systems and PCM tanks. The state of charge of these systems can be modified by some active intervention, such as using a solar thermal collector or a heat pump to change their temperature. Strategies for controlling these passive and active thermal energy storage systems must

be considered for use as early as possible, especially during the early design stages so that they must be considered as an essential part of the design.

2.2.2 Controls of High Performance Buildings

Controls are critical for the success of high performance buildings (Torcellini *et al.*, 2004). Advanced building control includes a large diversity of systems and technologies in residential and commercial buildings. Smart building systems include access control, communication, IT systems, elevator control and fire protection (Wong *et al.*, 2005), integrated within what is commonly called a "building automation system" (BAS).

In general, research on advanced control has focused more on commercial buildings than houses, as home automation (also known as "domotics") has not been widely adopted yet. Advanced control systems are still mainly used in the commercial sector, especially in large buildings (Braun, 2007), although recent developments have enabled their installation in smaller commercial buildings. The energy requirements and control needs of commercial and residential buildings are often quite different. For example, in commercial buildings, cooling and lighting play major roles, while in houses, especially in cold climates, space heating and domestic hot water (DHW) heating are the dominant factors in energy consumption. Despite these differences, control strategies can often be adapted from commercial to residential buildings, and vice versa.

Classifying building control technologies and strategies is a challenging task; boundaries between methodologies and systems are not clearly defined and there is significant overlap and hybridization between applications, algorithms and approaches. However, two trends have been followed in research on advanced building control: (a) methods based on physical models; and (b) model-free (or almost model-free) methods (Dounis and Caraiscos, 2009). In the first approach, a physical model of the system is used in optimal and predictive control algorithms. In the second approach, algorithms consist mostly of model-free techniques (e.g., reinforcement learning, expert systems) or black-box models (e.g., obtained with artificial neural networks, correlation techniques and polynomial curve fits). Figure 2.1, adapted from Wang and Ma (2008), presents an overview of supervisory control methodologies.

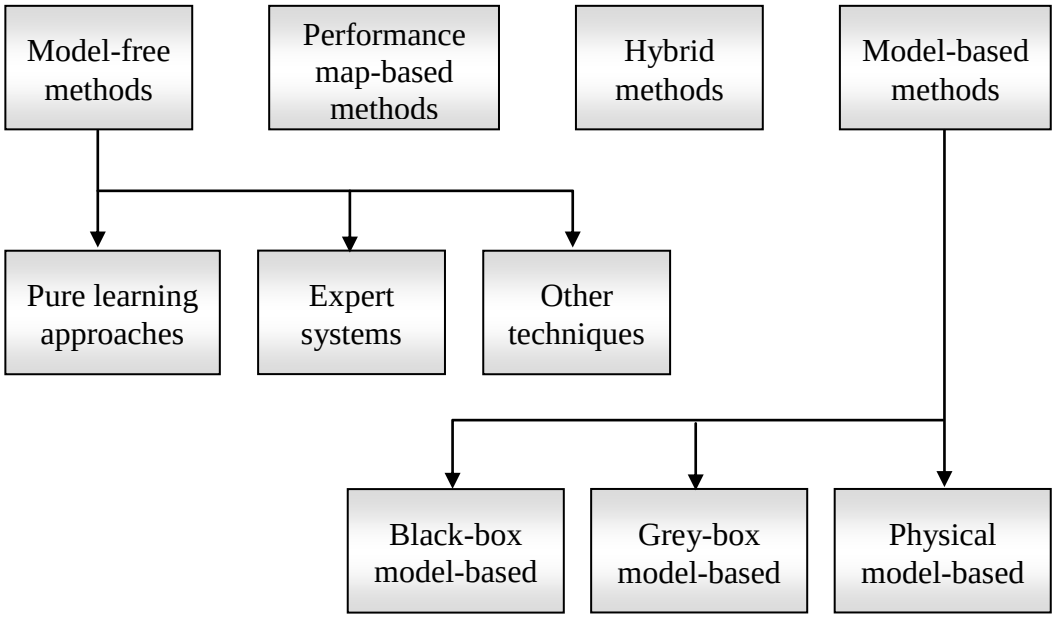

Figure 2.1 Classification of advanced building control methodologies, adapted from Wang and Ma (2008)

Again, there is no sharp separation between approaches: boundaries are blurry. Methods presented on the left of the graph are usually based on artificial intelligence (AI) techniques, while methods presented on the right tend to employ models of higher resolution with formal mathematical optimisation algorithms. The dashed line indicates that a black-box model, while not giving much information on the system, may be used in a "model-based" strategy. Conversely, a purely physically based model can be used with an optimization algorithm based on AI techniques (e.g., genetic algorithms). In "Grey-box" models, hypotheses are made on the configuration of a physical model (e.g., a thermal network); optimisation techniques are then used to find the best fit for the value of the parameters (Kampf and Robinson, 2007; McKinley and Alleyne, 2008).

2.3 Model-Based Building Control

2.3.1 Early Work on Dynamic Control of Buildings

The most basic supervisory control strategy consists of keeping a fixed temperature set-point. A slightly more sophisticated approach uses a lower set-point at night during the heating season ("night setback"), or a higher set-point at night during the cooling season ("night setup", although the wording "night setback" is also sometimes used for this strategy). Different temperature set-point profiles have been proposed. For example, a

typical scheme of a programmable residential thermostat, attempting to follow the needs of the occupants, uses four set-points: a wake-up set-point (approximately from 06:00 to 08:00), a daytime set-point (08:00 to 17:00), evening set-point (17:00 to 22:00), and a night set-point (22:00 to 06:00).

There are several advantages to integrating the building thermal mass in a well-conceived control strategy: improved comfort because of higher mean radiant temperature, reduction of peak loads, and dampening of fluctuations due to sudden changes in solar radiation or exterior temperature. The ASHRAE Handbook of Applications (ASHRAE, 2007) mentions other benefits: (a) reduction in demand costs where demand charges apply; (b) the use of electricity when it is less expensive; (c) the use of exterior air at night for ventilation pre-cooling in the cooling season; and (d) the improved performance of the system because of better ambient conditions.

Dynamic control, a strategy incorporating the use of the building's thermal mass into the HVAC control to reduce energy consumption, has been studied for decades, in particular for commercial buildings (Hartman, 1980, 1988). Dynamic control allows smaller HVAC equipment, improved part-load operation and a more even distribution of the energy supply over time. Despite these opportunities, implementing dynamic control of the thermal mass can be challenging since the long-time constants introduce significant delay between external stimuli (e.g., solar radiation, outdoor temperature) and their effects. Hartman discussed the potential of dynamic control for energy savings, describing basic features of this technique, including the use of weather forecasts to anticipate load conditions and the need for a supervisory control coordinating the actions of all the systems. Hartman (1988) mentions the need for collaboration among all the professionals involved in the design of a building, so that energy use is minimised.

The work by Borresen (1981) presented a basic approach to the mathematical modelling of a room and its use for control purposes. Borresen stated that a single capacitance for the air node might suffice for short-term control purposes. Modelling complexity becomes an issue for long term analysis. Borresen suggested a method for adjusting the time constants of the models with experimental data.

2.3.2 Optimal Control for Management of Active and Passive TES

Optimal control theory is the collective name given to the mathematical and numerical techniques focusing on the optimisation of a performance parameter (e.g., cost or energy consumption) called the "objective function" over time. The optimization is subject to constraints (e.g., thermal comfort limits), and is performed based on estimations or forecasts of future loads. Chapter 41 of the HVAC Handbook of Applications provides an overview of optimal control strategies used in supervisory control of buildings (ASHRAE, 2007). The review paper by Wang and Ma (2008) provides a summary of different optimization algorithms used in building control applications. Optimization algorithms are numerous, and highly dependent on the intended application. They include basic least square methods, simplex search, dynamic programming, and Lagrange methods.

In the last quarter of a century, the application of optimal control to buildings has received considerable attention. A landmark work is the study carried out by Braun (1990), essentially focused on cooling. By performing numerical simulations, Braun compared conventional night setback and three optimal dynamic control strategies. The three control strategies consisted of: (a) minimising energy consumption without time-of-use (TOU) rates, (b) minimising energy consumption with TOU rates, and (c) minimizing peak demand. Braun (1990) concluded that the use of free-cooling with optimal control reduces electricity peak loads even when peak load reduction is not the objective function, and that in general, optimal control outperforms conventional control. The optimization method used was the direct search complex method.

Rabl and Norford (1991) studied peak load reduction strategy by pre-cooling a building at night. In this study, a simplified model with relatively few inputs is used. Morris *et al.* (1994) published an experimental study applying Braun's optimisation method to a test facility. Optimal temperature set-points were designed using energy consumption and peak demand as objective functions. The results showed that the temperature set-point profile of the optimal control strategy differs considerably from a night setback. However, the performance of the optimal control strategy is remarkably good. Drees and Braun (1996) continued work in the field of ice storage systems by developing rule-based approaches based on optimal control strategies.

Kinter-Meyer and Emery (1995) presented one of the first studies considering optimal control of both active and passive storage. A simple model of a building and a mechanical system with a cooling tower and two chillers (one for direct supply of cooling and another for an ice-storage system) were examined. The plant model included a representation of the compressor as a simple function of the load and the temperatures of the cooling tower and the chilled water. Simple analogy relationships were used for the power consumed by the circulating pumps. The objective function to be minimized was defined as the sum of the electric power consumed by each device and a penalty for demand charges. Two variables were determined: the cooling power provided directly to the space, and the charge rate of the TES system (which can be positive or negative). Kintner-Meyer and Emery (1995) pointed out that matching a pre-determined cooling load is not a requirement for an HVAC system: what is important is to maintain satisfactory thermal comfort conditions when the building is occupied. Kintner-Meyer and Emery (1995) employed a commercial non-linear optimisation program (NPSOL) in their investigation.

Henze and collaborators have carried out extensive work on the application of optimal control techniques for predictive control of thermal energy storage (TES) in large buildings (Figure 2.2), in particular ice-storage systems. One of the key motivations for using TES is to take advantage of reduced utility rates during off-peak hours; however, lack of proper control strategies was cited as the cause of the poor performance of these systems (Henze *et al.*, 1997). Early research efforts of Henze's group focused on one controlled variable: the rate of charge of the ice thermal storage. This rate can take negative values (discharge) when stored cooling capacity is used to supply the building needs (Henze, 1995; Henze *et al.*, 1997; Henze and Krarti, 1999; Krarti *et al.*, 1999).

In the configuration shown in Figure 2.2, lower efficiencies are expected when the chiller is used to charge the ice TES than when it is used to supply the cooling load (ASHRAE, 2007). For this reason, a conventional control strategy is "chiller priority"; as its name indicates, the chiller is used in the first place to satisfy the cooling load and the use of the ice storage is minimized. "Chiller priority" is used when there are nearly flat rates for energy cost and there is no demand charge: the main benefit is then the reduction of the chiller rating. Another strategy is "storage priority", in which the chiller is used to make as much ice as possible during off-peak hours, and the ice TES is used

as much as possible to satisfy the cooling load. The chiller only provides cooling directly to the space when the capacity of the TES is exceeded.

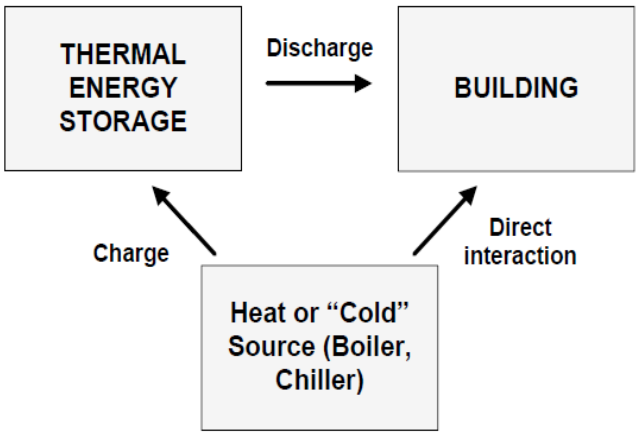

Figure 2.2 Schematic of a TES system, adapted from ASHRAE (2007). The chiller can provide cooling of the ice storage system or the building itself.

Henze and collaborators (Henze *et al.*, 2004a; Henze *et al.*, 2005; Liu, 2005; Zhou *et al.*, 2005) have published studies on numerical simulations and experimental applications of optimal control in the coordination of active and passive thermal storage for large commercial buildings. In these studies, two variables (temperature set-points and discharge rate of the TES) are used as controlled variables in a dynamic programming strategy. Other studies carried out by this group have addressed:

- The effect of using different levels of building modeling accuracy on the optimal control strategy (Henze *et al.*, 2005; Liu, 2005). Construction materials, internal heat gains and characteristics of the HVAC plant were found to be among the most important factors for the design of optimal control strategies.
- The effect of forecasting uncertainty (Henze and Krarti, 1999). It was found that even imperfect forecasts enable the optimal predictive controller to perform better than conventional strategies do.
- The impact of the accuracy of weather forecasting models on a predictive optimal controller (Henze *et al.*, 2004b). A "perfect prediction" was used as the reference. It was found that even simple weather forecasting models provide satisfactory results.
- The impact of the planning horizon length (Krarti *et al.*, 1999). It was concluded that a planning horizon of 24 hours is often enough, unless two conditions occur

simultaneously in the long term: (a) that all the energy stored in the TES is used and (b) the system needs more than one day to fully charge the TES.

- Parametric analysis of optimal control of active and passive cooling storage (Zhou *et al*., 2005). In general, the conclusions of this study confirmed previous intuitive expectations: (a) optimal control provided more benefits in buildings with larger thermal mass; (b) more potential for savings was found for stronger incentives in the TOU utility rate structure; (c) more savings were obtained for a hotter, drier location in summer; (d) optimal control had a tendency to keep the set-point in the upper limit if other thermal comfort considerations were not included with a penalty function; (e) the capacity of the system affected the proportion of active and passive TES used; (f) an economizer was more useful wherever nights were cooler.

2.3.3 Model-Based Predictive Control of Solar Buildings

Studies on the dynamic control of solar buildings have tended to focus on specific aspects (e.g., the control of one piece of equipment) rather than on a global, comprehensive approach. The main goal of these investigations has often been the control of passive solar buildings. Dorato and Knudsen (1979) studied the use of steady periodic models of solar radiation and exterior temperature, which were represented by Fourier series, to determine the optimal control strategy for auxiliary heating in a simplified model of an enclosure with a solar heating system. The objective function was analyzed by simple calculus (finding the values at which the derivative of the objective function is equal to zero). Albeit practical, this kind of strategy can only be used when simple curves are used to model the inputs (solar radiation and temperature).

Athienitis *et al.* (1990) stated that the proper design and operation of a building requires an integrated analysis of the building's response to load changes and the performance of its HVAC system. The study mentions two approaches traditionally followed to attain this integrated analysis: (a) detailed numerical simulation with specialized software and (b) simplified analytical models dealing with specific interactions. Athienitis *et al.* (1990) developed an alternative methodology based on thermal networks with distributed parameter elements and lumped elements. Distributed parameter elements, which are used to represent exterior walls as two-port networks, provide a mathematically exact solution for heat fluxes and temperatures through them. Lumped elements (typically a single thermal capacitance) are used to represent constituents such

as the room air and provide only an approximate solution. The resulting network model with two kinds of elements can then be solved in the frequency domain by applying methods borrowed from the analysis of electrical networks. In simple cases, the transfer functions between inputs and outputs can be determined analytically; in more complex cases, inputs and outputs are found at discrete frequencies, and numerical methods can then be used to obtain an approximate analytical expression. The building transfer functions can be used for control studies (Athienitis and Shou, 1991) and for energy and load calculations.

2.3.4 Recent Developments in Model-Based Predictive Control

In recent years, model-based predictive control has received significant attention and is gradually becoming more "main stream" (Cooperman *et al.*, 2010). Florita and Henze (2009) compared different models for weather forecasting (as opposed to using online weather forecasts) for predictive control. The authors point out that forecasts produced by meteorological institutions and companies may not provide the information required (hourly or sub-hourly forecasts of solar radiation), are subject to service interruption (e.g., communication failure), and may not be available for the specific location. Local forecasting has the advantage of enabling the creation of data-driven models, based on on-site measurements of weather variables and determination of trends. Florita and Henze (2009) conclude that although more complex models (typically, neural-network based) have been applied, the performance of simpler time series methods (e.g., simple prior moving average) is often satisfactory.

May-Ostendorp *et al.* (2011) have recently looked at the utilisation of model predictive control of window operation in commercial buildings, with the purpose of extracting rules which may be easily computed and implemented in commercial buildings.

The *OptiControl* project, carried out in Switzerland by several academic institutions, government agencies and industrial partners, has produced interesting developments in the area of model predictive control (Gyalistras and OptiControl Team, 2010). This team has looked at the utilization of thermally activated building systems (TABS) for energy storage (Gwerder *et al.*, 2008; Gwerder *et al.*, 2009), the development of advanced control algorithms for peak load reduction and climate control (Oldewurtel *et al.*, 2010a; Oldewurtel *et al.*, 2010b), and the improvement of weather forecasts for the purpose of building control (Stauch *et al.*, 2010).

Despite the emerging interest in the application of MPC for building control applications, MPC research projects specifically devoted to solar homes are still rather limited. Moreover, investigations tend to focus more on the optimisation algorithms for the controllers than the implementation in the building. Many papers have been presented or published in specialised conferences or journals for control engineering, with limited exposure to the HVAC and solar engineering research communities.

2.4 Relevant Technologies and Tools for Solar Homes

2.4.1 Passive Solar Design

Passive solar design (Anderson, 1990b; Balcomb, 1992; Athienitis and Santamouris, 2002; Haggard *et al.*, 2010) consists of a set of design techniques intended to take advantage of solar heat gains in order to supply a substantial portion of the heating needs of a building. The basic principles have been known since antiquity: Anderson (1990a) cites examples from ancient Egypt, Greece and Rome, including evidence of double-glazed windows in bathing rooms at Herculaneum (near Pompeii). Indian cultures in the American Southwest provided solar exposure to their dwellings (Anderson, 1990a). In spite of the intuitiveness of the concept, passive solar design requires a careful quantitative approach for its successful implementation. The term passive indicates that, in general, these methods do not require the intervention of mechanical systems or moving parts.

Passive solar design relies on features such as high levels of thermal insulation in the building envelope, air-tight construction, high-performance windows with an equatorial orientation (towards the South in Northern Hemisphere, and towards the North in Southern Hemisphere). Passives solar design also includes increased levels of thermal mass that can store heat while mitigating temperature fluctuations, properly sized overhangs to prevent solar gains in summer and measures to encourage natural ventilation and passive cooling. Passive solar design not only allows energy consumption and cost reduction; it also significantly improves thermal comfort.

The maximum contribution of passive solar gains to supply heating loads is difficult to quantify, as it is not clear which conditions should be used as a reference. When comparing solar gains to heat loss through the building envelope, figures between 30 and 50% have been reported, for example, for different cities (CMHC, 2006). However,

as pointed out in (CMHC, 2006), passive solar design is particularly suited for the cold and sunny winters.

Overheating is a common problem found in poor passive solar design (CMHC, 2006). In the countries where traditional construction materials are used, thermal mass can play a significant role in preventing this problem. Other measures, such as set-point adjustment and air circulation to distribute the heat in the space, are also advisable.

2.4.2 BIPV and BIPV/T Systems

Photovoltaic generation provides the most practical way to generate electricity at a building scale when compared, for instance, with wind generators or CHP systems. When PV panels are integrated seamlessly into the building envelope, they are called "building integrated photovoltaic" (BIPV) systems. This approach can reduce total cost since the PV panels are a working element of the building envelope, which replaces cladding or shingles, therefore even contributing to improving the aesthetics of the building. Most residential photovoltaic systems are "grid-connected" (Ayoub *et al.*, 2001). This approach provides a backup for the user of a BIPV system, obviating the need for a battery system or any other storage device. Photovoltaic generation can be used to offset the consumption of appliances and lighting. In 2001, a typical detached Canadian house consumed about 8720 kWh of electricity per year for lighting and appliances. Interestingly, even in the early 1990s, it was possible to reduce this figure to about 4,300 kWh by using energy-efficient appliances and lighting systems (Ayoub *et al.*, 2001). A quick calculation shows that this corresponds to the energy generated by a 3.5-4.0 kWe PV system in Montréal.

When BIPV installation has additional goal of recovering heat, it is called "building integrated photovoltaic/thermal" (BIPV/T) system. Research projects at Concordia University have studied the properties of BIPV/T systems by using air as heat recovery fluid (Charron and Athienitis, 2006; Liao *et al.*, 2007; Candanedo *et al.*, 2010). BIPV/T systems remain an important research area at the Concordia Solar Laboratory.

Two types of PV cells are commonly manufactured today: crystalline silicon (either single-crystal or polycrystalline) and thin-film panels. Crystalline panels are currently the dominant technology, but it is expected the thin-film technology will have a more important share of the market in the future (Hoffmann, 2006). Although the main

obstacle for BIPV systems remains their elevated cost, there is a continuous trend towards lower prices. Hoffmann (2006) indicates that a price of 1 € per W_p will be reached in the 2020s. As of May 2011, the price of PV is reported to be $3.12 per W_p in the US and about €2.73/W_p in Europe. Although for several years the price of PV remained steady, there is a clear downward trend, as seen in Figure 2.3.

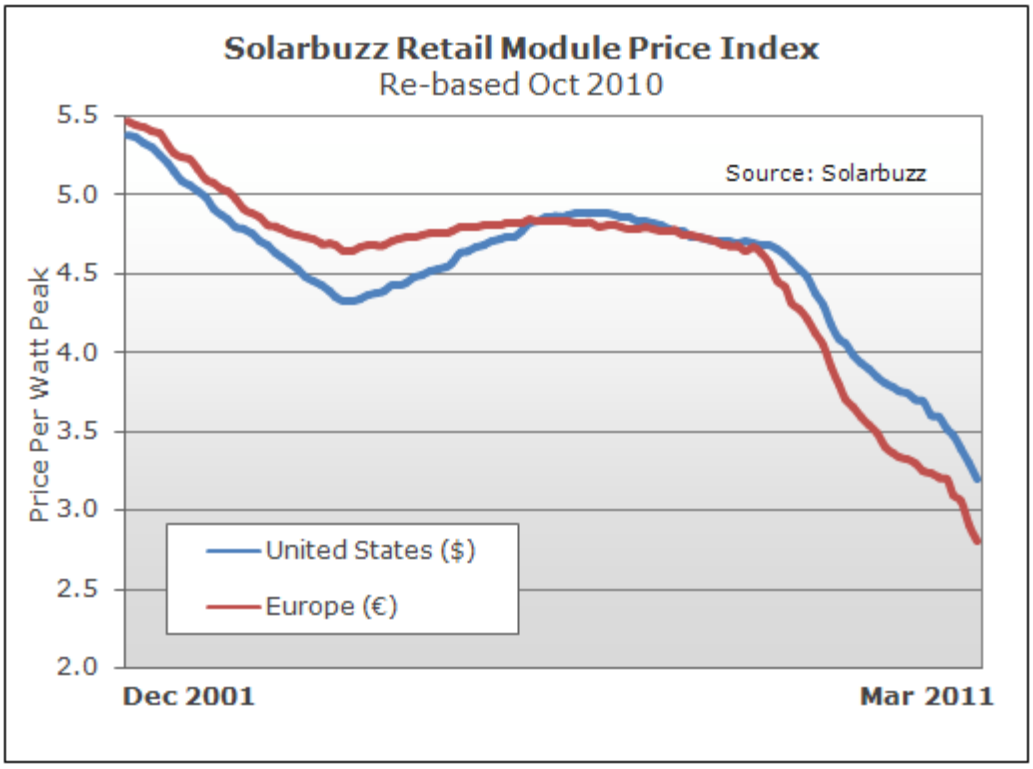

Figure 2.3 Progression of PV price over the last decade (Solarbuzz, 2011).

2.4.3 Solar Thermal Collectors

Perhaps the most commonly used collectors for the solar heating of DHW are the glazed flat-plate solar collector and the vacuum tube solar collector. For the theory of operation of flat plate solar thermal collectors, the text by Duffie and Beckman (2006) is an excellent reference. These collectors consist simply of a plate designed to absorb solar radiation (the "absorber plate"), typically covered by glazing, on top of a piping system in which a circulating fluid (water or water-glycol mixture) removes the heat from the absorber plate. A circulating pump, together with a storage tank, completes the system. The circulating pump may be eliminated by placing the storage tank above the collector and relying on the thermosiphon effect.

In a vacuum tube solar collector, a specially designed heat pipe is encapsulated within a glass tube in which a vacuum has been made to reduce heat losses to the exterior. The heat pipe collects the heat and delivers it to a fluid circulating around a metal tip (the condenser of the heat pipe) inserted within a header or manifold.

Figure 2.4, obtained from a manufacturer's website, displays typical curves for solar collectors. Efficiency, the fraction of energy recovered from solar radiation, is usually plotted versus the ratio of the temperature difference between the fluid's temperature and the ambient temperature divided by solar irradiance.

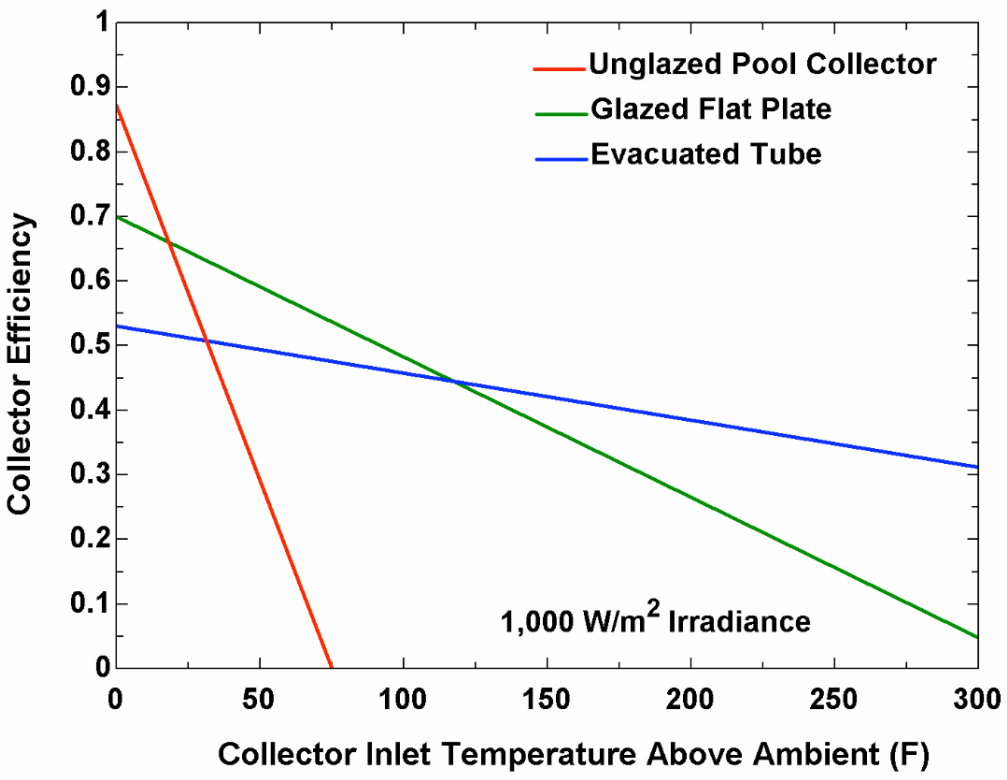

Figure 2.4 Comparison of the performance of different kinds of solar collectors (SunEarth Inc., 2005).

The curves are approximately linear. Although the y-axis intercept may vary, flat plate collectors tend to perform better at high solar radiation and smaller temperature differences (i.e., towards the left of the graph); however, their performance drops rapidly when these conditions change. Because of their low heat losses, vacuum tube solar collectors have excellent performance in cold winter conditions; they can also operate at higher water temperatures than flat-plate collectors (50 to 95°C versus 30 to

70°C) (NRCan, 2006). Evacuated tube collectors are, however, typically more expensive than flat-plate collectors (NRCan, 2006).

2.4.5 Thermal Energy Storage

Energy storage systems are essential for solar-optimized buildings, not only because of the obvious extension of energy availability, but also because they can be used to take advantage of changing electric utility rates.

Reviews of currently available thermal energy storage (TES) technologies have been presented by Dincer (2002), Nielsen (2003) and Bales *et al.* (2005). The latter presented the findings of Task 32 of the International Energy Agency (IEA), dedicated to advanced storage systems in single-family houses, with the purpose of obtaining a high solar fraction (i.e., fraction of thermal energy provided by the sun), focusing on latitudes of 45° (coincidentally, the latitude of Montréal). IEA's research has been focused on three types of active thermal storage systems: water-based, phase change materials (PCM) and thermochemical systems. This classification roughly coincides with the one presented by Dincer (2002) who mentions three storage methods: sensible heat storage (by changing the temperature of a medium like water or rock), latent heat storage (PCM materials, ice-water storage), and chemical systems.

a) Sensible heat storage

Water is a popular storage medium for solar applications because of its availability and high specific heat. Although the energy storage density of water systems is not as high as PCMs or thermo-chemical systems, the obvious advantages of these systems are their simplicity, low cost and experience with their use (Bales *et al.*, 2005). Thermal stratification helps to improve the performance of a water storage tank, as hot water from the top can be used to supply heat to the space, or as the source of domestic hot water (DHW); colder water from the bottom can be used to obtain heat from any primary heat source. Technologies exist to enhance thermal stratification and delay the onset of thermal equilibrium in the tank. For example, baffles are installed in the tank as obstacles to natural convection (Kulacki *et al.*, 2007) and perforated pipes or special manifolds are used to reduce the speed of the water entering or leaving the tank, thus avoiding mixing the water in the tank (Duffie and Beckman, 2006). Multiple-tank configurations, with tanks at different temperatures, can also be employed (Cruickshank and Harrison, 2006).

A limitation of water is the fact that it can only store heat below 100°C at atmospheric pressure. Above this temperature, pressure vessels are needed, a fact which considerably increases the price of the system (Dincer, 2002), and represents a safety issue. Heat resistant oils can store heat in a wide range of temperatures from -20°C to +320°C, but their specific heat is only about half that of water. Molten salts and molten metals are also used to store heat at high temperatures (Dincer, 2002).

Rocks have also been used for thermal storage (Dincer, 2002). They occupy more space per unit energy than water, but they are easy to implement. Dincer (2002) points out that combining water with air/rock thermal storage has become practically a standard TES system for solar applications.

b) Latent heat storage

Ice storage systems are a mature technology to store cooling power (Dincer, 2002). They require a chiller for ice making and a piping distribution system. The chiller can be the same that provides direct cooling to the space, or a different one. In general, ice storage systems represent savings because of the use of electricity in off-peak hours and the reduction of initial cost due to a smaller system, but as discussed by Henze *et al.* (1995), these advantages depend on the operation strategy. Dincer (2002) discusses two basic schemes: (a) full storage TES, providing all the cooling needs during on-peak hours; and (b) partial storage TES, aiming to reduce only the peak load (this is the preferred system when the peak load are much higher than the average load).

PCMs are specifically designed to undergo a phase change (generally liquid-solid, but also solid-solid) at a given temperature, the "Phase Change Temperature" (PCT) (Bales *et al.*, 2005). Typical PCM materials are paraffins, fatty acids, or inorganic salt hydrates. By keeping them in a vessel, PCMs can be used as a backup for the thermal storage system. PCMs can also be incorporated into the building envelope, contributing to the passive storage of the building's structure. According to Bales *et al.* (2005), typical PCTs are: 5 to 18°C for cold storage, 22°C for building envelope integration, and 60°C for hot storage.

c) Thermo-chemical storage

Sorption can be defined as "the process in which one substance takes up or holds another (by either absorption or adsorption)" (WordNet, 2008). In a thermo-chemical

storage system, heat from a solar collector or other source is supplied to separate a sorbate –the sorbed substance– from a sorbent –the material that contains it (Bales *et al.*, 2005; Jahnig *et al.*, 2006).This process, called the desorption stage, requires energy and is therefore endothermic. The sorbate and sorbent can then be stored in separate vessels for as long as required. When heat is needed, the substances can be combined, triggering the exothermic sorption stage, which releases energy. Most of the work of Task 32 has focused on systems using water as the sorbate, or operating substance.

Thermo-chemical systems have the advantage of providing a high density of energy storage. Nielsen (2003) gives the figure of 1 MWh/m^3. In comparison, 1.0 m^3 of water can store roughly 58 kWh of heat within a 50K temperature range.

Figure 2.5, borrowed from a recent presentation by Hauer (2010), compares the energy storage capacity of thermo-chemical (TCM) systems, PCMs and water. Evidently, there is significant potential in thermo-chemical storage. However, engineering solutions including TCM are still needed, due to the complexities of the technology required.

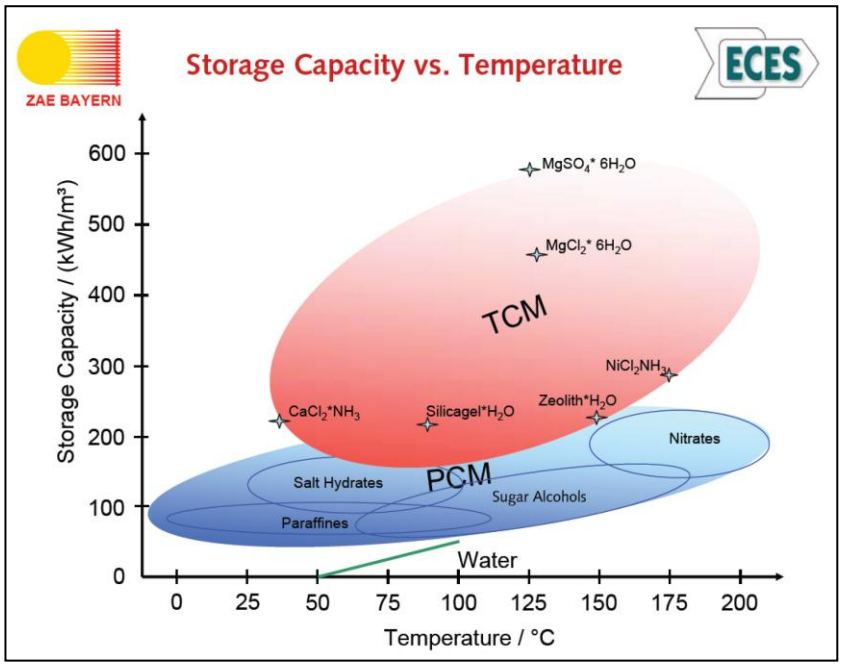

Figure 2.5 Comparison of different TES systems (Hauer, 2010)

2.4.6 Technology Trends in Building Controls

Wireless technologies, such as ZigBee^{TM} (Egan, 2005; Duan and Li, 2008) are becoming more widely available. Although wireless sensors are still relatively costly, the savings in terms of wiring and installation costs are turning them into an interesting

alternative for retrofit projects. Some wireless devices are able to harvest different kinds of energy (electromagnetic waves, solar, thermal and vibration). Moreover, the implementation of wireless devices converges with the trend towards distributed control architecture, in which smaller, low-cost processing devices are closer to sensors. Control system installations are shifting from centralised to de-centralised (Braun, 2007; Guo and Zhou, 2009), which contributes to their robustness and flexibility.

Recently, efforts have been made towards the creation of open-source network protocols expected to ease the design of integrated HVAC solutions, such as BACNet™ (Bushby, 1997; Holmberg and Bushby, 2009) and LonWorks (Echelon, 2009) in North America, and KNX/EIB in Europe (KNX, 2011). These protocols have opened the doors for the participation of more control companies in the HVAC market (Braun, 2007).

Emergence of embedded intelligence in devices allow supplying valuable information for building operators, maintenance crews and even building occupants (Braun, 2007). It will be possible to obtain information not only from the central control system, but also from individual components (air-handling units, fans, heat exchangers, etc.). This information will include documentation of the device, and it may include performance maps that could provide accurate estimates of power consumption, flow rates, temperatures and other variables, working as "virtual sensors" (Braun, 2007).

Web and mobile (e.g., iPhone™) interfaces (Negron and Hayes, 2009) and energy dashboards (Fehrenbacher, 2009) are bringing home automation closer to reality. By facilitating information exchange with occupants, these devices are expected to have significant impact on user behaviour (Agarwal *et al.*, 2009; Bartram *et al.*, 2010), by allowing occupants to change their consumption habits.

2.5 Advanced Fenestration

2.5.1 High Insulation Windows

Technological developments have allowed the increase of the insulation value (R-value) of windows, which is often much lower than the insulation value of walls. Windows have been described as the "weak spot" of the building envelope (Hutcheon and Handegord, 1983). According to Arasteh *et al.* (2006), windows account for 30% of the heating and cooling energy in buildings in the US, and despite recent significant advances. The window-to-wall ratio (WWR) has always been an important parameter in the design of a building. Choosing an appropriate WWR value usually implies a trade-off between increasing solar heat gains and day lighting and avoiding heat losses from the heated space.

In cold climates, two panes of glass have been traditionally used in windows to increase their total insulating value. The air gap between the window panes acts as an additional layer of insulation. Beyond a gap thickness of about 13 mm the R-value (i.e., thermal insulation) of the window does not change, since the most important heat transfer phenomenon is radiation between the two glazing (Athienitis and Santamouris, 2002). Frames made of conductive material such as aluminium can act as "thermal bridges", with thermal resistance values even lower than the window glazing. Advances have been made in the framing system to include insulating materials to "break" the thermal bridge (Hutcheon and Handegord, 1983). Thermal bridges can also favour the appearance of condensation, which can have serious detrimental effects on the building enclosure (Hutcheon and Handegord, 1983). The addition of a third pane of glass, to create "triple-glazed windows" has further increased the R-value of windows.

Low emissivity coatings improve the R-value dramatically by reducing long wave radiation heat transfer between window panes. They have become quite popular since the 1980s, since replacing conventional windows with low-e windows is one of the easiest and cheapest ways to improve the energy performance of a building. In 2005, these windows represented 50% of the US window market share, and their savings since their implementation have been estimated as $US 37 billion (Arasteh *et al.*, 2006).

Arasteh *et al.* (2006) indicated three promising areas of research: (a) aerogels which are silica-based porous coating materials, currently in the research stage, that trap air and

increase the insulating value while letting light through (Apte *et al.*, 2003); (b) vacuum glazing, already available in Japan, which try to completely eliminate convection and conduction heat losses, and (c) gas-filled low-e windows, which use three or more glazing, low emissivity coatings and cavities filled with argon.

Low-e coatings also affect the SHGC (solar heat gain coefficient), the fraction of solar heat that ultimately reaches the living space. Whereas a low SHGC can be beneficial in cooling-dominated regions, it can have a detrimental effect in cold climates, where heat gains are desirable in winter. Although low-e windows with high SHGC are being developed (Apte *et al.*, 2003), the trade-off is not easy to determine, as in summer it is still convenient to reduce solar heat gains.

2.5.2 Switchable Glazing and "Smart Windows"

Several new technologies, at different stages of research and development, offer the possibility of adjusting the impact of fenestration on heating loads, cooling loads and day lighting in a building. For example, it might be convenient to increase the opacity of a window during the summer months in order to reduce the cooling load, and increase their transmittance during winter to increase solar heat gains. Some of these new technologies are briefly presented below:

a) Electrochromic (EC) windows. This technology takes advantage of chemical reactions, triggered by the sudden application of a voltage, to change the opacity of a material. Electrochromic windows, usually formed by several layers, can vary their transmittance over a wide range, between a few and 70 percent (Apte *et al.*, 2003).

b) Thermochromic windows. These windows change their optical properties as a function of temperature. Thermochromism is a well-known phenomenon that is used in a wide range of applications (Fraunhofer IAP, 2008). The main disadvantage of thermochromic windows is that they are not as easily controllable as electrochromic windows.

c) Photochromic windows. Photochromic windows change colour when exposed to bright lights (CEC, 2006). Their main application could be glare prevention. They may not be the best technology for cold climates, as they can limit solar heat gains in winter.

d) Gasochromic windows. A gasochromic window has a layer of an active film (WO_3) which reacts when extremely dilute hydrogen fills the cavity, changing the colour and transparency of the window (Wilson *et al.*, 2002). This change can be reverted by filling the cavity with dilute oxygen. Their switching speed can be faster than that of electrochromic windows (Carmody, 2003).

e) Other technologies. Windows using polymer dispersed liquid crystals (PDLC), the technology used in LCD screens, have been considered for modifying properties of window glazing (Bonsor, 2001; Richardson *et al.*, 2001). This technology offers privacy by scattering light, but there is no control of solar heat gains. Suspended particle devices (SPDs) were created as a commercial product by Research Frontiers, Inc. (Bonsor, 2001), although other companies are developing the idea based on principles discovered nearly a hundred years ago: millions of particles in a liquid suspension block the light when in random distribution (Bonsor, 2001). When a voltage is applied, they become aligned, consequently allowing the light to pass through.

2.5.3 Controllable Motorized Blinds

Although blinds, curtains and shades have been used for centuries to adjust the passage of light through windows, it is only in the last decades that they have been used as automated "control actuators" of solar heat gains and day lighting. Taking into account the architectural trend towards buildings with large glazing areas (Bessoudo, 2008), these devices will play an increasing role in building energy management.

The inherent complexity of the physical heat transfer phenomena and their effects on thermal comfort makes controlling the position of blinds, curtains or shades a difficult task. However, automatic control of these devices is a necessity.

The published literature in the field of blind controls is vast. Some of the relevant recent investigations have been carried out at the Concordia Solar Laboratory (Tzempelikos, 2005; Tzempelikos and Athienitis, 2003). The potential of controllable blinds for reducing electricity load and energy consumption in buildings has been underscored as illustrated in Figure 2.6.

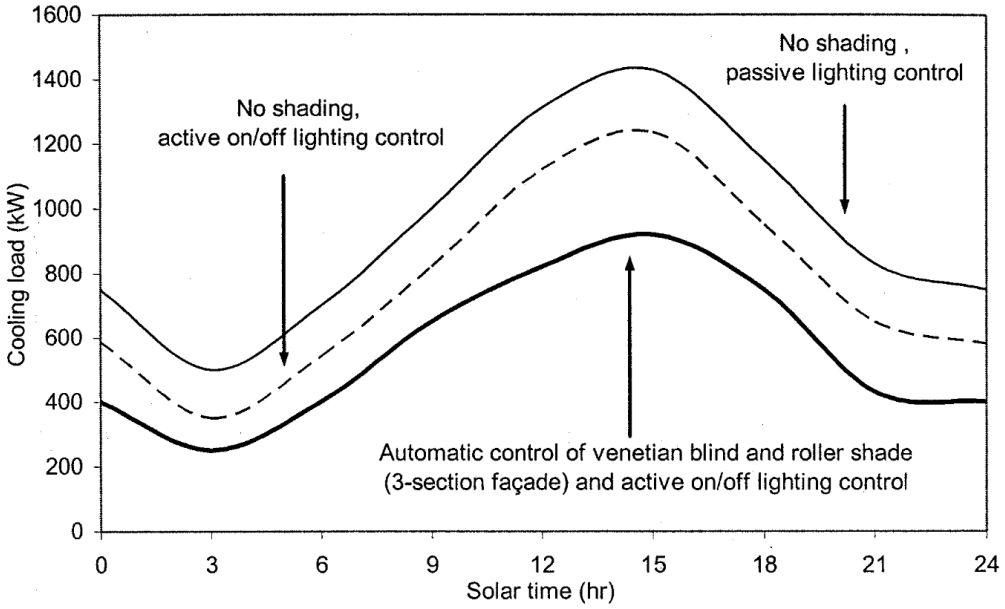

Figure 2.6 Cooling load curves for hot summer day under different control conditions of lighting, Venetian and roller blind control (Tzempelikos, 2005).

Controlling solar heat gains and internal temperature in a house by adjusting the position of roller blinds according to an algorithm working with weather forecasts has been explored at the Concordia Solar Laboratory (Candanedo *et al.*, 2007). Example of studies conducted on control of venetian blinds has been carried out by Kuhn (2006).

2.6 Overview of Absorption Refrigeration Systems

2.6.1 Operating Principles

In the typical absorption refrigeration system (ARS), the latent heat that accompanies any phase change process will be transmitted between different levels of operating temperature. Also the typical absorption system employs two different working media, which are the refrigerant and the absorbent. Accordingly, the temperature related to the change of phase can be affected by altering the working pressure and also by altering the concentration of the refrigerant used in the system (Dincer and Kanoglu, 2010). Moreover, the typical absorption refrigeration system includes combination of two key processes which are the *absorption* and the *desorption process* as shown in Figure 2.7.

As clearly shown in Figure 2.7, the cycle includes four essential components namely the evaporator (E) in which the cooling effect is achieved, the generator (G) in which the thermal heat is transferred to the working medium, the absorber (A) and the condenser

(C) from which the heat is rejected from the refrigerant and from the solution. Inside the condenser unit of the cycle, the refrigerant vapour is to be condensed, throttled in the expansion device and then delivered to the evaporator unit in which it evaporates as the case of the normal compression refrigeration systems. After refrigerant evaporation inside the evaporator unit to provide the needed cooling effect, the refrigerant vapour is to be absorbed by the solution of the refrigerant/absorbent during the cooling process that takes place inside the absorber unit. The result of the refrigerant absorption is the change of the solution concentration so that it can be pumped to the generator. Insider the generator unit, thermal energy is added so that the refrigerant vapour will be regenerated to be directed to the condenser whereas the remaining solution will be throttled through an expansion device to flow back to the absorber unit and so on (Dincer and Kanoglu, 2010).

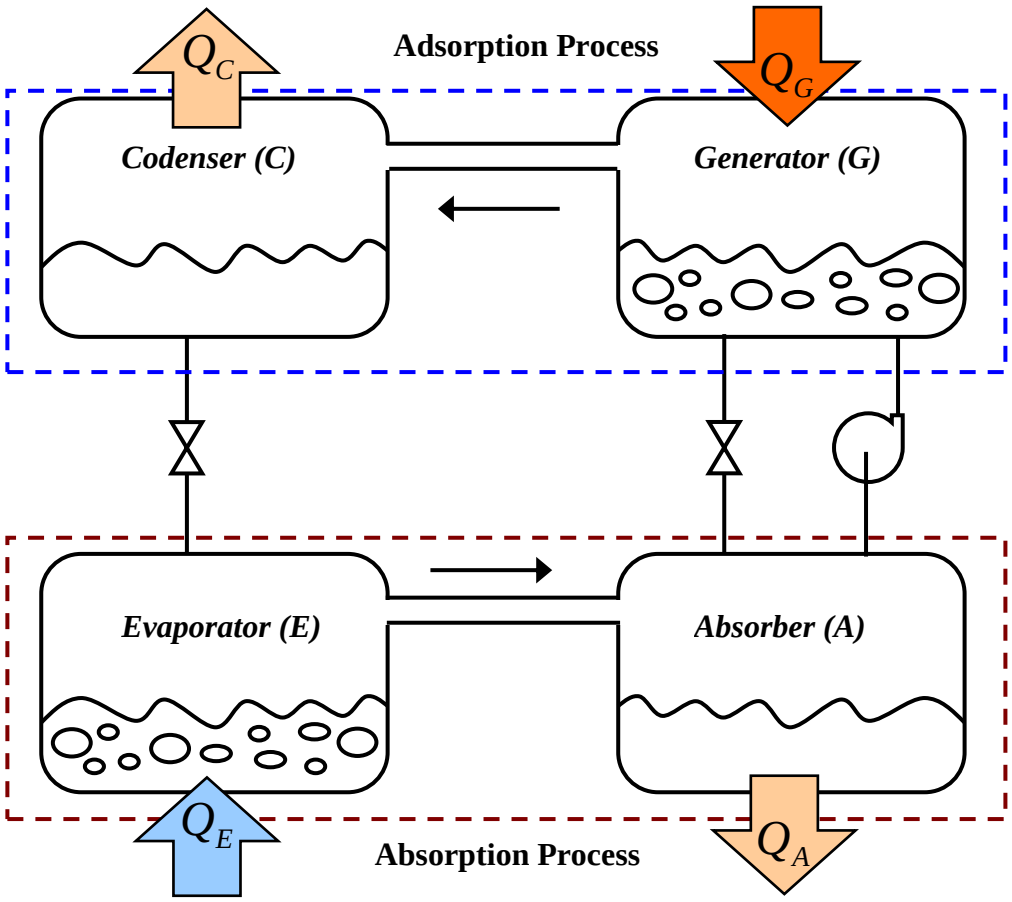

Figure 2.7 Main processes of typical ARS (adopted from Srikhirin *et al.*, 2001)

The operating efficiency of the absorption refrigeration system depends mainly on the two amounts of thermal energies exchanged in the evaporator and the generator.

Therefore, to enhance the efficiency of the system without changing its key operational concepts, solution heat exchanger (SHX) is usually used. The SHE is used to allow transfer part of the thermal energy to the pumped solution (flowing to the generator) from the hot solution coming out from the generator to flow back to the absorber). Normally, the efficiency of the system is expressed in terms of the coefficient of performance (COP), which is defined as the ratio between the useful cooling load achieved in the evaporator and the thermal energy transferred to the working medium inside the generator unit. In most cases, the mechanical work required for the pump operation is ignored because it is very small compared with the amount of thermal energy added to the generator unit. This means that the pump work is usually ignored to ease the analyses processes of the system (Hundy, 2008).

The typical absorption refrigeration system mainly exchanges thermal energy with three different external energy reservoirs of low, intermediate, and high levels of temperature. During the normal operation of the ARS, the thermal energy is to be transferred from the high temperature reservoir. The useful form of energy of the system which is the refrigeration effect is to be achieved at the lower temperature. In addition, the thermal energy will be rejected from both the absorber and the condenser units at an intermediate temperature (Hundy, 2008).

2.6.2 Working Fluids Selection for ARS

The performance of the typical ARS varies significantly with the variation of both the chemical and thermodynamic properties of the working mediums (Perez-Blanco, 1984). Working fluid plays a significant role in the performance of the absorption systems. Therefore, selecting the proper working fluid pair is very crucial for the efficient and safe working of the system.

Various restrictions are there when selecting the suitable working fluids, which are the absorbent and the refrigerant fluids. The adequate working fluid to be used for the absorption system should have various properties. It must be non-corrosive, non-toxic and harmless to the environment. It also should be inflammable and non explosive in addition to being cheap and available. There are also important properties needed for the efficient operation of the system. For example, the working fluid must have satisfactory mass and heat transfer properties over the operating temperature range. It must be of high solubility in absorbent solution at the absorber operating temperature and low

solubility in absorbent at the generator operating range. Moreover, the working fluid must be of irreversible reaction with absorbent within operating temperature range. Moreover, the absorbent fluid should have lower vapour pressure compared with the refrigerant fluid and it should have lower heat capacity (Crepinsek *et al.*, 2009).

Several working fluid pairs have been considered for the absorption systems, which satisfy most of the above mentioned characteristics. Examples of the used working pairs include water/sodium hydroxide, water/sulphuric acid, and ammonia/sodium thioczanat. The working fluids also include the water/ammonia and the water/ lithium bromide (LiBr). The most commonly used working fluid pair is water/ammonia and water/LiB. But, the working fluid pair of water/LiBr has a temperature constraint because the water is the refrigerant which can not reach temperatures below zero. Therefore, this pair of working fluid is commonly used for air conditioning applications (Crepinsek *et al.*, 2009). Accordingly, this pair of the working fluid is selected to be the working medium of the absorption system considered in the present investigation. Alefeld (1982) presented a comparison between water/ammonia and water/LiBr system. Summary of the points of comparison is shown in Table 2.1.

Table 2.1 Water/ammonia versus water/LiBr systems (Adopted from Alefeld, 1982)

Property	**Working Medium Pair**	
	Water/Ammonia	**Water/ LiBr**
Refrigerant	Ammonia	Water
Absorbent	Water	LiBr solution
Vapour pressure	Too high	Too low
Increased latent heat	Good	Excellent
Reduced freezing temperature	Excellent	Limited applications
No solid phase	Excellent	Limited applications
Lower viscosity	Good	Good
Lower vapour pressure	Poor	Excellent
Lower toxicity	Poor	Good
Temperature lift	High	Low
Affinity between refrigerant and absorbent	Good	Good

2.6.3 Crystallisation and Corrosion Risks in ARS

2.6.3.1 Crystallisation

Aqueous lithium bromide has advantages comparing to other solutions. However, there are few restrictions such as crystallisation which could result in damages to the system and system shutdown. The nature of the salt solution is that the salt component precipitates when the mass fraction of the salt exceeds the solubility limits. The solubility limit is a strong function of the mass fraction and temperature and a weak function of the pressure. Supersaturation can occur where the salt content of the liquid is greater than the solubility limit. Once crystals begin to form it will be a favourite nucleation site for larger crystals to grow on themselves, nevertheless no other nucleation sites presence (Crepinsek *et al.*, 2009).

Various methods can be used to minimize the possibility of crossing the phase boundary. The simplest method used is to ensure a sufficiently low temperature sink for cooling the absorber. Based on the properties of aqueous lithium bromide, low temperatures in the absorber require lower absorber solution concentration and thus tend to avoid the phase boundary. Since crystallisation produces a slush-like, viscous liquid, it results in blocking the pump or drying the generator (Alefeld, 1982; Hundy, 2008; Crepinsek *et al.*, 2009).

Water cooled absorption machines generally can operate without crystallisation problems. However, crystallisation occurrence requires considerable time and effort to correct. The preferred recovery method is to raise the temperature of the portion that is crystallised to a point where the viscosity is reduced sufficiently so that the pumps can circulate the solution. Once the solution is in circulation, it can be easily diluted using water from the evaporator. In a typical installation, manufacturers include controls to identify crystallisation and take appropriate action to avoid the condition by reducing heat input to the generator or by diverting liquid water from the evaporator to the absorber to dilute the solution.

2.6.3.2 Corrosion

In the presence of dissolved oxygen, aqueous LiBr is highly aggressive to many metals including carbon steel and copper. Although, in the hermetic environment inside an absorption machine, very little oxygen is present and corrosion rates are much slower. For the temperature range a typical single-effect application, carbon steel and copper are

the preferred materials of construction. Over the extended life of a machine, significant corrosion can still occur (or in case of improper operation). In order to minimise the effect, there are primary measures available such as pH control or corrosion inhibitors (Crepinsek *et al.*, 2009).

2.6.4 Commonly used Working Fluids in ARS

There are several pairs of working fluids suggested to be applied in the ARS applications. Extensive survey of these fluids is given by Marcriss (1988) who reported the availability of more than forty compounds to be used as refrigerants and more than two hundred compounds to be used as absorbents. However, the most commonly used working fluids in the various absorption refrigeration system applications are the ammonia/water (NH_3/H_2O) systems and lithium bromide/water ($LiBr/H_2O$) systems (Kaynakli and Yamankaradeniz, 2007)

The ammonia/water system uses ammonia as the refrigerant and water as the absorbent. This system has been widely used for the various applications of cooling and heating. Both ammonia (refrigerant) and water (absorbent) are both remarkably stable over an extended range of working condition i.e. temperature and pressure. Ammonia characterised by its increased latent heat of vaporisation, which is very essential for enhanced performance of the system (Lewis *et al.*, 2007). This system can be used for lower temperature applications because the freezing temperature of ammonia is –77°C. But, the toxicity of ammonia is also a key restriction that causes its restricted use solely for the well-ventilated spaces. Since both ammonia and water are both volatile, the system will need rectifier to eliminate any water vapour that normally evaporates with ammonia. If the rectifier use is ignored, the water can reach the evaporator and freezes affecting the system performance and can stop operation (Hundy, 2008). There are other drawbacks of the system include the increased operating pressures, the corrosion effects on the copper alloys. But, ammonia/water systems are considered environmentally friendly systems and characterise by the decreased costs. Absorption refrigeration machines that use ammonia/water as fluid pairs are commercially available with capacity of 10 to 90 kW with COP around 0.5 (Hundy, 2008). The various thermodynamic properties of ammonia/water are available in the literature (Park and Sonntag, 1990; Ziegler and Trepp, 1984; Herold *et al.*, 1988).

The use of lithium bromide/water solutions in ARS applications started about 1930 (Berestneff, 1949). The two excellent characteristics of this system are the absorbent non-volatility (no need to add rectifier to the system) and the higher vaporisation heat of refrigerant. But the use of water as refrigerant restricts the minimum temperature of the system to be higher than the water freezing point of 0°C. According to the working temperature, the use of water as refrigerant cause the corresponding vapour pressures to be considerably lower than atmospheric which cause the whole system to work under vacuum conditions. As stated before, at higher lithium bromide concentrations in the solution, there will be more chance to experience risks of crystallisation that can block the pipes and stop the operation of the system. Moreover, the working fluid pairs can be of corrosive effects to some metals and they are considerably expensive compared with the working pairs of the ammonia/water systems. Absorption machines using $LiBr/H_2O$ as working fluids are usually used as absorption chillers for the air conditioning applications, especially for the large capacity needs. They are commonly available in different sizes varies from 10 to 1500 Ton of Refrigeration (TR) keeping in mind that the one TOR is equivalent to 3.517 kW. The coefficient of performance (COP) of the LiBr/water ARS can be changeable as $0.7<COP<1.2$ according to the system design. Several studies are available in the literature to cover the thermodynamic properties of $LiBr/H_2O$ (McNeely, 1979; Patterson and Perez-Blanco, 1988; Lee *et al.*, 1990; Jeteter *et al.*, 1992; Lenard *et al.*, 1992). Moreover, other additives can be used with the $LiBr/H_2O$ systems to stop the corrosion effects (Modahl and Lynch, 1971; Verma *et al.*, 1999) or to enhance both the heat and mass transfer characteristics (Alberston and Krueger, 1971; Chang *et al.*, 1971; Elkassabgi and Perez-Blanco, 1991; Daiguji *et al.*, 1997; Hihara and Saito, 1993).

2.7 Common Designs of ARS

In addition to the proper selection of the working fluids, the structural design of the absorption system is significant to the performance of the system. According to the basic design concepts of the absorption refrigeration system, different modifications can be used to enhance the performance of the system. The most commonly used designs are explained in the following sections.

2.7.1 Single-Effect Absorption System

The simplest design and the most commonly used ARS is the single-effect design. Figure 2.8 illustrates the single-effect ARS using lithium bromide/water.

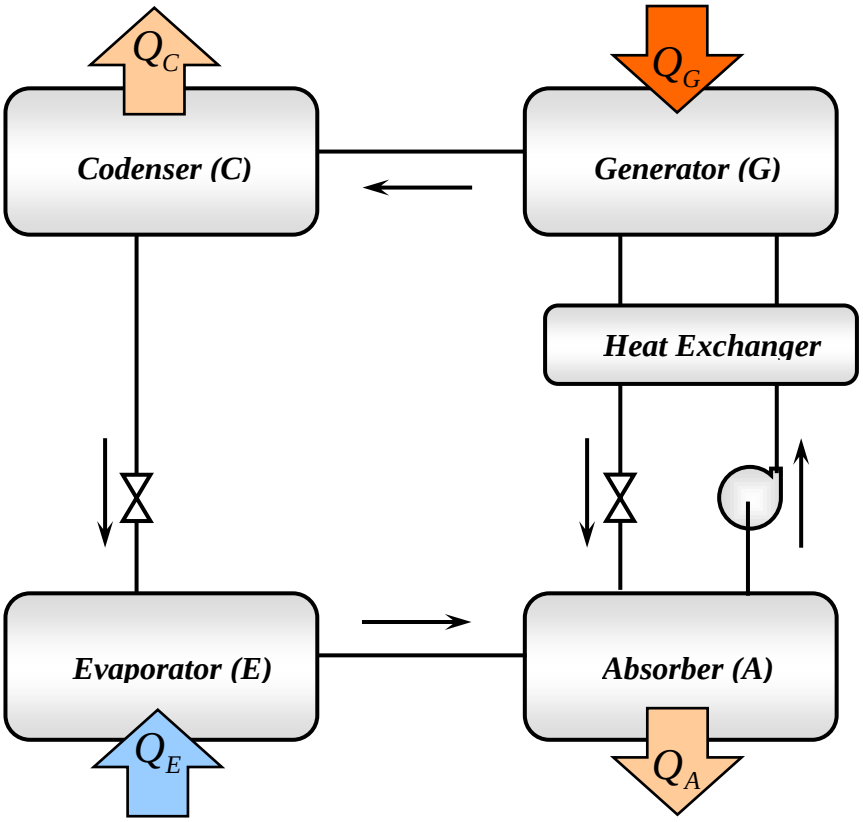

Figure 2.8 Single-effect absorption refrigeration system with solution heat exchanger (adopted from Srikhirin *et al.*, 2001)

Based on the design shown in Figure 2.8, high temperature thermal energy is transferred to the generator unit. The thermal energy is used for evaporating of the refrigerant from the LiBr/water solution. Part of this energy is then removed to the surroundings from the condenser unit during refrigerant condensation. Also part of this energy is transferred to the absorber solution and also to be transferred to the surrounding from

the absorber unit. Therefore, there will be considerable energy waste from the heat supplied to the generator which can decrease the COP of the system. Accordingly, the design modification to improve the system performance takes place by using solution heat exchanger, as illustrated in Figure 2.8. The function of the heat exchanger in the system is clear so that it allows transfer part of the thermal energy from the solution leaving the generator unit to the solution entering the generator. This decrease the amount of thermal energy needed to be supplied to the generator unit. The net result will be COP improvement and decreased thermal energy input. Also the use of the heat exchanger will decrease the amount of thermal energy to be rejected from the absorber unit so that the size of the absorber will be reduced and becomes cost effective. In ARS employing solution heat exchanger, the COP can be improved up to 60% (Kaynakli and Yamankaradeniz, 2007).

2.7.2 Double-Effect Absorption System

The key target of the higher effect ARS is to enhance the performance of the system when higher temperature thermal energy source is accessible. In the typical *multi-effect* ARS, the system is to be designed so that the thermal energy outlet from the higher temperature stage is employed as input source of thermal energy to the lower temperature stage. This will ensure having increased cooling effect (which is the key target of the ARS used for refrigeration and air conditioning) especially in the lower temperature stage.

The double-effect ARS was firstly employed during the period 1956 and 1658 (Vliet *et al.*, 1982). There are two main designs for the double-effect ARS namely parallel and series double-effect ARS. Figure 2.9 demonstrated the typical series double-effect ARS using $LiBr/H_2O$. In this system, the high temperature thermal energy from the external source (for example, thermal energy from set of solar collectors) is transferred to the first-effect generator unit. This thermal energy is used to evaporate part of the refrigerant fluid which will be directed the second-effect generator to be condensed in at higher pressure. In this unit, the rejected thermal energy from the condensed refrigerant vapour will be used to generate additional amounts of refrigerant vapour out of the lithium bromide/water solution. The combined refrigerant streams will be condensed in water cooled condenser, throttled and then directed to the evaporator. Moreover, two heat exchangers arranged in series are used to heat the weak solution pumped from the

absorber towards the high temperature generator. In this system there are three different concentrations of the $LiBr/H_2O$ solution i.e. strong, intermediate and weak solutions.

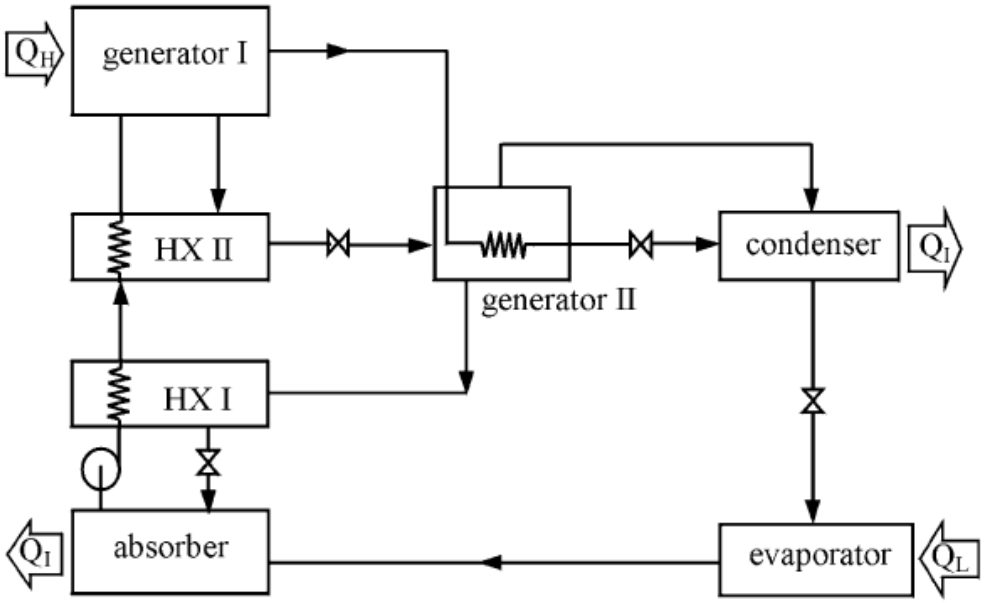

Figure 2.9 Series double-effect ARS (Srikhirin *et al.*, 2001)

Srikhirin *et al.* (2001) reported that the double-effect ARS is seen as a combination of 2 single-effect ARS each of which has COP value known as COP_{single}. For each unit of thermal energy (transferred from the external source), the cooling effect cause by the refrigerant produced at the first-effect generator will be $1\times COP_{single}$. For the single-effect ARS, it can be assumed that the thermal energy exit from the condenser is nearly equal the resulting cooling capacity. Therefore, the thermal energy to be supplied to the generator component becomes $1\times COP_{single}$. Accordingly, the cooling effect that can be achieved from the second-effect generator will be $1\times COP_{single}\times COP_{single}$. Then, the COP of the double-effect ARS can be evaluated as:

$$COP_{double} = COP_{single} + \left(COP_{single}\right)^2 \tag{2.1}$$

According to the analysis of Srikhirin *et al.* (2001), the double-effect ARS can have a COP of about 0.96 when the COP of its corresponding single-effect is 0.6. According to the basic of double-effect ARS, other designs of multi-effect systems have been considered such as the triple-effect ARS design. As understood from Equation 3.1, the

increase of number of effects increases the COP but the real situation is not that simple. It can be said then that the COP increase cannot of direct result of increasing the number of effects. This is mainly because the more increase of the number of effects decrease the COP of the single-effect system, which overall will decrease the whole COP along with increased costs.

For the parallel double-effect ARS, as shown in Figure 2.10, the weak solution coming from the absorber is pumped using the weak solution pump and then divided between the two parallel flow lines.

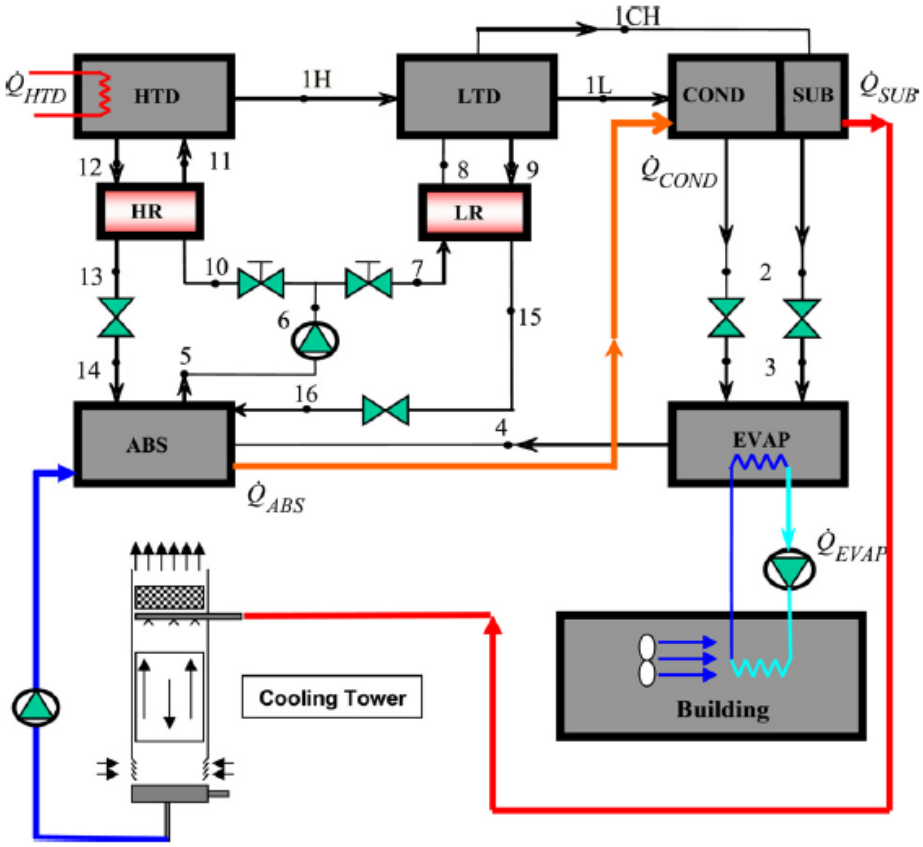

Figure 2.10 Parallel double-effect ARS (Marcos *et al.*, 2011)

As shown in Figure 2.10, the portion of weak solution for each branch is controlled via control valves then delivered to heat exchanger and then to generator unit. The two generator units are at different temperatures. One generator (high temperature desorber HTD on Figure 2.10) works at high generator temperature, to which the thermal energy is supplied. The second generator (low temperature desorber LTD) uses the refrigerant generated in the HTD as heat source to generate more refrigerant.

2.8 Research on ARS Performance

During the last few decades, more research has been focused to improve the operation of the ARS. ARS can rely on using cheap and renewable energy sources for operation including solar and biomass energy. Also, the working media required for ARS are environmentally good compared with the traditional vapour compression system fluids (Herold *et al.*, 1996). Yoon and Kwon (1999) reported the performance features of novel working media to replace H_2O/LiBr. They carried out system simulation study to determine the best design and working parameters of ARS. They carried out their analysis (thermodynamically) focusing on the effect of heat exchangers on the system COP. Other researchers (Dincer and Dost, 1996; Sun, 1997; Romero *et al.*, 2000) evaluated and compared the system COP by performing energy analysis for the different system various components. Moreover, Srikhirin *et al.* (2003) reviewed the various ARS technologies, configurations, designs, and working fluids for enhancing the system performance. In their study, Joudi and Lafta (2001) presented simulation model, based on assumption of steady state condition of ARS, to evaluate the ARS performance when LiBr/H_2O are used as the working fluids of the system.

Bereche *et al.* (2009) conducted thermoeconomic analysis of ARS. They considered single- and double-effect systems for their analysis. Based on the exergetic analysis, the single-effect system is appropriate for the cogeneration work or when waste heat at decreased temperature is available with temperature ranged from 80 to 120°C. But, the double effect shows better exergetic analysis while they require increased temperatures to operate. Moreover, Dorgan *et al.* (1995) reported that the COP of the single-effect ARS can be in the range of 0.6 to 0.7. However, Herold *et al.* (1996) reported that the double-effect can have COP in the range 1.0 to 1.2, which make it more feasible compared with the single-effect, according to the operating parameters of the system.

In 2007, Kaynakli and Kilic conducted thermodynamic analysis of the operating factors of single-effect ARS. In order to validate their predictions, Kaynakli and Kilic (2007) made a comparison with data available in the literature. The others reported an increase of the single-effect COP with the generator temperature at two different evaporator temperatures as shown in Figure 2.11. They reported good agreement with the experimental values reported in the literature. As shown in Figure 2.11, the using of

higher evaporator temperature increased the COP of the system at any generator temperature used in their simulation.

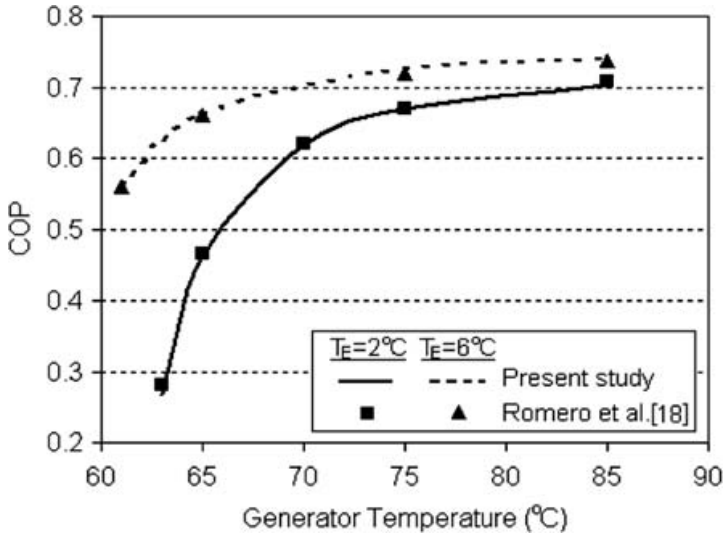

Figure 2.11 Comparison of COP values (Kaynakli and Kilic, 2007)

Considerable number of research performed on ARS system performance considered either single-effect or double-effect system for the analysis. Few studies compared the COP of the system for the two designs but not at the same generator temperature. Therefore, the comparison seems would be more reasonable if conducted on the two systems using exactly the same operating parameters, which is the target of this study.

Chapter III

Modelling and Simulation of Absorption Refrigeration System

3.1 Introduction

Cooling is very essential for different aspects of modern life. One of the important applications is to use the cooling systems for the air conditioning applications. With the increases prices of oil, alternative means are investigated to decrease the required needs of thermal energy. One of the possible means is to use the solar energy for the cooling purposes. The absorption refrigeration system uses thermal energy at the generator unit to have cooling at the evaporator unit. These systems are already available in the market but researches on improving their performance are still needed. In order to investigate the performance of the ARS, it can be tested experimentally. Alternatively, simulation studies can be performed to allow more chances to test more variables with reduced testing costs.

In this chapter simulation procedures to evaluate the ARS performance are presented. In order to compare the performance of various designs, single- and double-effect ARS are considered for simulation. In each system, the temperature in the evaporator unit is varied to allow more cooling. Also, the temperatures in the generator, at which the thermal energy are supplied, are changed. The effects of these parameters on the performance of the system are simulated. Moreover, the control on the mixing process needed at different units of the ARS is presented. Simulink is used to build the control system and the simulation procedures are explained.

The first part of this chapter describes the solar cooling system using ARS. The simulation procedures for both the single- and double-effect ARS are then presented. The last part of this chapter presents the Simulink modelling procedures to evaluate the response time while charging the storage tank with thermal energy.

3.2 System Description

The system considered in this study comprised different sub-systems. Figure 3.1 shows schematic diagram of solar cooling system employing single-effect ARS.

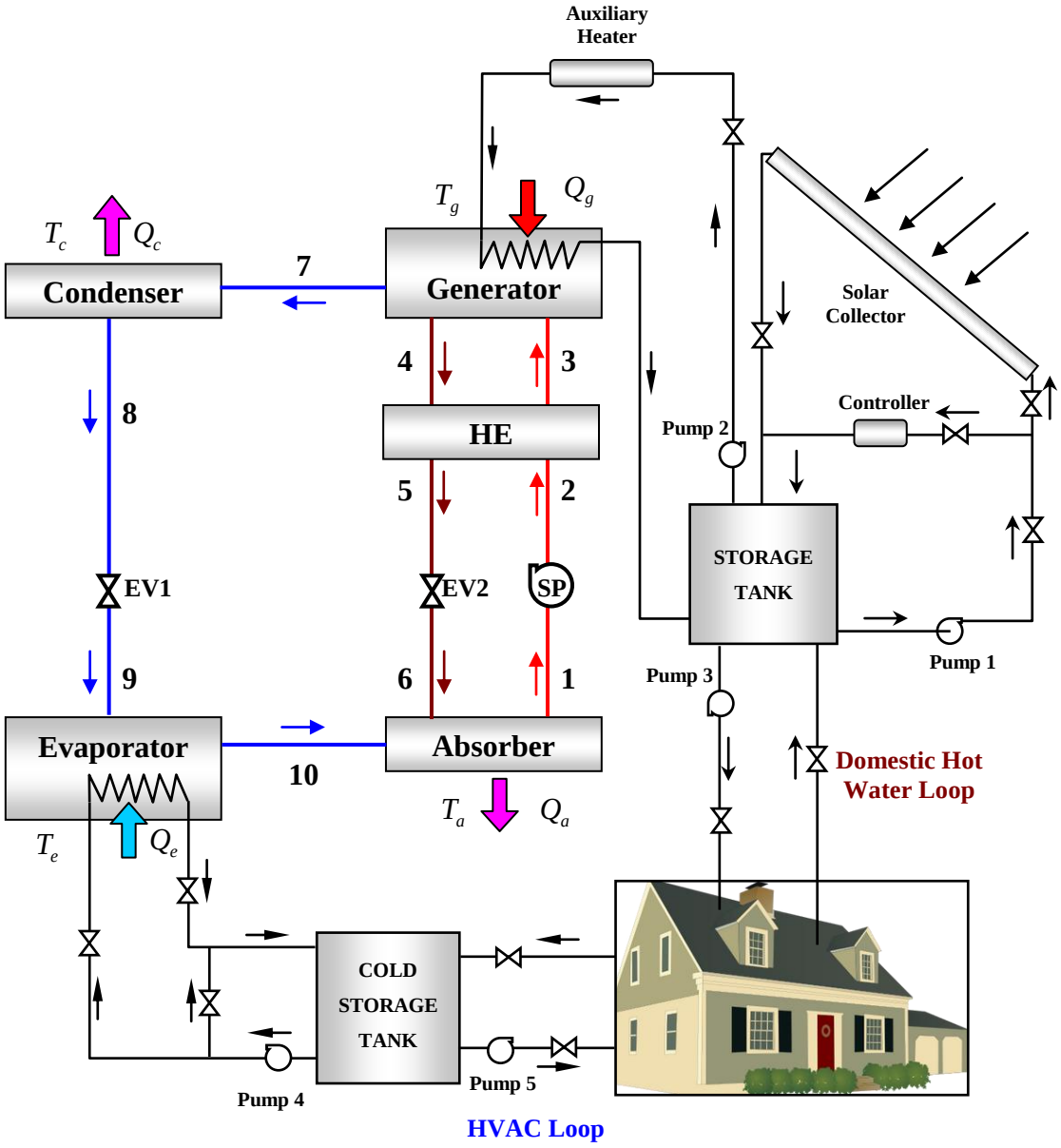

Figure 3.1 Schematic diagram of solar cooling using single-effect ARS

As shown in Figure 3.1, the system utilises solar energy in the form of thermal and electrical energies to fulfil the system needs. These energies are needed to operate the system pumps, provide thermal energy to the generator unit of the ARS and to satisfy the domestic hot water needs. The system in Figure 3.1 comprises several sub-systems. These include solar heating system, absorption refrigeration system, cold storage system and PVC solar system (not shown in Figure 3.1).

3.2.1 Solar Heating Sub-system

The solar heating system comprises sets of solar collectors used to heat water, which is stored water in storage tank. The stored hot water is used to fulfil the domestic hot water needs and to operate the generator unit of the ARS. In this system, pump (1) is used to circulate the water via a valve to the solar collectors. While water is flowing through the collectors, it absorbs thermal energy so its temperature will increase. The heated water is to be directed to the storage tank via control valve. In the system, there is a bypass line equipped with controller and control valve. Based on the outlet water temperature of the solar collectors, the controller allows the water to flow from the storage tank through the collectors for further heating. If the solar radiation intensity is not sufficient to further increase the water temperature, the controller and valves change the flow direction to the bypass line and closes the pass through the collectors, especially during night time operation.

3.2.2 Generator Unit Heating System

Hot water system is used to provide the generator of the ARS with thermal energy. In this stem, pump 2 circulates the hot water from the storage tank to the generator unit via control valve. An auxiliary heater unit is used on this flow line. This heater is used to control the hot water temperature needed for the generator unit. Indirect heat exchanger is used to exchange the thermal energy between the hot water and the working medium of the ARS. Solar panels are used to convert solar energy into electricity and store it in batteries. This electricity can be used for the auxiliary heaters to control the temperature of the generator unit.

3.2.3 Absorption Refrigeration System

Absorption refrigeration system (ARS) does not use mechanical power for operation. It uses what is also called thermal pumping to transfer the heat. It operates with a pair of working fluid, where one fluid acts as the refrigerant and the other fluid acts as the absorbent. In this study, Lithium Bromide (LiBr)/water system is used in which water is the refrigerant and LiBr solution is the absorbent.

Single-effect and double-effect ARS are considered in this study. The single effect comprises absorber, generator, evaporator, condenser, and solution heat exchanger. It also comprised expansion valves on both the refrigerant and the strong solution lines in addition to the weak solution pump. In typical ARS, the solution containing higher

percentage of LiBr is called strong solution whereas the weak solution is the solution containing lower percentage of LiBr.

As shown in Figure 3.1, the weak solution at condition (1) leaves the absorber as a saturated mixture and is pumped towards the generator where heat is supplied by the solar heating system. The operating temperatures are controlled by the working fluid properties and the operation of the system components. The temperature inside the generator unit is the highest temperature in the system. As the weak solution is pumped to condition (2), it flows through the heat exchanger (HE) so that it will be heated to reach condition (3). The heated weal solution then enters the generator unit. The HE is used to reduce the needed amount of thermal energy in the generator unit. Inside the generator unit, thermal energy is transferred to the weak solution so that part of its water is vaporised with condition (7) and flows to the condenser. Therefore, the concentration of the LiBr in the remaining solution increases so that strong solution will leave the generator at higher pressure and condition (4). This solution will be hot enough to heat the weak solution in the HE and leave the HE at condition (5). This solution then flows through the expansion valve so its pressure is decreased to condition (6) before it enters the absorber. When the strong solution enters the absorber unit, it absorbs the water vapour coming out of the evaporator at condition (10). With the vapour absorption process, the strong solution will be converted to the weak solution at condition (1) to exit from the absorber, and so on.

The water vapour (refrigerant) comes out of the generator unit at condition (7) is in the form of superheated steam of generator temperature and condenser pressure. This steam flows through the condenser to be fully condensed into saturated water at condition (8). The condensation process takes place at constant condenser pressure. The saturated water is then flows through the expansion valve to be throttled to the lower pressure. It then becomes water-vapour mixture at condition (9). This mixture enters the evaporator so that its liquid part absorbs thermal energy to provide cooling. Accordingly the liquid part of the mixture will evaporate so that the exit of the evaporator at condition (10) will be fully saturated vapour. This vapour enters the absorber to be absorbed by the strong solution and, so on.

3.2.4 Chilled water system for HVAC Loop

As the case of storing the hot water, it is also essential to store chilled water in this system. It should be noted that the heat loss from the hot water storage tank will be considerably higher than the heat transfer to the chilled water tank because of the decreased temperature difference with respect to the surrounding temperature. It is also important to install the chilled water storage tank closer to the air conditioned area in order to minimise the heat gain by the storage tank.

3.3 Single-Effect ARS Modelling

The single-effect system components are shown in Figure 3.2. The main components of the system are the absorber, generator, condenser, evaporator and the heat exchanger.

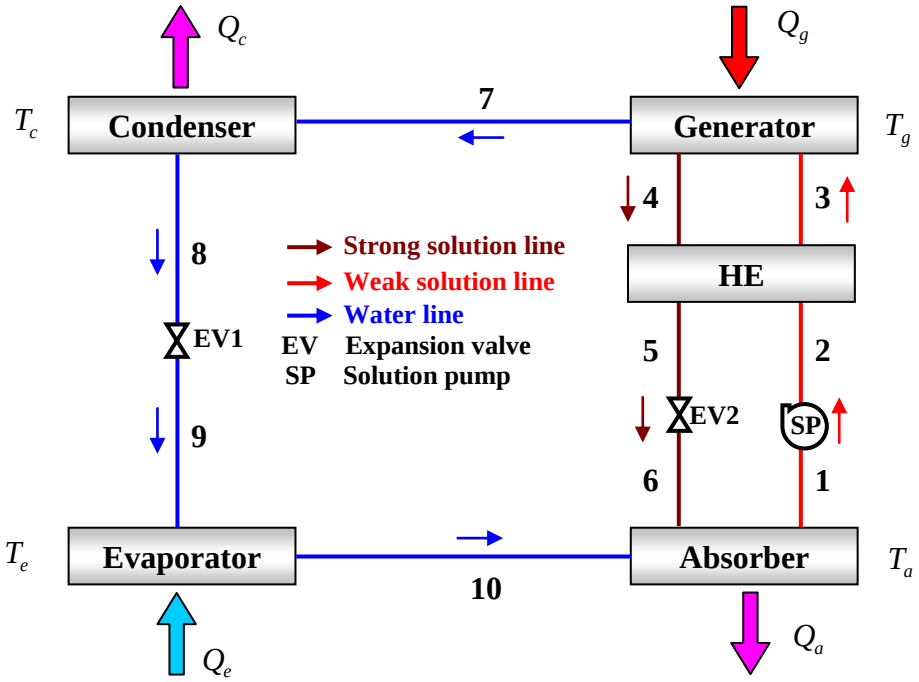

Figure 3.2 Schematic diagram of single-effect ARS components

3.3.1 Design Parameters

As shown in Figure 3.2, the system operates between two pressure limits namely high pressure (in the generator and condenser) and low pressure (in the evaporator and absorber). Since phase change process takes place inside the condenser, the condenser temperature determines the higher pressure of the system. Since condenser and absorber reject heat to the surroundings, therefore both can operate at the same temperature.

Accordingly, the first assumption is to assume condenser temperature (T_c) at 40°C which equals the absorber temperature (T_a).

Since the ARS considered for simulation uses LiBr/H_2O, the refrigerant fluid of the system will be the water vapour. Therefore, the evaporator temperature will be limited by the water freezing temperature. Therefore, the evaporator temperature (T_e) must be higher than zero. Accordingly, the system performance will be simulated at different evaporator temperature of 4, 5, 6 and 7°C.

For solar cooling system, the thermal energy source is solar collector sets. However, any solar collector type receives variable amounts of solar radiations. The operating nature of the solar system is then dynamic as there is continuous change of the incident solar radiation and the surrounding atmospheric temperature. There is variation of these quantities during the day (i.e. it has hourly values) and based on the day of the year (termed average daily values). Meanwhile, the ARS needs thermal energy supply at nearly fixed temperature. Consequently, storage tank is used with the solar cooling system to store the collected thermal energy (dynamic in nature) to enable steady supply of thermal energy to the ARS. For the performance evaluation of the ARS, the generator unit temperature (T_g) will be changed as 100, 110, 120, 130, 140, and 150°C.

In order to improve the performance of the system, HE is used to allow heating of the weak solution by the hot strong solution coming out of the generator. This heat exchange process will decrease the amount of thermal energy to be supplied to the ARS in the generator. In the heat exchanger, the heat exchange process will take place indirectly so that no contact between the two solutions can happen. Since the thermal energy exchange takes place through surfaces, the heat transfer resistance is high. Therefore, the effectiveness of the HE can be assumed as 0.7.

During heat exchange inside the HE, the strong solution out from the generator will be cooled. Therefore, to avoid solution crystallisation, careful attention should be paid to the solution temperature after cooling. So, the minimum solution temperature after cooling can be assumed 50°C (T_5=50°C). The cooling capacity is assumed 35.17 kW.

3.3.1.1 Mass flow rate at each branch

As shown in Figure 3.2, the single-effect system comprises three main branches (flow streams). The mass flow rate in each branch is:

$$\dot{m}_1 = \dot{m}_2 = \dot{m}_3 = m_I \qquad \text{Weak solution} \qquad (3.1)$$

$$\dot{m}_4 = \dot{m}_5 = \dot{m}_6 = m_{II} \qquad \text{Strong solution} \qquad (3.2)$$

$$\dot{m}_7 = \dot{m}_8 = \dot{m}_9 = \dot{m}_{10} = m_{III} \qquad \text{Water and vapour} \qquad (3.3)$$

3.3.1.2 Solution concentration

The concentration of the solution is defined as the mass of Lithium Bromide (LiBr) divided by the mass of the solution i.e. the mass of LiBr and water. Therefore, the solution concentration is defined as:

$$x = \frac{m_{LiBr}}{m_{LiBr} + m_{water}} \qquad (3.4)$$

The concentration changes if water is added or removed to or from the solution. However, heating or cooling processes (without mass exchange) will not affect the concentration. The LiBr concentration in each branch is:

$$x_1 = x_2 = x_3 = x_I \qquad \text{Weak solution} \qquad (3.5)$$

$$x_4 = x_5 = x_6 = x_{II} \qquad \text{Strong solution} \qquad (3.6)$$

$$x_7 = x_8 = x_9 = x_{10} = x_{III} = Zero \qquad \text{Water and vapour (no LiBr)} \qquad (3.7)$$

The concentration at each solution state varies with solution temperature and pressure (pressure can be replaced by its corresponding saturation temperature of the refrigerant). To obtain solution concentration ASHRAE (2001) proposed the following equation:

$$T_{sat)p} = \left(\sum_{n=0}^{n=3} B_n \; x^n \right) + \left(T_{sol}\right) \left(\sum_{n=0}^{n=3} A_n \; x^n \right) \qquad (3.8)$$

where

$\left(T_{sat)p}\right)$ is the saturation temperature of the refrigerant at solution pressure.

$\left(T_{sol}\right)$ is the solution temperature.

It should be noted that Equation (3.8) is valid (ASHRAE, 2001) in the range:

Concentration: $45 < x < 70\,\%$.

Saturation temperature: $-15 < T_{sol} < 110\,°\text{C}$.

Solution temperature: $5 < T_{sol} < 175\,°\text{C}$.

The coefficients A_n and B_n can be obtained from ASHRAE (2001):

$$\begin{aligned} A_o &= -2.00755 & B_o &= 124.937 \\ A_1 &= -0.16976 & B_1 &= -7.71649 \\ A_2 &= -3.133362E^{-3} & B_2 &= 0.152286 \\ A_3 &= 1.97668E^{-5} & B_3 &= -7.9509E^{-4} \end{aligned} \tag{3.9}$$

3.3.1.3 Solution enthalpy

The enthalpy at any solution state varies with solution temperature and concentration. In order to evaluate the enthalpy of the solution, ASHRAE (2001) proposed the following equation:

$$h = \left(\sum_{n=0}^{n=4} A_n\ x^n\right) + \left(T_{sol}\right)\left(\sum_{n=0}^{n=4} B_n\ x^n\right) + \left(T_{sol}\right)^2\left(\sum_{n=0}^{n=4} C_n\ x^n\right) \tag{3.10}$$

It should be noted that Equation (3.10) is valid (ASHRAE, 2001) in the range:

Concentration: $40 < x < 70\,\%$

Solution temperature: $15 < T_{sol} < 165\,°\text{C}$.

The coefficients A_n, B_n and C_n can be obtained from ASHRAE (2001):

$$\begin{aligned} A_o &= -2024.33 & B_o &= 18.2829 & C_o &= -3.7008214E^{-2} \\ A_1 &= 163.309 & B_1 &= -1.1691757 & C_1 &= 2.8877666E^{-3} \\ A_2 &= -4.88161 & B_2 &= 3.248041E^{-2} & C_2 &= -8.1313015E^{-5} \\ A_3 &= 6.302948E^{-2} & B_3 &= -4.034184E^{-4} & C_3 &= 9.9116628E^{-7} \\ A_4 &= -2.913705E^{-4} & B_4 &= 1.8520569E^{-6} & C_4 &= -4.4441207E^{-9} \end{aligned} \tag{3.11}$$

3.3.2 Mass and Energy Balance at Each component

3.3.2.1 Evaporator balance

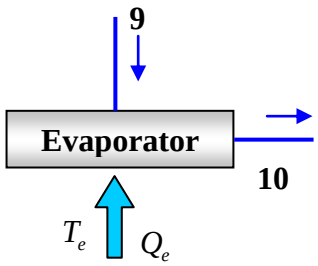

Energy balance

$$\dot{Q}_e + \dot{m}_9 \, h_9 = \dot{m}_{10} \, h_{10}$$

$$Q_e + m_{III} \, h_9 = m_{III} \, h_{10} \tag{3.12}$$

3.3.2.2 Absorber mass and energy balance

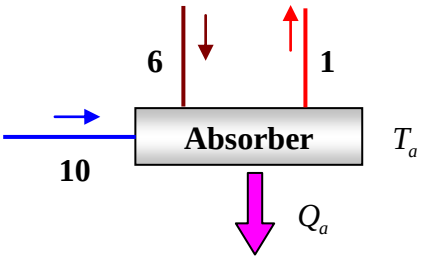

Mass balance

$$\dot{m}_1 = \dot{m}_6 + \dot{m}_{10}$$

$$m_I = m_{II} + m_{III} \tag{3.13}$$

Partial mass balance

Partial mass balance means the balance of the LiBr mass. Therefore:

$$\dot{m}_1 \, x_1 = \dot{m}_6 \, x_6 + \dot{m}_{10} \, x_{10}$$

$$m_I \, x_I = m_{II} \, x_{II} + m_{III} \, x_{III}$$

But, the concentration of the water and vapour is zero. Then, $x_{III} = 0.0$.

$$m_I \, x_I = m_{II} \, x_{II} \tag{3.14}$$

Energy balance:

$$\dot{Q}_a + \dot{m}_1 \, h_1 = \dot{m}_6 \, h_6 + \dot{m}_{10} \, h_{10}$$

$$Q_a + m_I \, h_1 = m_{II} \, h_6 + m_{III} \, h_{10} \tag{3.15}$$

3.3.2.3 Generator mass and energy balance

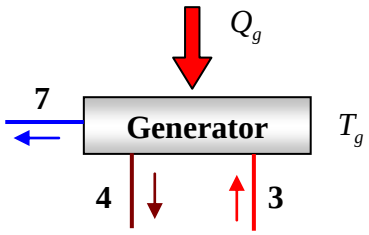

Mass balance

$$\dot{m}_3 = \dot{m}_4 + \dot{m}_7$$

$$m_I = m_{II} + m_{III}$$

Partial mass balance

$$\dot{m}_3\ x_3 = \dot{m}_4\ x_4 + \dot{m}_7\ x_7$$

$$m_I\ x_I = m_{II}\ x_{II} + m_{III}\ x_{III}$$

$$m_I\ x_I = m_{II}\ x_{II}$$

Energy balance

$$Q_g + \dot{m}_3\ h_3 = \dot{m}_4\ h_4 + \dot{m}_7\ h_7$$

$$Q_g + m_I\ h_3 = m_{II}\ h_4 + m_{III}\ h_7 \tag{3.16}$$

3.3.2.4 Condenser balance

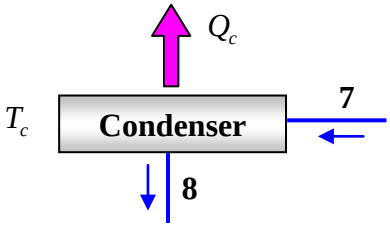

Energy balance

$$Q_c + \dot{m}_7\ h_7 = \dot{m}_8\ h_8$$

$$Q_c + m_{III}\ h_7 = m_{III}\ h_8 \tag{3.17}$$

3.3.2.5 Heat Exchanger balance

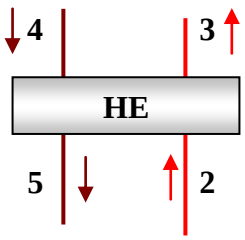

The heat exchanger effectiveness (ε) is the ratio between the actual heat transfers to the cold fluid divided by the heat transfer from the hot fluid. So:

$$\varepsilon = \frac{m_I \left(h_3 - h_2\right)}{m_{II} \left(h_4 - h_5\right)}, \text{ or } m_I \left(h_3 - h_2\right) = \left(\varepsilon\right) m_{II} \left(h_4 - h_5\right)$$

Then:

$$h_3 = \left[\left(\varepsilon\right) \frac{m_{II}}{m_I} \left(h_4 - h_5\right) \right] + h_2 \tag{3.18}$$

3.3.3 System Performance and Mass Ratio

The performance of the system can be evaluated using the coefficient of performance (COP) which is the ratio of the useful heat (cooling load at the evaporator) divided by the required energy (heat added at the generator). Then:

$$COP = \frac{Q_e}{Q_g} \tag{3.19}$$

In order to size the solution branches, mass ratio of each solution branch is to be referred to the required mass flow rate of the refrigerant. Therefore, weak solution mass ratio and the strong solution mass ratio become:

$$R_{ws} = \frac{m_I}{m_{III}} \tag{3.20.a}$$

$$R_{ss} = \frac{m_{II}}{m_{III}} \tag{3.20.b}$$

3.4 Double-Effect ARS Modelling

Series double-effect ARS is used for simulation in this study. The main components of the system are shown in Figure 3.3. These include absorber, generator (I), generator (II), condenser, evaporator and heat exchangers (I) and (II).

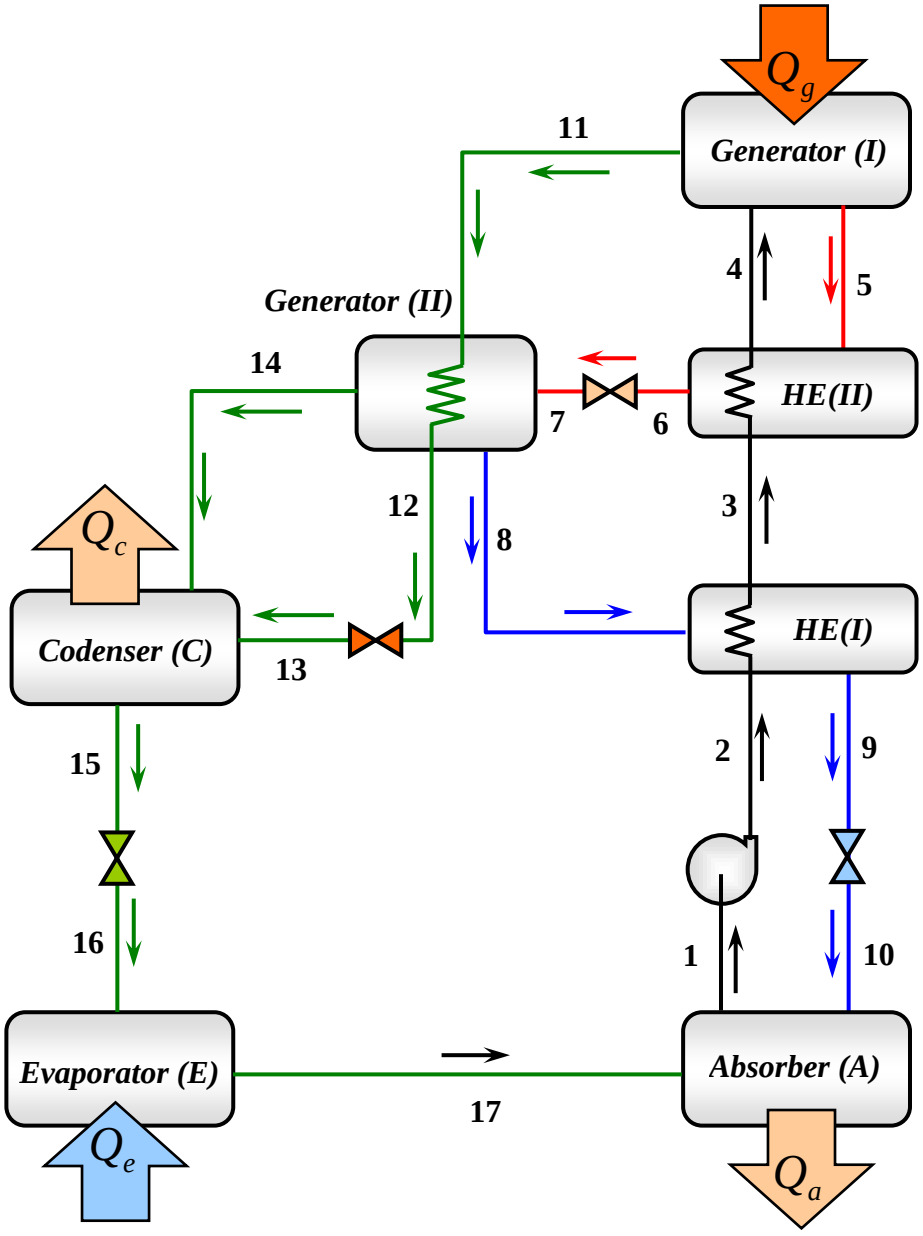

Figure 3.3 Schematic diagram of series double-effect ARS

3.4.1 Design Parameters

As shown in Figure 3.3, the system operates using three pressure levels. These pressures are maximum pressure (inside generator (I) and HE-II), intermediate pressure (inside generator (II), condenser and HE-I) and minimum pressure (inside the evaporator and

absorber). Phase change process takes place inside the evaporator and condenser units. Therefore, the temperatures inside these units determine the values of the minimum and the intermediate pressure levels. Since condenser and absorber reject thermal energy to the surroundings, these units operate at same temperature. So, the temperature in the condenser (T_c) is assumed 40°C which is equal to the absorber temperature (T_a).

Since the system uses LiBr/H_2O as working fluids, the refrigerant fluid is water vapour. Therefore, the evaporator temperature will be limited by water freezing temperature. Therefore, evaporator temperature (T_e) must be higher than zero. For performance simulation of the series double-effect ARS, the generator and evaporator temperatures (T_g & T_e) will be varied. The effectiveness of each heat exchanger is assumed 0.7. The minimum strong solution temperature after cooling is assumed 50°C (T_9=50°C). The cooling capacity is assumed as 35.17 kW.

3.4.1.1 Mass flow rate at each branch

The series double-effect ARS shown in Figure 3.3 has five branches. The mass flow rate in each branch is:

$$\dot{m}_1 = \dot{m}_2 = \dot{m}_3 = \dot{m}_4 = m_I \quad \text{Weak solution} \quad (3.21)$$

$$\dot{m}_5 = \dot{m}_6 = \dot{m}_7 = m_A \quad \text{Intermediate solution} \quad (3.22)$$

$$\dot{m}_8 = \dot{m}_9 = \dot{m}_{10} = m_{II} \quad \text{Strong solution} \quad (3.23)$$

$$\dot{m}_{11} = \dot{m}_{12} = \dot{m}_{13} = m_B \quad \text{Refrigerant line I} \quad (3.24)$$

$$\dot{m}_{15} = \dot{m}_{16} = \dot{m}_{17} = m_{III} \quad \text{Refrigerant line} \quad (3.25)$$

3.4.1.2 Solution concentration

The LiBr concentration in each branch is:

$$x_1 = x_2 = x_3 = x_4 = x_I \quad \text{Weak solution} \quad (3.26)$$

$$x_5 = x_6 = x_7 = x_A \quad \text{Intermediate solution} \quad (3.27)$$

$$x_8 = x_9 = x_{10} = x_{II} \quad \text{Strong solution} \quad (3.28)$$

$$x_{11} = x_{12} = x_{13} = x_{14} = x_{15} = x_{16} = x_{17} = x_{III} = 0 \quad \text{Water and vapour} \quad (3.29)$$

3.4.2 Mass and Energy Balance at Each component

3.4.2.1 Evaporator energy balance

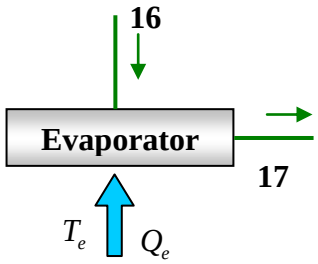

Energy balance

$$Q_e + \dot{m}_{16}\, h_{16} = \dot{m}_{17}\, h_{17}$$

$$Q_e + m_{III}\; h_{16} = m_{III}\; h_{17} \tag{3.30}$$

3.4.2.2 Absorber mass, partial mass and energy balance

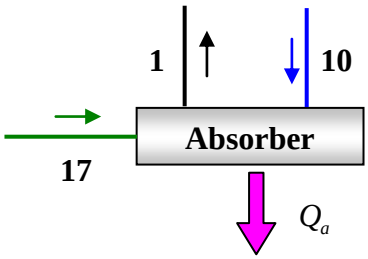

Mass balance

$$\dot{m}_1 = \dot{m}_{10} + \dot{m}_{17}$$

$$m_I = m_{II} + m_{III} \tag{3.31}$$

Partial mass balance

$$\dot{m}_1\; x_1 = \dot{m}_{10}\; x_{10} + \dot{m}_{17}\; x_{17}$$

$$m_I\; x_I = m_{II}\; x_{II} + m_{III}\; x_{III}$$

But, the concentration of the water and vapour is zero ($x_{III} = 0.0$), then:

$$m_I\; x_I = m_{II}\; x_{II} \tag{3.32}$$

Energy balance:

$$Q_a + \dot{m}_1\; h_1 = \dot{m}_{10}\; h_{10} + \dot{m}_{17}\; h_{17}$$

$$Q_a + m_I\; h_1 = m_{II}\; h_{10} + m_{III}\; h_{17} \tag{3.33}$$

3.3.2.3 Mass, partial mass and energy balance of control volume

The control volume subjected to analysis contains generator (II), heat exchanger (I) and heat exchange (II).

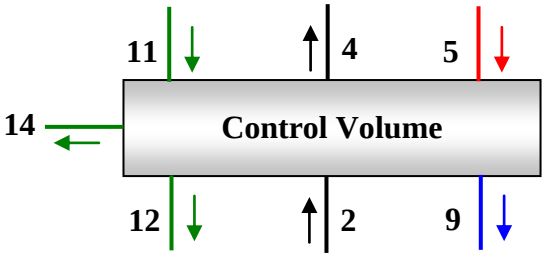

Mass balance

$$\dot{m}_2+\dot{m}_5+\dot{m}_{11}=\dot{m}_4+\dot{m}_9+\dot{m}_{11}+\dot{m}_{14}$$

$$m_I+m_A+m_B=m_I+m_{II}+m_B+m_{14}$$

$$m_A=m_{II}+m_{14} \tag{3.34}$$

Partial mass balance

$$\dot{m}_2x_2+\dot{m}_5x_5+\dot{m}_{11}x_{11}=\dot{m}_4x_4+\dot{m}_9x_9+\dot{m}_{12}x_{12}+\dot{m}_{14}x_{14}$$

$$m_Ix_I+m_Ax_A+0=m_Ix_I+m_{II}x_{II}+0+0$$

$$m_Ax_A=m_{II}x_{II} \tag{3.35}$$

Energy balance

$$\dot{m}_2h_2+\dot{m}_5h_5+\dot{m}_{11}h_{11}=\dot{m}_4h_4+\dot{m}_9h_9+\dot{m}_{12}h_{11}+\dot{m}_{14}h_{14}$$

$$m_Ih_2+m_Ah_5+m_Bh_{11}=m_Ih_4+m_{II}h_9+m_Bh_{12}+m_{14}h_{14} \tag{3.36}$$

3.4.2.4 Generator (I) mass, partial mass and energy balance

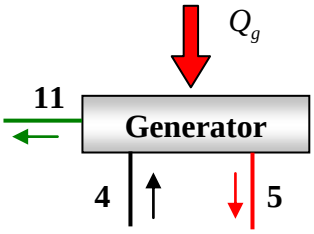

Mass balance

$$\dot{m}_4=\dot{m}_5+\dot{m}_{11}$$

$$m_I = m_A + m_B \tag{3.37}$$

Partial mass balance

$$\dot{m}_4\ x_4 = \dot{m}_5\ x_5 + \dot{m}_{11}\ x_{11}$$

$$m_I\ x_I = m_A\ x_A + m_B\ x_B$$

$$m_I\ x_I = m_A\ x_A \tag{3.38}$$

Energy balance

$$Q_g + \dot{m}_4\ h_4 = \dot{m}_5\ h_5 + \dot{m}_{11}\ h_{11}$$

$$Q_g + m_I\ h_4 = m_A\ h_5 + m_B\ h_7 \tag{3.39}$$

3.4.2.5 Condenser energy balance

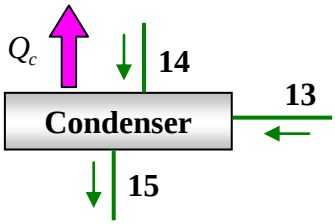

Energy balance

$$Q_c + \dot{m}_{15}\ h_{15} = \dot{m}_{13}\ h_{13} + \dot{m}_{14}\ h_{14}$$

$$Q_c + m_{III}\ h_{15} = m_B\ h_{13} + m_{14}\ h_{14} \tag{3.40}$$

3.4.2.6 Generator (II) mass, partial mass and energy balance

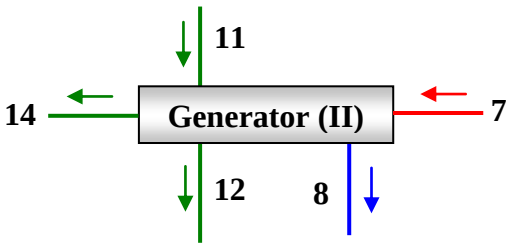

Mass balance

$$\dot{m}_7 + \dot{m}_{11} = \dot{m}_8 + \dot{m}_{12} + \dot{m}_{14}$$

$$m_A + m_B = m_{II} + m_B + m_{14} \tag{3.41}$$

Partial mass balance

$$\dot{m}_7\ x_7 + \dot{m}_{11}\ x_{11} = \dot{m}_8\ x_8 + \dot{m}_{12}\ x_{12} + \dot{m}_{14}\ x_{14}$$

$$m_A\ x_A + 0 = m_{II}\ x_{II} + 0 + 0$$

$$m_A\ x_A = m_{II}\ x_{II} \tag{3.42}$$

Energy balance

$$\dot{m}_7\ h_7 + \dot{m}_{11}\ h_{11} = \dot{m}_8\ h_8 + \dot{m}_{12}\ h_{12} + \dot{m}_{14}\ h_{14}$$

$$m_A\ h_7 + m_B\ h_{11} = m_{II}\ h_8 + m_B\ h_{12} + m_{14}\ h_{14} \tag{3.43}$$

3.4.2.7 Heat Exchanger (I) energy balance

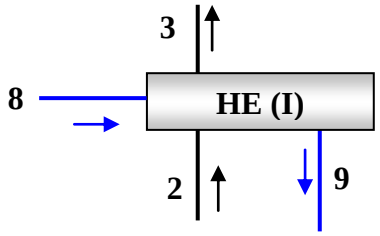

The heat exchanger effectiveness (ε) is expressed as:

$$\varepsilon = \frac{m_I\ (h_3 - h_2)}{m_{II}\ (h_8 - h_9)}, \text{ or } m_I\ (h_3 - h_2) = (\varepsilon)\, m_{II}\ (h_8 - h_9)$$

Then:

$$h_3 = \left[(\varepsilon) \frac{m_{II}}{m_I} (h_8 - h_9) \right] + h_2 \tag{3.44}$$

3.4.2.8 Heat Exchanger (II) energy balance

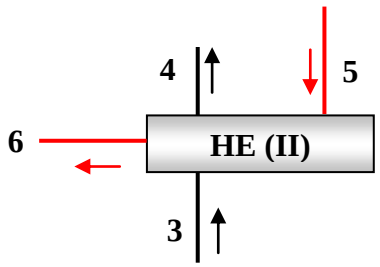

The heat exchanger effectiveness (ε) is expressed as:

$$\varepsilon = \frac{m_I\ (h_4 - h_3)}{m_A\ (h_5 - h_6)}, \text{ or } m_I\ (h_4 - h_3) = (\varepsilon)\, m_A\ (h_5 - h_6)$$

Then:

$$h_4 = \left[(\varepsilon) \frac{m_A}{m_I} (h_5 - h_6) \right] + h_3 \tag{3.45}$$

3.4.3 System Performance and Mass Ratio

The coefficient of performance (COP) is evaluated from:

$$COP = \frac{Q_e}{Q_g} \tag{3.46}$$

The weak solution mass ratio is evaluated from:

$$R_{ws} = \frac{m_I}{m_{III}} \tag{3.47}$$

This gives the ratio between the mass flow rate of the weak solution needed per unit refrigerant mass flow rate of the system.

The strong solution mass ratio is evaluated from:

$$R_{ss} = \frac{m_{II}}{m_{III}} \tag{3.48}$$

This gives the ratio between the mass flow rate of the strong solution needed per unit refrigerant mass flow rate of the system.

The intermediate solution mass ratio is evaluated from:

$$R_{is} = \frac{m_A}{m_{III}} \tag{3.49}$$

This gives the ratio between the mass flow rate of the intermediate solution needed per unit refrigerant mass flow rate of the system.

The percentage of refrigerant mass flow rate generated in generator-I to the total mass flow rate of refrigerant of the system is evaluated from:

$$R_{gi} = \frac{m_{14}}{m_{III}} \times 100 \tag{3.50}$$

The percentage of refrigerant mass flow rate generated in generator-II to the total mass flow rate of refrigerant of the system is evaluated from:

$$R_{gii} = \frac{m_{14}}{m_{III}} \times 100 \tag{3.50}$$

3.5 Control of the Storage Tank Temperature

3.5.1 Description of the Process

It is essential for the efficient operation of the ARS, to ensure that the generator unit is working at nearly constant temperature. The heat source for the generator is the hot water at the specific generator temperature delivered from the storage tank unit of the solar system. Accordingly, the temperature of the water inside the storage tank should be as constant as possible. Therefore, the amount of thermal energy supplied to the storage tank (either from solar collectors or from electric heaters) must be controlled to ensure nearly constant storage tank temperature. During the daytime operation, the storage tank is fed with thermal energy from the solar collector. But, during the night operation or insufficient solar intensity, electric heaters are used to supply the storage tank with the thermal energy. In either case, the amount of thermal energy is fed to the storage tank to compensate the energy used by the generator unit of the ARS. Therefore, the control philosophy is to manipulate the amount of thermal energy supplied to the storage tank to keep the storage tank temperature as constant as possible.

3.5.2 Control Goals, Variables and Structure

a) Control goal: The control goal is to ensure that the storage tank temperature is nearly constant while feeding thermal energy to the generator unit of the absorption system.

b) Control variables: (Input variables)

Manipulated input variables: The manipulated input variable is the amount of thermal energy added to the storage tank (Q_a), either from the electric heaters (night operation) or from the solar collector unit (daytime operation). This amount of thermal energy is to be manipulated by changing the control valve settings to change the electric energy to the heater (night operation) or the heating fluid mass flow rate (daytime operation).

Disturbances (non-manipulated) variable: The disturbance of the system is the generator return water temperature (T_b), which comes from the generator to the tank.

c) Control variable (Output variable)

The output variable is the temperature of the storage tank unit.

3.5.3 Modelling the Process

The process of energy exchange in the storage tank is shown in Figure 3.4. The amount of thermal energy supplied to the storage tank (Q_a) will be manipulated to compensate for the thermal energy delivered to the generator unit. For simplification, the storage tank will be assumed perfectly insulated so that the amount of thermal energy loss to the surrounding will be ignored.

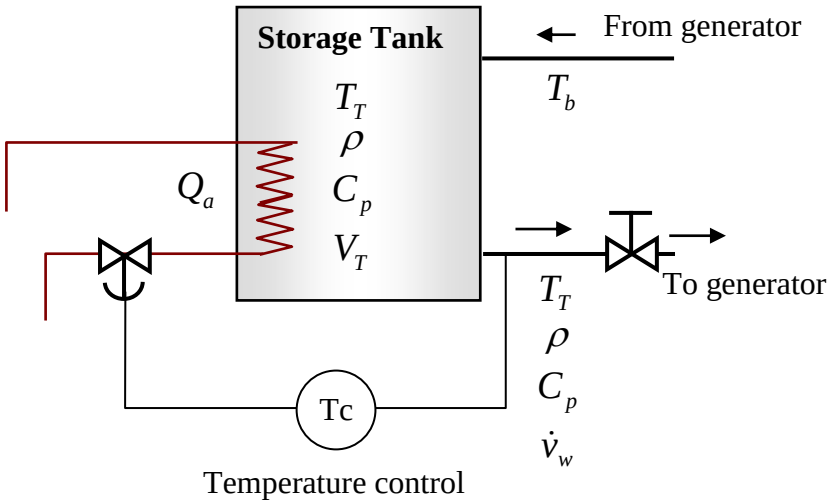

Figure 3.4 Schematic diagram of storage tank energy exchange process

The variables of the system shown in Figure 3.4 are:

T_T = storage tank water temperature = hot water temperature supplying generator, °C

T_b = hot water temperature return from the generator, °C

$\dot{v}_w$ = water volume flow rate to the generator, m^3/s

V_T = storage tank volume, m^3

ρ = water density, kg/m^3

C_p = water specific heat, J/kg K

Q_a = thermal energy supplied to the storage tank, W

Applying the first law of thermodynamics to the system:

$$\begin{bmatrix}\text{Time rate of energy}\\ \text{change inside the tank}\end{bmatrix}=\begin{bmatrix}\text{Net enrgy flow into}\\ \text{the tank}\end{bmatrix}-\begin{bmatrix}\text{Net enrgy flow from}\\ \text{the tank}\end{bmatrix} \quad (3.51)$$

Therefore,

$$\left(\rho\, C_p\, V_T\right)\frac{dT_T}{dt} = Q_a - \rho\, C_p\, \dot{v}_w\left(T_T - T_b\right) - Q_{loss} \tag{3.52}$$

Assumptions:

- $\rho = 1000$ kg/m^3
- $C_p = 4200$ J/kg K
- $V_T = 1.0$ m^3
- $\left(\Delta T\right)_g = 10$ °C = temperature difference across the generator unit
- $Q_{loss} = 0$
- $Q_g = 80$ kW = 80,000 W = design load of the generator unit

The generator load can be expressed as $Q_g = \rho\, \dot{v}_w\, C_p\, \left(\Delta T\right)_g$, so:

$80000 = 1000 \times \dot{v}_w \times 4200 \times 10$

$\dot{v}_w = 0.0019$ m^3/s, which is the required mass flow rate of water needed as energy carrier fluid to the generator unit

Accordingly, equation (3.52) becomes:

$$\left(\rho\, C_p\, V_T\right)\frac{dT_T}{dt} = Q_a - \rho\, C_p\, \dot{v}_w\left(T_T - T_b\right)$$

$$\left(\rho\, C_p\, V_T\right)\frac{dT_T}{dt} = Q_a - \rho\, C_p\, \dot{v}_w\, T_T + \rho\, C_p\, \dot{v}_w\, T_b$$

$$\left(\rho\, C_p\, V_T\right)\frac{dT_T}{dt} + \rho\, C_p\, \dot{v}_w\, T_T = Q_a + \rho\, C_p\, \dot{v}_w\, T_b$$

Divide both sides by $\left(\rho\, C_p\, \dot{v}_w\right)$:

$$\left(\frac{\rho\, C_p\, V_T}{\rho\, C_p\, \dot{v}_w}\right)\frac{dT_T}{dt} + T_T = \frac{Q_a}{\left(\rho\, C_p\, \dot{v}_w\right)} + T_b$$

$$\left(\frac{V_T}{\dot{v}_w}\right)\frac{dT_T}{dt} + T_T = \frac{Q_a}{\left(\rho\, C_p\, \dot{v}_w\right)} + T_b$$

$$\left(\frac{V_T}{\dot{v}_w}\right)\frac{dT_T}{dt} + T_T = \frac{Q_a}{\left(Q_g / \Delta T\right)} + T_b$$

$$\left(\frac{1.0}{0.0019}\right)\frac{dT_T}{dt} + T_T = \frac{Q_a}{\left(80000/10\right)} + T_b$$

$$(526)\frac{dT_T}{dt} + T_T = \frac{Q_a}{(8000)} + T_b \tag{3.53}$$

Using Laplace Transform:

$$(526)\,S\,T_T(s) + T_T(s) = \frac{Q_a(s)}{(8000)} + T_b(s)$$

Rearrange:

$$(526S+1)T_T(s) = \frac{Q_a(s)}{(8000)} + T_b(s)$$

$$T_T(s) = \left[\frac{(1/8000)}{(526S+1)}\right]Q_a(s) + \left[\frac{1}{(526S+1)}\right]T_b(s) \tag{3.54}$$

3.5.4 Simulation of night time operation

According to Equation (3.54), the open loop block diagram of the system, for the night time operation, is shown in Figure 3.5.

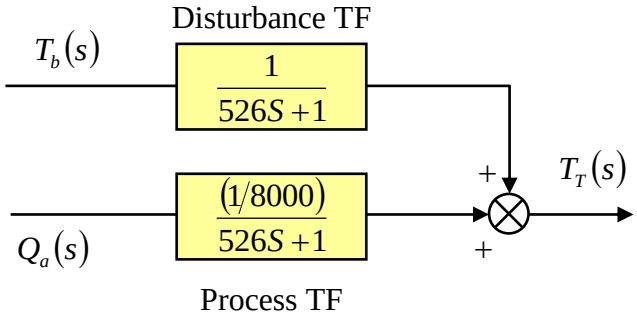

Figure 3.5 Open loop block diagram (night operation)

In order to study the open loop step input response of the system, MatLab Simulink model is built as shown in Figure (3.6). The upper limit of the system input representing the disturbance is set to zero to ignore the disturbance effects.

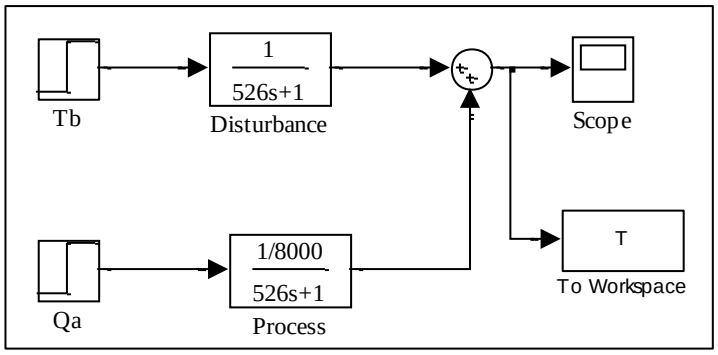

Figure 3.6 Simulink model to study open loop step response

The closed loop response of the system can be obtained using unity feedback. The closed loop block diagram is shown in Figure (3.7).

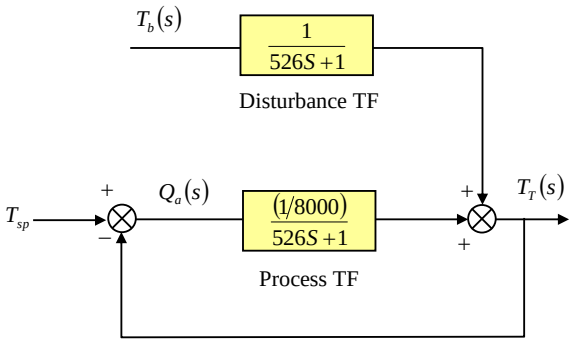

Figure 3.7 Closed loop block diagram

In order to study the step input response of the closed loop, MatLab Simulink model is built as shown in Figure (3.8). In this model, the effect of disturbance on the system response is ignored for simplification of the simulation.

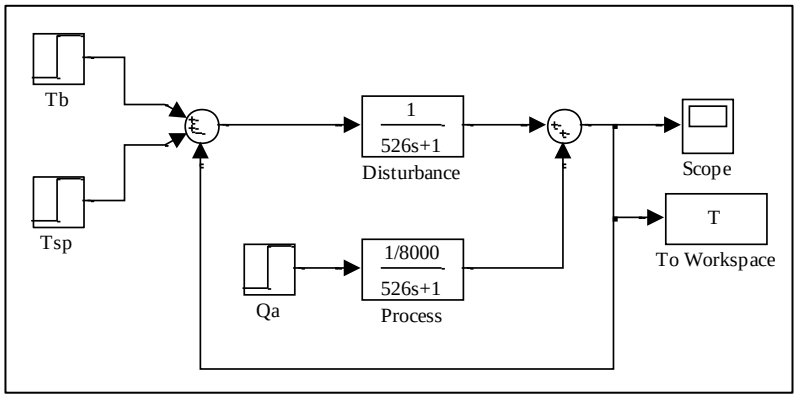

Figure 3.8 Simulink model to study closed loop step response

The response of the system is improved by introducing PID controller, as shown in Figure (3.9). This model is used to study the system response and to evaluate the design values of the controller parameters.

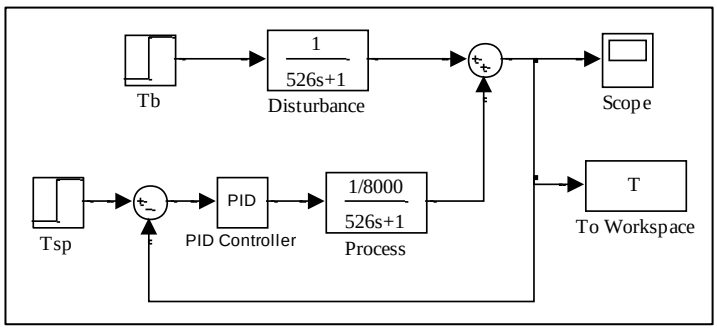

Figure 3.9 Simulink model to study closed loop step response of the controlled system

3.5.5 Simulation of daytime operation

During the daytime operation, the solar system is used to supply thermal energy to the storage tank. However, the solar intensity is changeable according to the day of the year and also from sunrise to sunset. Therefore, the amount of thermal energy to be supplied to the storage tank from the solar system will be time dependent. The solar radiation data for Dubai will be used for the simulation. Radhi (2010) reported the following location data for Dubai city:

- Longitude angle = 55°19' East
- Latitude angle = *l*= 25°15' North = 25.25°
- Elevation above sea = 5 m

The simulation is to be conducted considering the variation of the solar intensity with time during the day. It also will consider the variation of the solar intensity with season. Therefore, following solar data are used (El Chaar and Lamont, 2010):

For summer operation, the solar data for June (21st):

- The sun rising duration during the day = 13.5 hours
- Sunrise time 5:30 am
- Sunset time 7:00 pm

For winter operation, the solar data for December (21st):

- The sun rising duration during the day = 10.5 hours
- Sunrise time 7:30 am
- Sunset time 5:30 pm

The solar heat Q_{solar} is a function of time and is evaluated as recommended by McQuiston *et al.* (2005) as follows:

$$Q_{solar}(t) = I(t)\, A\, \eta \tag{3.55}$$

where:

A = cross sectional area of the solar panel

η = efficiency $\cong 85\% = 0.85$

$I(t)$ = total solar radiation incident on a non-vertical surface

The value of the total solar radiation incident on a non-vertical surface can be evaluated using procedures reported by McQuiston *et al.* (2005). The calculation procedures are

conducted for winter season (on 21st Dec) and for summer season (21st June). The procedures are as follows.

a) Evaluation of total solar radiation

Step (1): Hour angle (h) evaluation:

The solar hour angle is evaluated from:

$$h(t) = (hour - 12{:}00) * 15 \tag{3.56}$$

where hour will change sunrise to sunset. The hour angle before noon time will be negative and reach zero at noon then becomes positive after noon.

Step (2): Solar altitude angle (β) evaluation:

The solar altitude angle is evaluated based on the latitude angle (l), solar declination angle (δ), and the solar hour angle (h) from:

$$\beta(t) = \sin^{-1}(\cos l\ \cos\delta\ \cos h - \sin l\ \sin\delta) \tag{3.57}$$

Step (3): Solar azimuth angle (ϕ) evaluation:

The solar azimuth angle is to be evaluated based on the latitude angle (l), solar declination angle (δ), and the solar hour angle (h) and solar altitude angle (β) from:

$$\emptyset(t) = \cos^{-1}\left(\frac{\sin\delta\ \cos l - \cos\delta\ \sin l\ \cos h}{\cos\beta}\right) \tag{3.58}$$

Step (4): Surface azimuth angle (γ) evaluation:

The surface azimuth angle is to be evaluated based on the solar azimuth angle (ϕ) from:

$$\gamma(t) = |\emptyset - 180| \tag{3.59}$$

It should be noted that γ is always positive.

Step (5): Solar incidence angle (θ) evaluation:

The solar incidence angle is to be evaluated based on surface azimuth angle (γ), solar altitude angle (β) and the surface tilt angle (α) from:

$$\theta(t) = \cos^{-1}(\cos\beta\ \cos\gamma\ \sin\alpha + \sin\beta\ \cos\alpha) \tag{3.60}$$

The surface tilt angle (α) should be changed with season to ensure optimum operation. Duffie and Beckman (1991) reported that for winter operation, the optimum tilt angle is 15 degrees higher than latitude angle (l). In summer, the tilt angle is 15 degrees lower than of the latitude. Reasonable values will be assumed.

Step (6): Normal direct solar radiation evaluation:

The normal direct solar radiation is to be evaluated from:

$$I_{ND}(t) = \left[\frac{A}{e^{\left[\frac{B}{\sin\beta}\right]}}\right] C_N \tag{3.61}$$

where

β is the solar altitude angle

C_N is constant = 1.0 (McQuiston *et al.*, 2005)

A and *B* change monthly (to be obtained from the table given by McQuiston *et al.* (2005), p. 187). The values are:

	Winter	Summer
A (W/m^2)	1204	1092
B	0.141	0.185

Step (7): Normal direct solar radiation evaluation:

The total solar radiation is to be evaluated from:

$I(t) = \left[max(\cos\theta, 0) + C\ F_{ws} + \rho_g\ F_{wg}(\sin\beta + C)\right] I_{ND}$

$$I(t) = \left[max(\cos\theta, 0) + C\ F_{ws} + \rho_g\ F_{wg}(\sin\beta + C)\right] \left(\frac{A}{e^{\left(\frac{B}{\sin\beta}\right)}}\right) \tag{3.62}$$

where

	Winter	Summer
C	0.103	0.137

F_{ws} is the fraction of the energy that leaves the surface and to strike the sky. It can be evaluated as $F_{ws} = 0.5(1 + \cos\alpha)$

F_{wg} is the fraction of the energy that leaves the surface to strike the ground. It can be evaluated as $F_{wg} = 0.5(1 - \cos\alpha)$

ρ_g is the reflectance of the ground level = constant = 0.33

b) Values of total solar radiation

	Winter (21st Dec)	Summer (21st June)
Daylight duration (hour)	10.5	13.5
Sunrise time	7:30	17:30
Sunset time	5:30	19:00
Solar declination angle (δ)	-23.45°	23.45°
Surface tilt angle (α)	40°	15°

The variation of the total solar radiation with time on 21st December (winter day) is shown in Figure 3.10.

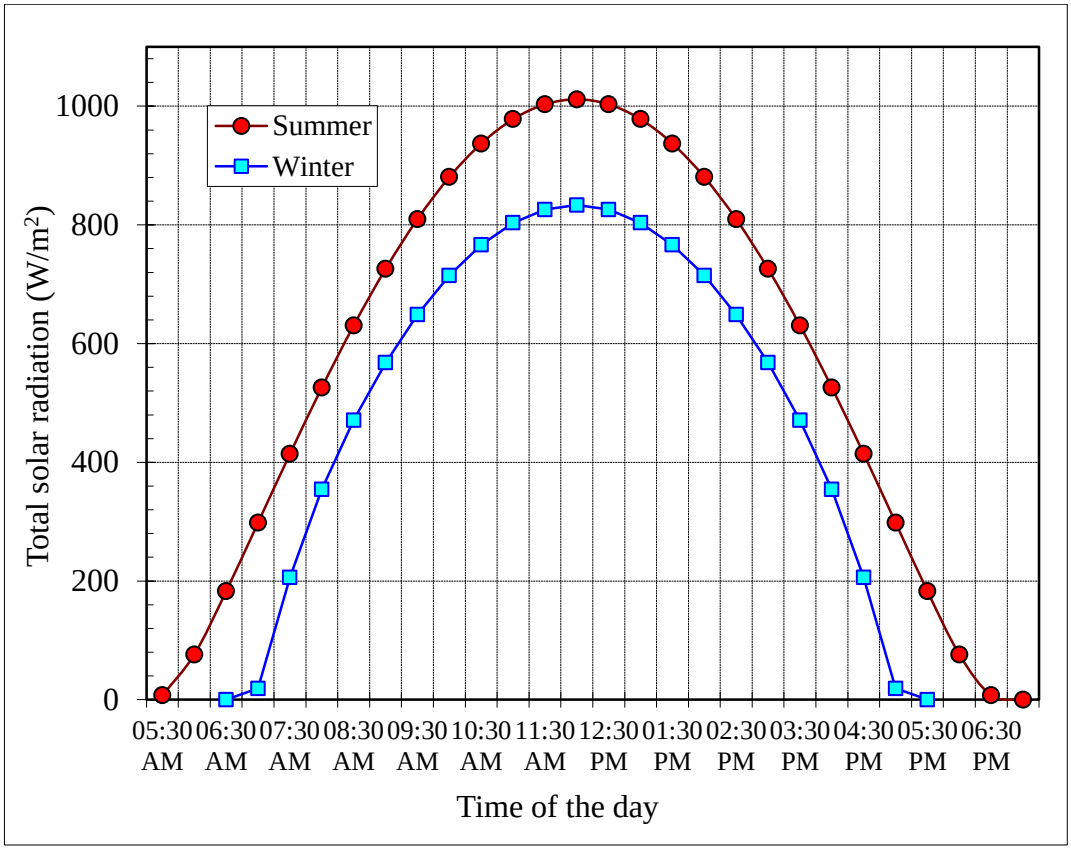

Figure 3.10 Hourly variation of the solar radiation for during summer and winter days

As shown in Figure 3.10, the intensity of the total solar radiation increases with time from sunrise to reach maximum at the mid of the day (solar noon time) then decreased to be zero at the sunset. In order to evaluate the required area of solar panel, average values of the solar index are evaluated. For winter operation, the maximum total solar radiation is 833.3 W/m^2 and the average total solar radiation is 503.8 W/m^2. For summer operation, the maximum is 1011.5 W/m^2 and the average is 569.6 W/m^2. The

area of the solar panels can be used using the average total solar radiation from equation (3.55) considering the designed amount of energy of the generator unit is 80000 W.

$$Q_{solar} = I_{av}\, A\, \eta$$

$$80000 = I_{av}\, A\,(0.85)$$

In winter, the required surface area of the panels is 186.8 m^2 whereas in summer, the required area is 165.22 m^2.

c) Simulation of the winter operation

The variation of the total solar radiation as a fraction of the maximum total solar radiation, for the winter operation, is as follows:

Hour	6:30 AM	7:00 AM	7:30 AM	8:00 AM	8:30 AM	9:00 AM	9:30 AM	10:00 AM
t (hr)	0.0	0.5	1.0	1.5	2.0	2.5	3.0	3.5
t (sec)	0	1800	3600	5400	7200	9000	10800	12600
I/I_{max}	0.000	0.023	0.247	0.425	0.565	0.681	0.778	0.858

Hour	10:30 AM	11:00 AM	11:30 AM	12:00 PM	12:30 PM	1:00 PM	1:30 PM	2:00 PM
t (hr)	4.0	4.5	5.0	5.5	6.0	6.5	7.0	7.5
t (sec)	14400	16200	18000	19800	21600	23400	25200	27000
I/I_{max}	0.920	0.964	0.991	1.000	0.991	0.964	0.920	0.858

Hour	2:30 PM	3:00 PM	3:30 PM	4:00 PM	4:30 PM	5:00 PM	5:30 PM
t (hr)	8.0	8.5	9.0	9.5	10.0	10.5	11.0
t (sec)	28800	30600	32400	34200	36000	37800	39600
I/I_{max}	0.778	0.681	0.565	0.425	0.247	0.023	0.000

These values are used to construct the signal builder in Simulink to facilitate the data entry to the software.

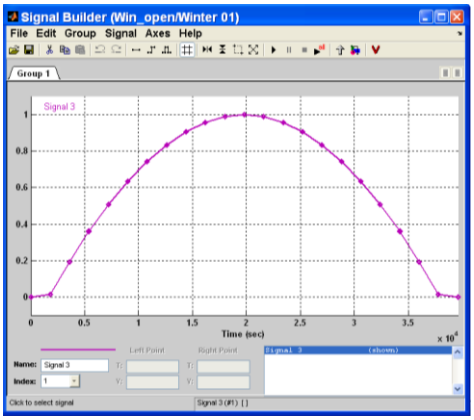

To study open loop response, MatLab Simulink model is built as in Figure (3.11).

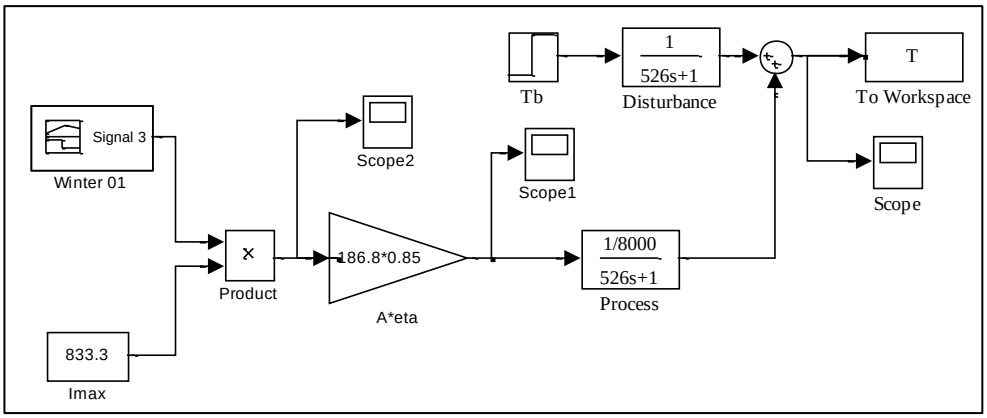

Figure 3.11 Simulink model to study open loop in winter

The closed loop response of the system is obtained using unity feedback. In order to study the closed loop response, MatLab Simulink model is built as in Figure (3.12).

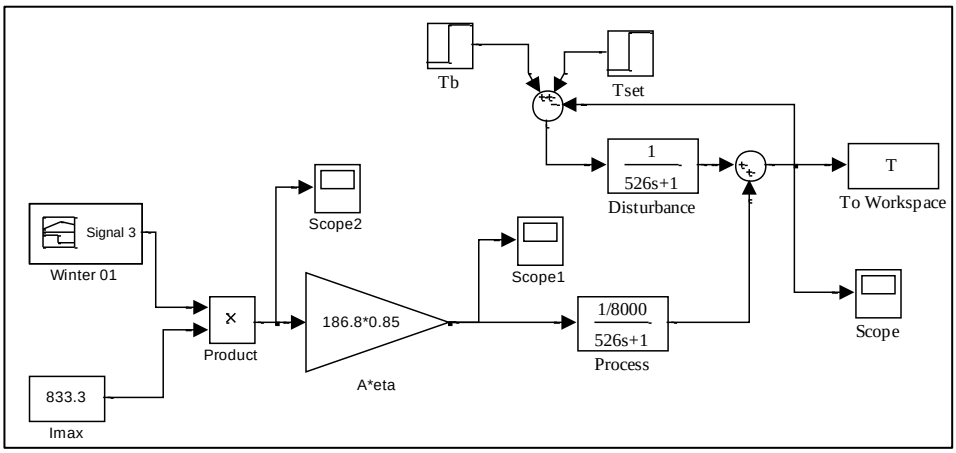

Figure 3.12 Simulink model to study closed loop in winter

The closed loop response of the system after control action is studied. In order to study the response, MatLab Simulink model is built as in Figure (3.13).

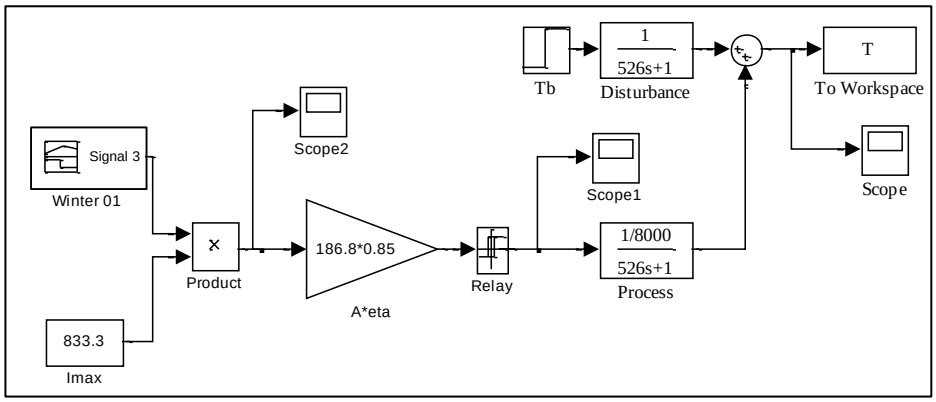

Figure 3.13 Simulink model to study controlled closed loop in winter

d) Simulation of the summer operation

The variation of the total solar radiation as a fraction of the maximum total solar radiation, for the summer operation, is as follows:

Hour	5:30 AM	6:00 AM	6:30 AM	7:00 AM	7:30 AM	8:00 AM	8:30 AM	9:00 AM
t (hr)	0.0	0.5	1.0	1.5	2.0	2.5	3.0	3.5
t (sec)	0	1800	3600	5400	7200	9000	10800	12600
I/I_{max}	0.007	0.075	0.181	0.295	0.409	0.520	0.623	0.718

Hour	9:30 AM	10:00 AM	10:30 AM	11:00 AM	11:30 AM	12:00 PM	12:30 PM
t (hr)	4.0	4.5	5.0	5.5	6.0	6.5	7.0
t (sec)	14400	16200	18000	19800	21600	23400	25200
I/I_{max}	0.800	0.870	0.926	0.967	0.992	1.000	0.992

Hour	1:00 PM	1:30 PM	2:00 PM	2:30 PM	3:00 PM	3:30 PM	4:00 PM
t (hr)	8.0	8.5	9.0	9.5	10.0	10.5	11.0
t (sec)	28800	30600	32400	34200	36000	37800	39600
I/I_{max}	0.967	0.926	0.870	0.800	0.718	0.623	0.520

Hour	4:30 PM	5:00 PM	5:30 PM	6:00 PM	6:30 PM	7:00 PM
t (hr)	8.0	8.5	9.0	9.5	10.0	10.5
t (sec)	28800	30600	32400	34200	36000	37800
I/I_{max}	0.409	0.295	0.181	0.075	0.007	0.000

These values are used to construct the signal builder in Simulink to facilitate the data entry to the software. To study open loop response, MatLab Simulink model is built as in Figure (3.14).

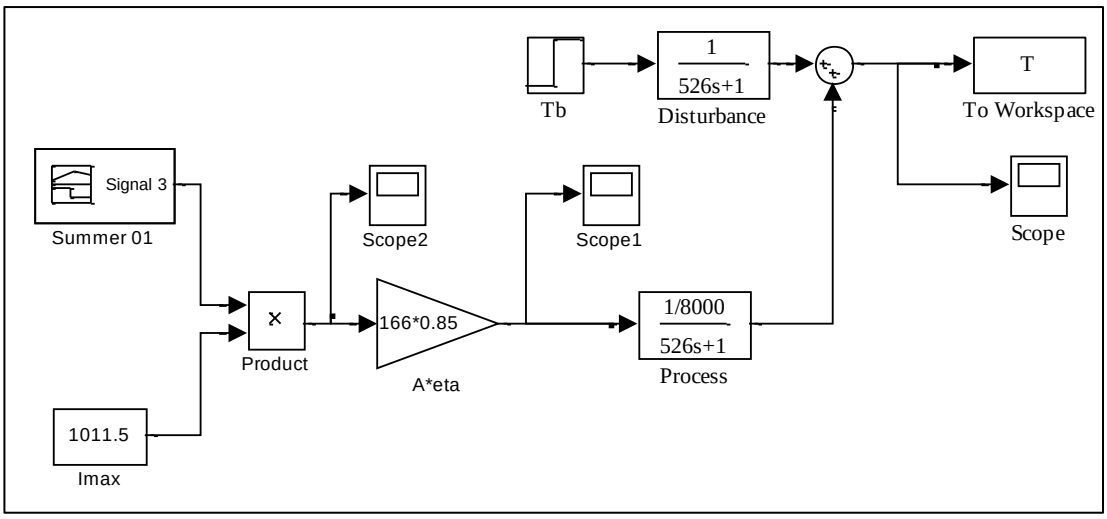

Figure 3.14 Simulink model to study open loop in summer

The closed loop response of the system is studied using MatLab Simulink model as shown in Figure (3.15).

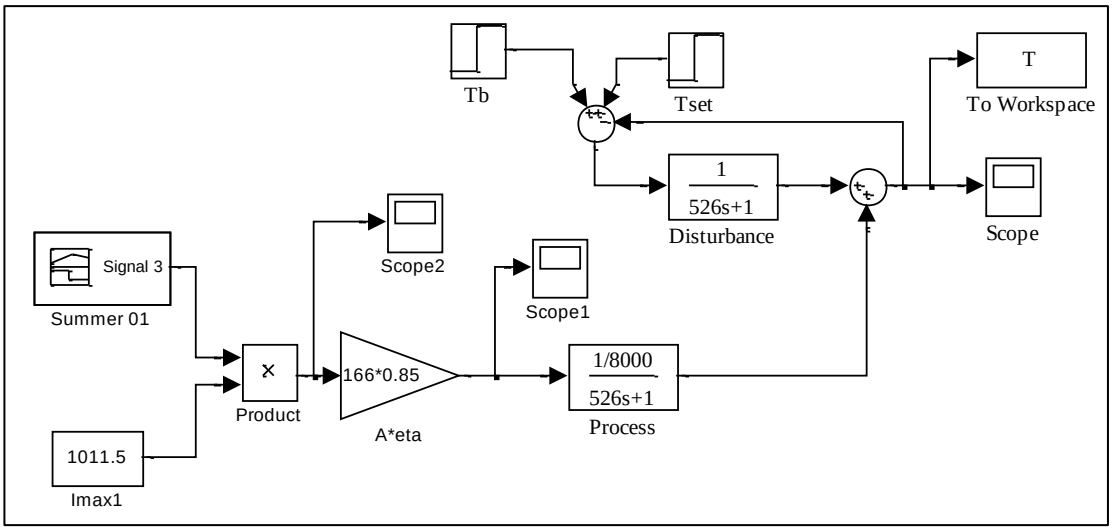

Figure 3.15 Simulink model to study closed loop in summer

The closed loop response of the system after control action is studied. In order to study the response, MatLab Simulink model is built as in Figure (3.16).

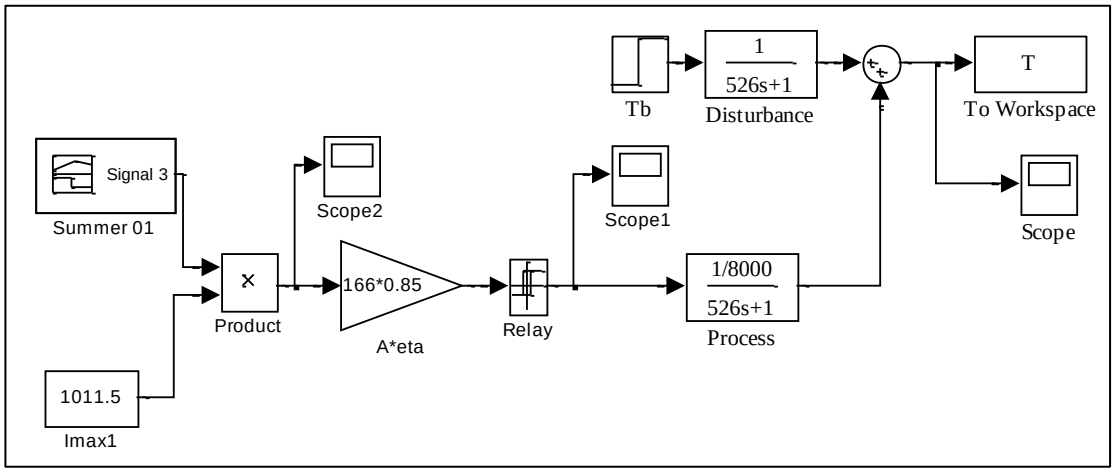

Figure 3.16 Simulink model to study controlled closed loop in summer

Chapter IV

Simulation Results and Discussion

4.1 Introduction

Simulation results of performance evaluation of ARS are given in this chapter. These results include the predictions of both the single- and double effect ARS. For each system, the assumptions, needed for the simulation process, are made and explained followed by the presentation of the effects of simulation parameters. The parameters considered in this study include the effects of the evaporator and generator temperatures on the performance parameters of the two designs of the system. The investigated performance parameters evaluated include the amounts of thermal energy at several components of the system such as the absorber, condenser and generator. The parameters also include the mass flow rates of the different types of LiBr-water solutions used for the ARS. It also includes the prediction of the system coefficient of performance.

The second part of the chapter presented comparison of the performance parameters for the two different designs namely single- and double-effect ARS. The performance parameters includes amounts of thermal energy, mass flow rates of solution and system COP. The last part of this chapter presents the results of controlling temperatures and mass flow rates after mixing process. The results of the system response at different values of the controller gain are introduced.

4.2 Simulation Results of Single-Effect ARS

4.2.1 Assumptions

The simulation of single-effect ARS performance is performed based on the following assumptions:

- Condenser and absorber temperatures are $T_c = T_a = 40°C$.
- Strong solution temperature after cooling = $T_5 = 50°C$
- Cooling capacity is 35.17 kW
- HE effectiveness = 0.7

The simulation procedures are repeated at generator temperature of 100, 110, 120, 130, 140, and 150°C. At each generator temperature, the evaporator temperature was varied as 4, 5, 6, and 7°C. Example of the simulation procedures, using generator temperature of 150°C and evaporator temperature of 5°C, is given in Appendix (A).

4.2.2 Effect of Generator Temperature

During the simulation at constant evaporator temperature and different generator temperatures, several parameters remain constant. These include the weak solution concentration, the refrigerant mass flow rate and the enthalpy at each point (except points 3, 4, 5, 6 and 7). Variations of enthalpy at points 4, 5, and 7, with generator temperature, at different evaporator temperatures are given in Table 4.1. Moreover, variations of weak solution enthalpy before entering the generator unit, point (3), with generator temperature, at different evaporator temperatures, are given in Table 4.2.

Table 4.1 Variations of enthalpy at points 4, 5 and 7 with generator temperature

T_g (°C)	h_4 (kJ/kg)	h_5 (kJ/kg)	h_7 (kJ/kg)
150	354.94	182.96	2783.2
140	332.78	175.78	2764.0
130	310.19	168.43	2745.0
120	287.16	161.00	2725.8
110	263.69	153.60	2706.8
100	239.80	146.31	2687.8

Table 4.2 Variations of weak solution enthalpy at generator inlet

T_g (°C)	Weak solution enthalpy, h_3 (kJ/kg)			
	$T_e = 4$ °C	$T_e = 5$ °C	$T_e = 6$ °C	$T_e = 7$ °C
150	211.12	207.32	203.67	200.06
140	203.71	199.98	196.41	192.87
130	195.93	192.27	188.78	185.32
120	187.66	184.09	180.68	177.31
110	178.82	175.35	172.02	168.74
100	169.31	165.93	162.71	159.52

The strong solution concentration varies significantly with the generator temperature. In order to compare the performance of single- and double-effect ARS, same concentration values of strong solution are used. Therefore, strong solution concentration, used for performance simulation of the double-effect ARS, is used for the simulation of the single-effect ARS. The method used to evaluate the strong solution concentration will be explained later. Variations of strong solution concentration with the generator temperature are shown in Table 4.3.

Table 4.3 Variations of strong solution concentration with generator temperature

T_g (°C)	100	110	120	130	140	150
x_{II} %	62.100	63.348	64.564	65.750	66.908	68.039

In order to properly size the generator unit of the system, which is heat exchanger, the amount of needed thermal energy is important to evaluate. This amount of energy varies with the temperature at which the energy is supplied to the generator fluid. Variations of the generator thermal energy with generator temperature, at an evaporator temperature of 5°C, are shown in Figure 4.1. As shown in this figure, the increase of generator temperature decreases the amount of generator thermal energy. Similar trends were found at different evaporator temperatures. The increase of generator temperature causes the strong solution at generator exit to be hotter. When this hot strong solution is

used to heat the weak solution before entering the generator, the weak solution temperature will increase which decrease the required generator thermal energy.

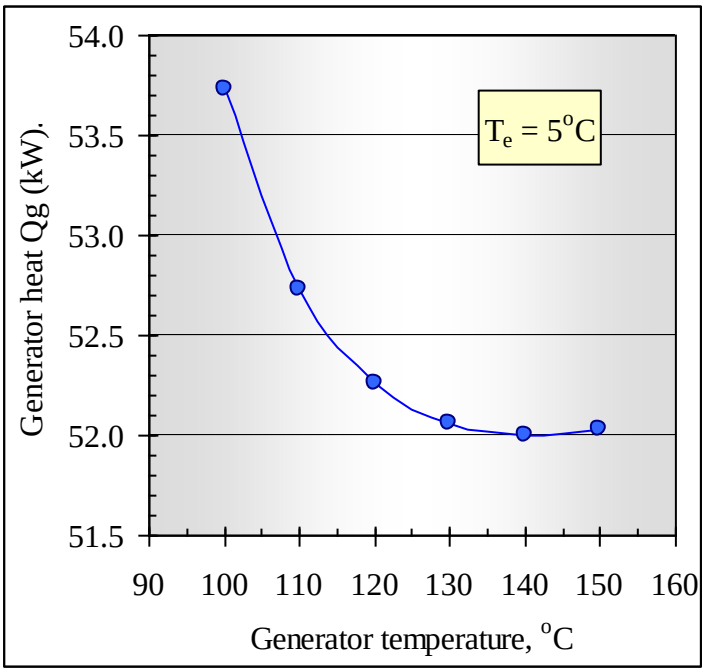

Figure 4.1 Variations of generator thermal energy with generator temperature for single-effects ARS (Te = 5°C)

As shown in Figure 4.1, at generator temperature of 100°C, the generator thermal energy needed is 53.73 kW. The increase of generator temperature from 100 to 120°C decreases the generator energy to 52.26 kW (2.7% reduction). Meanwhile, the increase of temperature from 100 to 150°C decreases the generator thermal energy by 3.11%. This reduction of energy with generator temperature can be attributed to the decreased mass flow rates of the strong and weak solutions, as shown in Figure 4.2.

As shown in Figure 4.2, the mass ratio of strong and weak solutions decreases with increased generator temperatures. In this figure, $R_{ss} = \left(m_{ss}/m_{ref}\right)$ is the mass ratio of the strong solution to the refrigerant and $R_{ws} = \left(m_{ws}/m_{ref}\right)$ is the mass ratio of the weak solution to the refrigerant. As seen in Figure 4.2, R_{ss} is less than R_{ws} at any generator temperature. This solution mass reduction with generator temperature has positive effect as it reduces the system costs by decreasing the required pipe size of both solution pipelines which saves materials and costs.

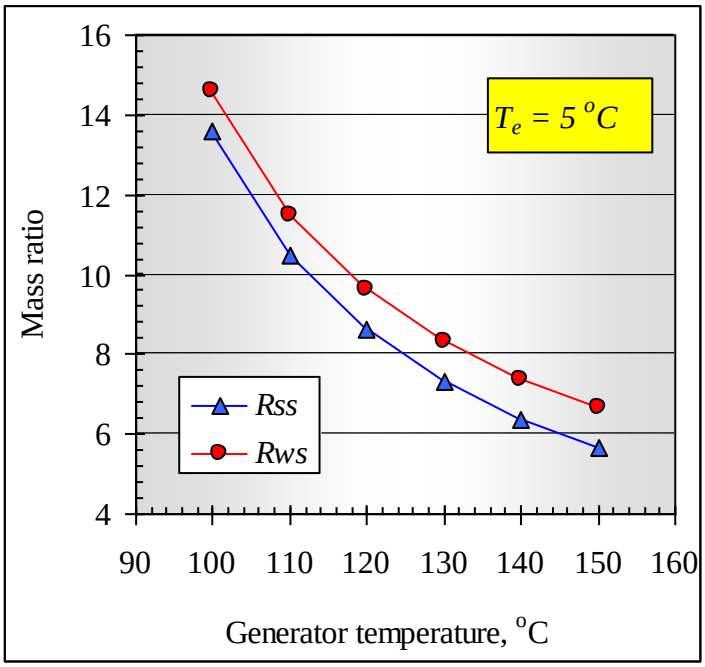

Figure 4.2 Variations of strong and weak solution mass ratio with generator temperature for single-effect ARS (Te = 5°C)

The system performance is usually assessed using coefficient of performance (COP), which depends on the generator temperature. Figure 4.3 shows the variations of COP of single-effect ARS with the generator temperature at different evaporator temperatures.

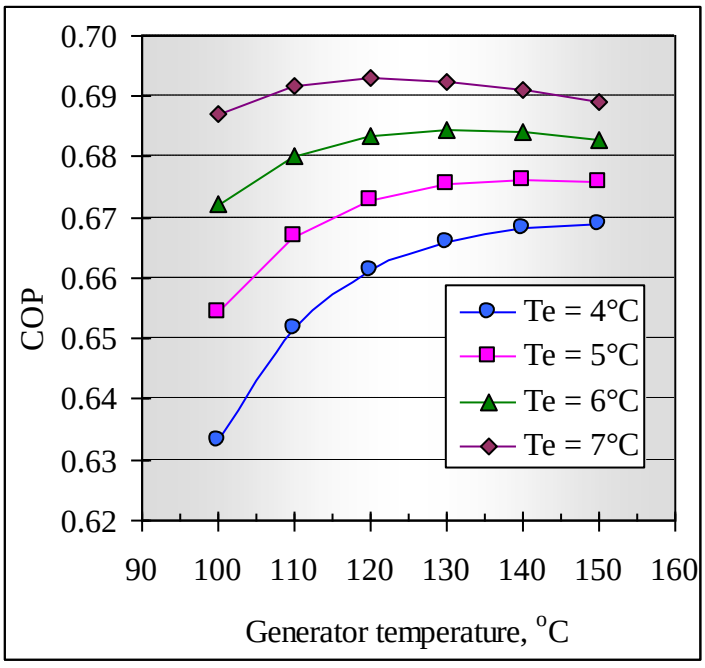

Figure 4.3 Variations of COP with generator temperature for single-effect ARS at different evaporator temperatures

As depicted in Figure 4.3, the increase of generator temperature increases the system COP, at any evaporator temperature. The system COP reached maximum of (0.693) at generator temperature of 120°C and evaporator temperature of 7°C. The increase of the system COP with generator temperature can be attributed to the reduction of the required generator thermal energy with generator temperature. At constant cooling load, the COP is inversely proportional to the amount of generator thermal energy needed, see Equation (3.19). The increase of COP with generator temperature was found at evaporator temperatures of 4 and 5°C.

As shown in Figure 4.3, the rate of increase of COP decreases with increasing the evaporator temperature. Therefore, slower rate of COP increase with generator temperature, at an evaporator temperature of 6°C, was found. At evaporator temperature of 7°C, the increase of generator temperature increases the system COP to reach maximum at 120°C and the further temperature increase decreases the system COP.

The simulation results at any evaporator temperature showed decreased mass ratio of both strong and weak solutions with generator temperatures. The variations of strong solution mass ratio with generator temperature are shown in Figure 4.4.

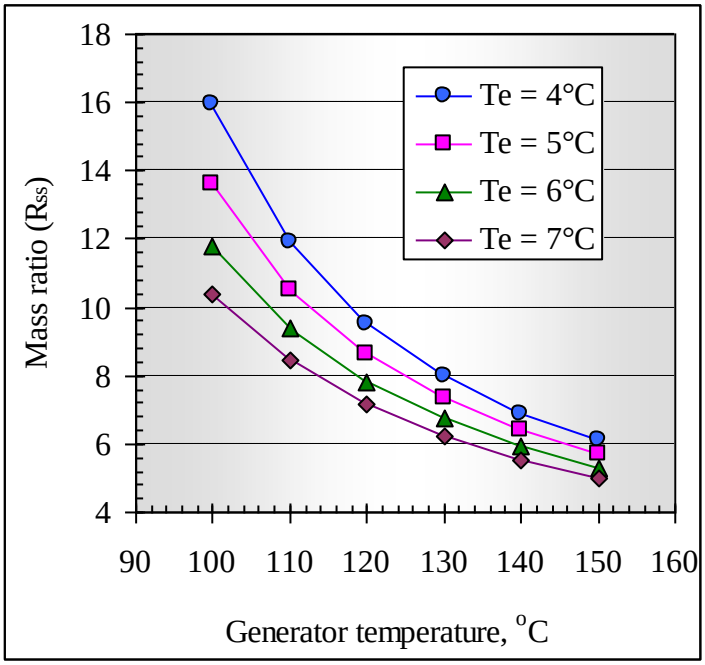

Figure 4.4 Variations of strong solution mass ratio with generator temperature at different evaporator temperatures for single-effect ARS

As shown in Figure 4.4, the decrease of evaporator temperature is always accompanied by an increase of the required weak and strong solution mass ratio. Accordingly, the increase of generator temperature not only increases the system COP but also decreases the required piping sizes, materials and cost. But, the increase of generator temperature is affected by the design of the solar heating system. Thus, to have higher generator temperatures, flat plate collectors with evacuated tubes or parabolic trough collectors can be used.

One of the important parameters needed to design the system absorber is the amount of energy. Variations of absorber thermal energy with generator temperature of single-effect ARS at different evaporator temperatures are shown in Figure 4.5.

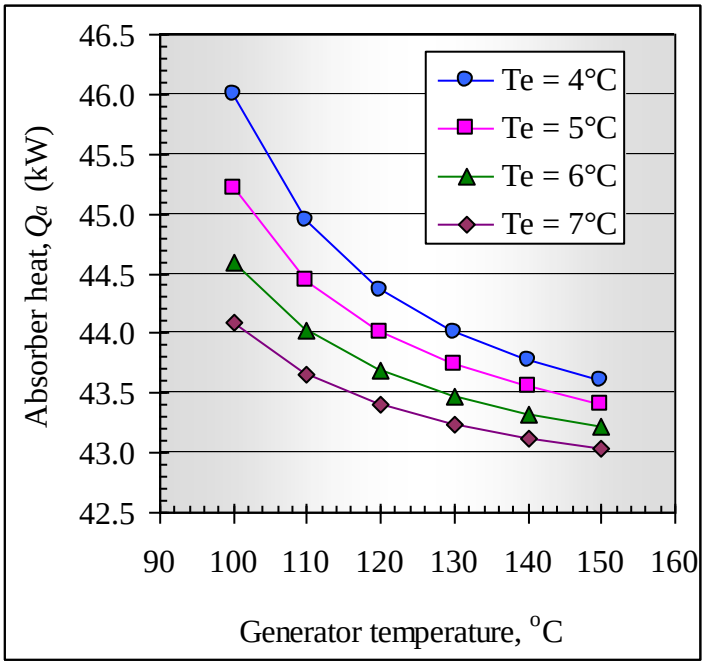

Figure 4.5 Variations of absorber heat with generator temperature at different evaporator temperatures for single-effect ARS

As shown in Figure 4.5, the increase of generator temperature decreases the absorber thermal energy, at any evaporator temperature. Therefore, lowering the evaporator temperature requires the use of bigger size absorber unit. At an evaporator temperature of 4°C, the increase of generator temperature from 100 to 150°C decreased the absorber thermal energy by 5.2%. Moreover, at evaporator temperatures of 5, 6, and 7°C, the percentage reduction of absorber thermal energy with generator temperature were 4.0, 3.1, and 2.4%, respectively.

4.2.3 Effect of Evaporator Temperature

For simulation at constant generator temperature and varied evaporator temperatures, several parameters remain constant. These include the strong solution concentration and the enthalpy at each point, except points 1, 3 and 10. Variations of conditions (3) enthalpy with evaporator and generator temperatures are reported before in Table 4.2. At constant cooling load, the variation of enthalpy at condition (10) with evaporator temperature slightly changes the refrigerant mass flow rate, as shown in Table 4.4.

Table 4.4 Variations of refrigerant mass flow rate with evaporator temperature

T_e (°C)	h_{10} (kJ/kg)	$\dot{m}_{ref}$ (kg/s)
4	2508.2	0.01526
5	2510.0	0.01524
6	2511.9	0.01523
7	2513.7	0.01522

Variations of the system COP, of single-effect ARS with evaporator temperature, at generator temperatures of 110, 130 and 150°C, are shown in Figure 4.6.

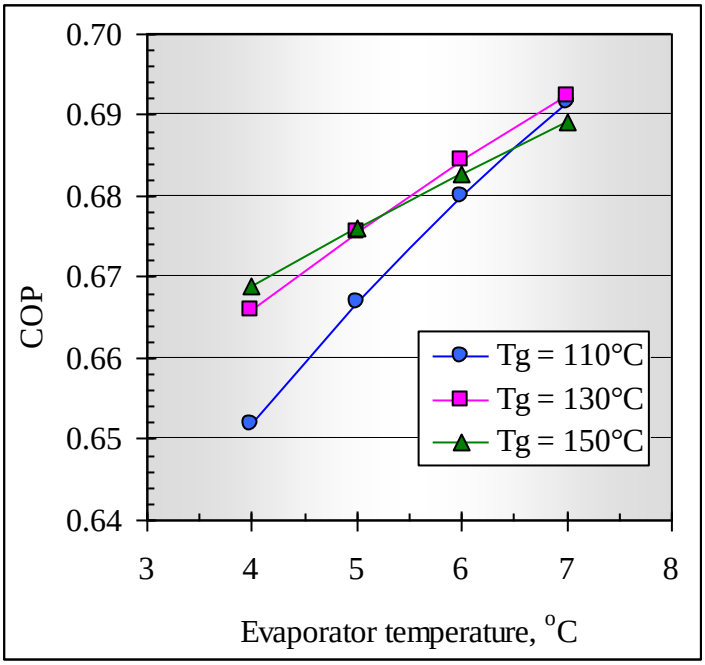

Figure 4.6 Variations of COP with evaporator temperature at different generator temperatures for single-effects ARS

As depicted in Figure 4.6, lowering the evaporator temperature decreases the COP, at any generator temperature. Nearly, linear relationship is found between the system COP and the generator temperature. At generator temperature of 110, 130, and 150°C, lowering the evaporator temperature from 7 to 4°C decreases the COP by 5.7, 3.8, and 2.9%, respectively. Therefore, the system performance is degraded with lowering the evaporator temperature. The other parameter to consider is the weak and strong solution masses. Variations of strong solution mass ratio with evaporator temperature, at generator temperature of 110, 130, and 150°C, are shown in Figure 4.7.

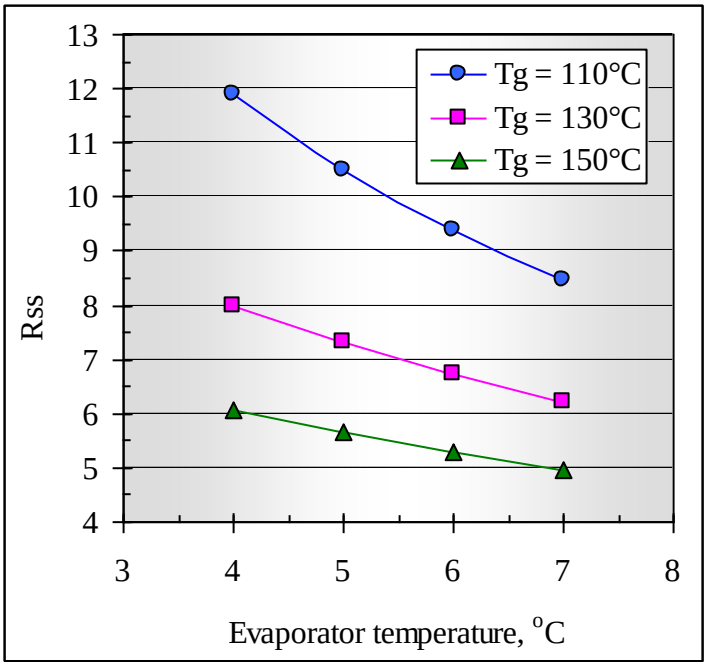

Figure 4.7 Variations of strong solution mass ratio with evaporator temperature at different generator temperatures for single-effect ARS

As shown in Figure 4.7, lowering the evaporator temperature requires the use of increased strong solution, and accordingly weak solution, mass flow rate (at nearly constant refrigerant mass flow rate). At generator temperature of 110, 130, and 150°C, lowering the evaporator temperature from 7 to 4°C increases the required mass flow rate of the strong solution by 40.5, 28.2, and 22.3%, respectively.

As stated earlier, one of the key values needed for proper absorber design, which is heat exchanger, is the absorber thermal energy. Variations of absorber thermal energy with evaporator temperature of single-effect ARS are shown in Figure 4.8.

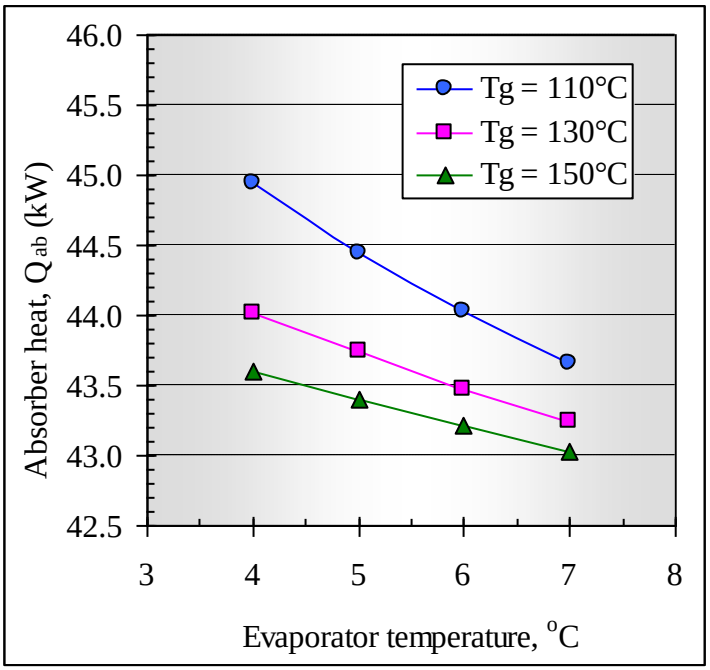

Figure 4.8 Variations of absorber heat with evaporator temperature at different generator temperatures for single-effect ARS

As shown in Figure 4.8, lowering the evaporator temperature increases the amount of thermal energy (heat) to be rejected by the absorber unit. It is also shown in this figure that the use of higher generator temperatures decreases the absorber thermal energy to minimum. At generator temperatures of 110, 130, and 150°C, lowering the evaporator temperature from 7 to 4°C increases the amount of thermal energy of the absorber unit by 2.9, 1.8, and 1.3%, respectively.

4.3 Simulation Results of Double-Effect ARS

4.3.1 Assumptions

The double-effect ARS simulation is performed based on the following assumptions:

- Condenser and absorber temperatures are $T_c = T_a = 40°C$.
- Strong solution temperature after cooling = $T_5 = 50°C$
- Cooling capacity is 35.17 kW and effectiveness of HE-I and HE-II = 0.7

The simulation procedures are repeated at generator-I temperatures of 100, 110, 120, 130, 140, and 150°C. At each generator-I temperature, the evaporator temperature was varied as 4, 5, 6, and 7°C. At each generator-I temperature, the pressure (in generator-I) is assumed as 120.9, 102, 97.8, 87.8, 78.6, and 70.2 kPa. The corresponding saturation temperatures at these pressures are 105, 102, 99, 96, 93 and 90°C, respectively. Example of simulation procedures at generator-I temperature of 150°C and evaporator temperature of 5°C, is given in Appendix (A).

4.3.2 Effect of Generator Temperature

During the simulation of double-effect, at constant evaporator but different generator-I temperatures, several parameters remain constant. These include the weak solution concentration, the refrigerant mass flow rate, and the enthalpy at each point, except 3, 4, 5, 8, 9, 10, 11, 12 and 13.

The series double-effect system has three concentration levels. The concentration of the weak solution (at absorber outlet) varies with evaporator temperature but remains constant with generator-I temperature. The concentration of the strong solution (at generator-II outlet) varies with solution pressure inside generator-II (which equals the condenser pressure) and solution temperature (which equals the saturation temperatures at generator-I pressure). These concentrations are evaluated using Equation (3.8).

The solution exit from generator-I is at the higher system pressure. But it is has an intermediate concentration. In their study, Marcos *et al.* (2011) reported that the system concentration increment is to be divided equally between the two generators to ensure system optimisation. Therefore, the intermediate solution concentration is evaluated as the sum of lower concentration and half of concentration increment. Variations of strong solution concentration are previously reported in Table 4.3. Variations of weak

solution concentration, with evaporator temperature are shown in Table 4.5. Moreover, changes of intermediate solution concentration are shown in Table 4.6.

Table 4.5 Variations of weak solution concentration

T_e (°C)	4	5	6	7
x_I %	58.431	57.84	57.247	56.65

Table 4.6 Variations of intermediate solution concentration

T_g (°C)	100	110	120	130	140	150
x_A %	59.970	60.594	61.202	61.795	62.374	62.940

The amount of thermal energy of generator-I varies with generator-I temperature. This variation, at an evaporator temperature of 5°C, is shown in Figure 4.9.

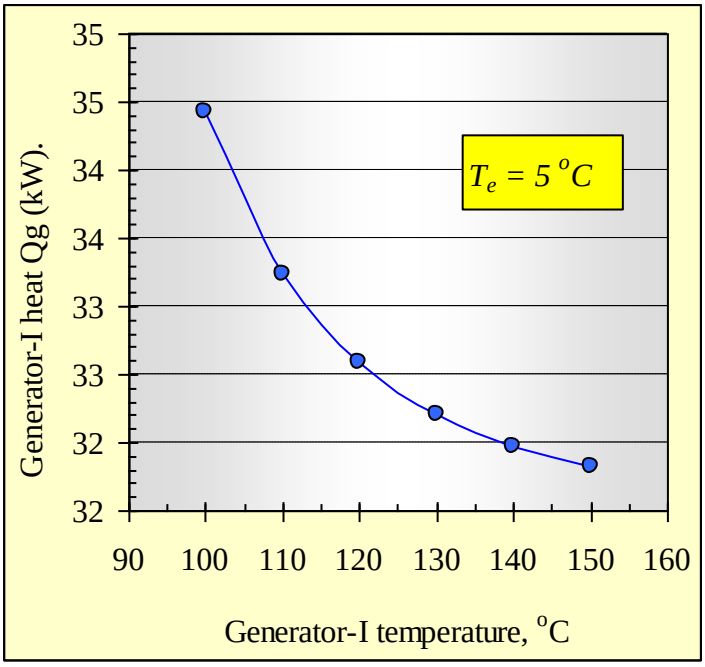

Figure 4.9 Variations of generator-I thermal energy with generator-I temperature for double-effect ARS (Te = 5°C)

As shown in Figure 4.9, increasing the generator-I temperature decreases generator-I thermal energy at evaporator temperature of 5°C. Similar trends were found at other evaporator temperatures. At generator-I temperature of 100°C, the energy needed is 34.42 kW. The increase of generator-I temperature from 100 to 150°C decreases the

thermal energy to 31.83 kW (7.52% reduction). This reduction can be attributed to the decreased solution mass flow rates, as shown in Figure 4.10. Moreover, variations of the double-effect COP with generator-I temperature at different evaporator temperatures are shown in Figure 4.11.

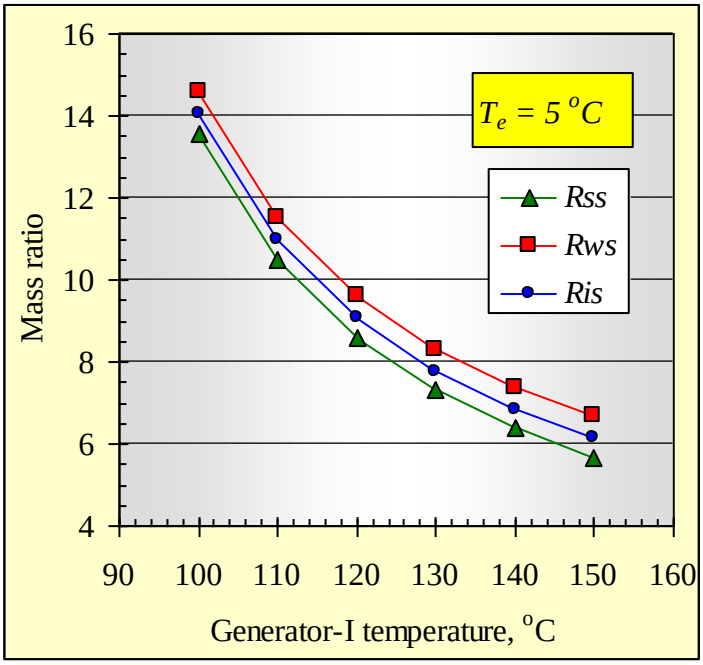

Figure 4.10 Variations of solution mass ratios with generator-I temperature for double-effect ARS (Te = 5°C)

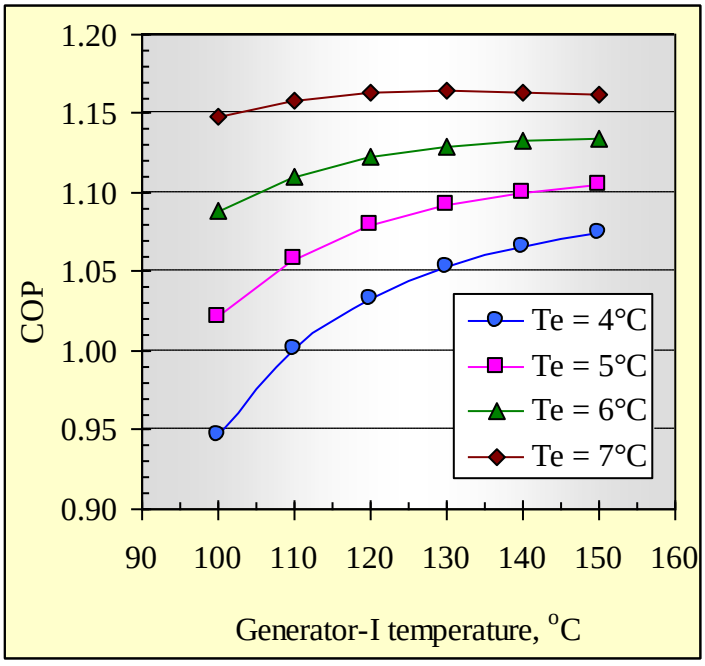

Figure 4.11 Variations of COP with generator temperature for double-effect ARS at different evaporator temperatures

As depicted in Figure 4.11, increasing generator-I temperature increases the system COP, at any evaporator temperature. The system COP reached maximum of (1.164) at generator-I temperature of 130°C and evaporator temperature of 7°C. The increase of the COP with generator-I temperature can be related to the reduction of the required generator-I energy with temperature. As shown in Figure 4.11, the rate of COP increase decreases with increased evaporator temperature. So, slower rate of COP increase was found with generator-I temperature, at an evaporator temperature of 6°C. At evaporator temperature of 7°C, the increase of generator-I temperature increases the COP to reach maximum at 130°C but further increase of temperature decreases the system COP.

At evaporator temperature 5°C, increasing generator-I temperature increases the refrigerant mass portion produced in generator-I unit whereas the refrigerant mass portion produced in generator-II unit was decreased. The variations of refrigerant mass portions with generator-I temperature are shown in Figure 4.12.

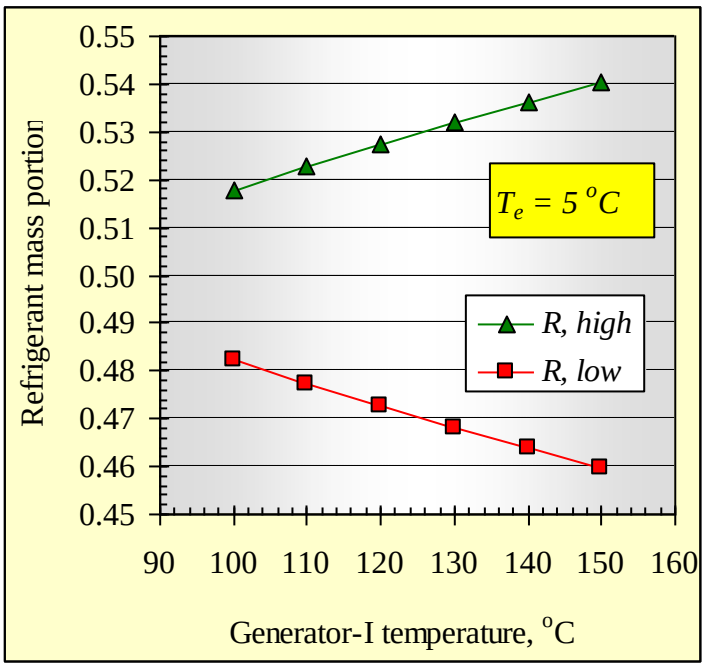

Figure 4.12 Variations of refrigerant mass portions with generator-I temperature for double-effect ARS (Te = 5°C)

Variations of condenser thermal energy, needed for proper condenser design, with generator-I temperature of double-effect ARS is shown in Figure 4.13.

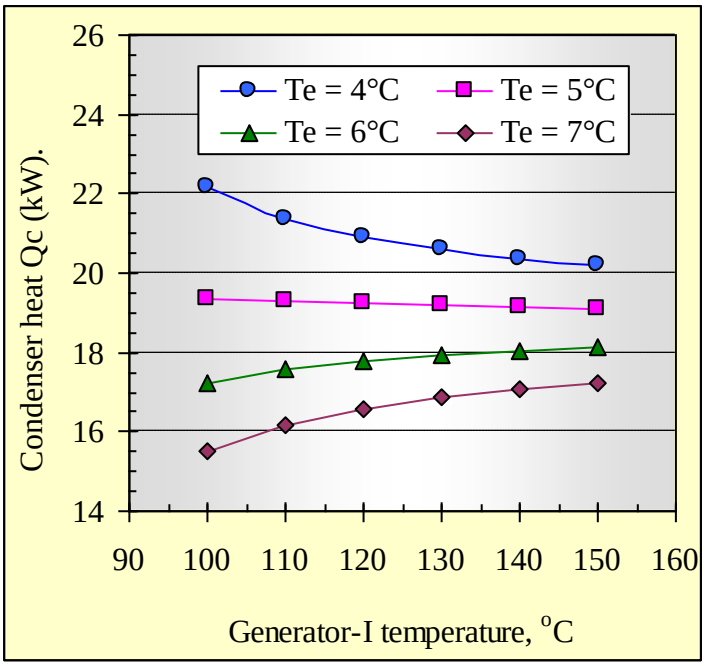

Figure 4.13 Variations of condenser thermal energy with evaporator temperature at different generator-I temperatures for double-effect ARS

As shown in Figure 4.13, increasing generator-I temperature differently changes the condenser thermal energy based on the evaporator temperature. For example, at evaporator temperature of 4°C, the increase of generator-I temperature from 100 to 150°C decreases the condenser energy by 8.8%. As the evaporator temperature was raised to 5°C, the condenser energy was slightly decreased by only 1.24%. At evaporator temperatures of 6 and 7°C, the increase of generator-I temperature increases the condenser thermal energy by 5.3, and 11.0%, respectively.

4.3.3 Effect of Evaporator Temperature

For simulation at constant generator-I but variable evaporator temperatures, several parameters remain constant. These include the strong solution concentration and the enthalpy at each point, except points 1, 3, 4, 6 and 11. Variations of weak solution enthalpy at absorber outlet (condition (1)), with evaporator temperature are shown in Table 4.7. Variations of weak solution enthalpy at HE-I outlet (condition (3), with evaporator and generator-I temperatures are shown in Table 4.8.

Table 4.7 Weak solution enthalpy, at absorber outlet, with evaporator temperature

T_e (°C)	4	5	6	7
$h_1 = h_2$ (kJ/kg)	107.74	104.98	102.38	99.825

Table 4.8 Weak solution enthalpy, at HE-I outlet, with temperature

T_g (°C)	Weak solution enthalpy, h_3 (kJ/kg)			
	$T_e = 4$ °C	$T_e = 5$ °C	$T_e = 6$ °C	$T_e = 7$ °C
150	164.60	161.26	158.09	154.95
140	163.18	159.86	156.70	153.57
130	161.74	158.43	155.28	152.18
120	160.25	156.96	153.82	150.73
110	158.67	155.40	152.28	149.21
100	156.99	153.74	150.64	147.58

Variations of weak solution enthalpy at HE-II outlet before entering generator-I unit (condition (4)), with evaporator and generator-I temperatures are shown in Table 4.9.

Table 4.9 Weak solution enthalpy, at HE-II outlet, with temperature

T_g (°C)	Weak solution enthalpy, h_4 (kJ/kg)			
	$T_e = 4$ °C	$T_e = 5$ °C	$T_e = 6$ °C	$T_e = 7$ °C
150	207.75	220.51	233.49	246.61
140	195.87	208.70	221.75	234.95
130	184.19	197.10	210.22	223.49
120	172.71	185.68	198.88	212.22
110	161.43	174.47	187.73	201.15
100	150.36	163.47	176.80	190.28

Variations of strong solution enthalpy at HE-II outlet before entering generator-II unit (condition (6)), with evaporator and generator-I temperatures are shown in Table 4.10.

Table 4.10 Strong solution enthalpy, at HE-II outlet, with temperature

T_g (°C)	Strong solution enthalpy, h_6 (kJ/kg)			
	$T_e = 4$ °C	$T_e = 5$ °C	$T_e = 6$ °C	$T_e = 7$ °C
150	269.47	243.77	217.45	190.40
140	265.68	240.28	214.27	187.53
130	260.99	235.90	210.20	183.79
120	255.38	230.60	205.21	179.13
110	248.78	224.31	199.25	173.49
100	241.12	216.98	192.24	166.82

Variations of system COP of double-effect ARS with evaporator temperature, at generator-I temperatures of 110, 130 and 150°C, are shown in Figure 4.14.

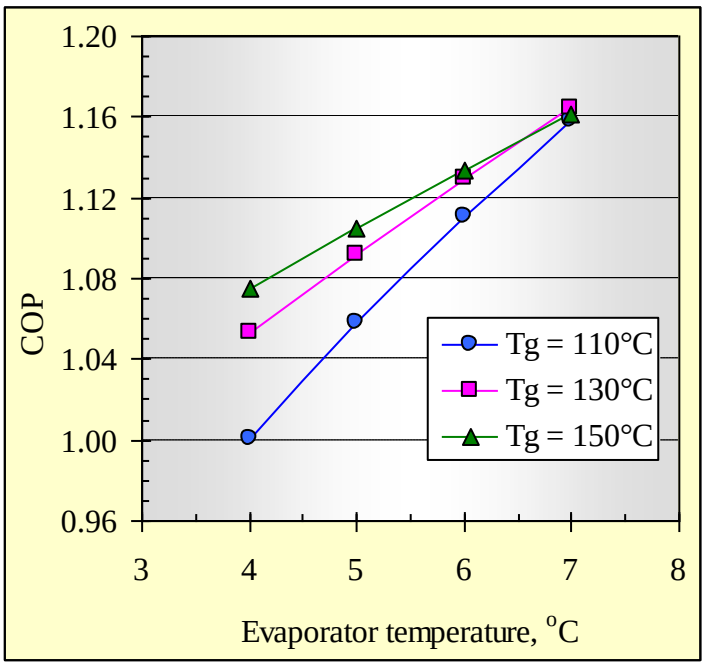

Figure 4.14 Variations of COP with evaporator temperature at different generator-I temperature for double-effects ARS

As shown in Figure 4.14, lowering evaporator temperature decreases (nearly linearly) the system COP, at any generator-I temperature. At generator temperature of 110, 130, and 150°C, lowering the evaporator temperature from 7 to 4°C decreases the system COP by 13.6, 9.5, and 7.5%, respectively. Therefore, the performance system is

degraded with lower evaporator temperature. In addition to COP, solution masses are important. So, variations of weak solution mass ratio with evaporator temperature, at generator-I temperatures of 110, 130, and 150°C, are shown in Figure 4.15.

As shown in Figure 4.15, lowering the evaporator temperature necessitates the use of increased weak solution, and thus intermediate and strong solution mass flow rates (at nearly constant refrigerant mass flow rate). Also Figure 4.15 shows that at generator-I temperatures of 110, 130, and 150°C, lowering the evaporator temperature from 7 to 4°C increases the required weak solution mass flow rate by 36.2, 24.3, and 18.5%, respectively. Also, lowering the evaporator temperature is, at all times, come with an increase of weak, intermediate and strong solution mass flow rates. Consequently, the increase of mass flow rates increases the required pipe sizes and the system cost.

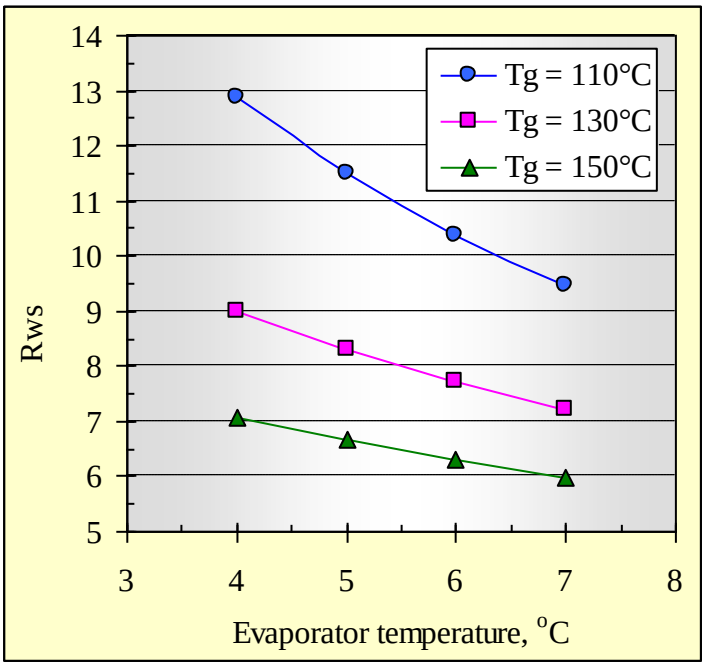

Figure 4.15 Variations of weak solution mass ratio with evaporator temperature at different generator-I temperatures for double-effect ARS

As stated earlier, one of the key values required for proper condenser design is the amount of thermal energy. Variations of condenser energy with evaporator temperature of double-effect ARS are shown in Figure 4.16.

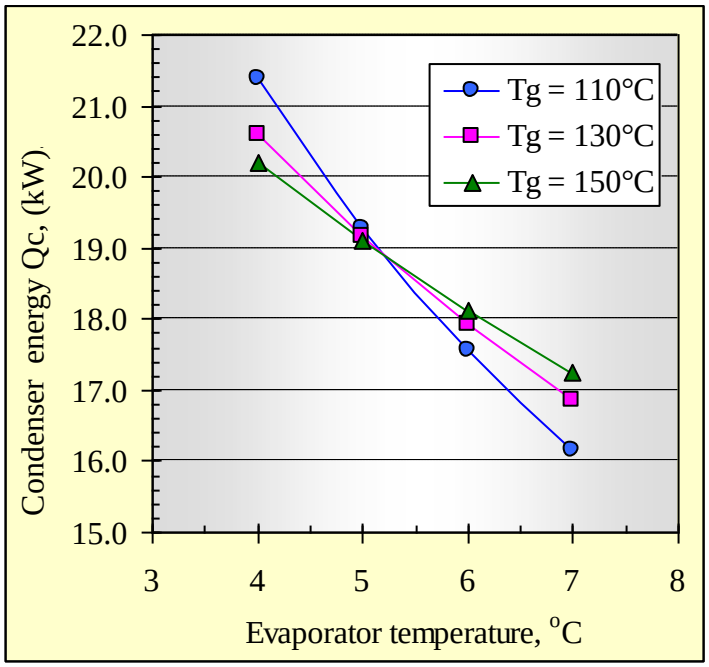

Figure 4.16 Variations of condenser thermal energy with evaporator temperature at different generator-I temperatures for double-effect ARS

As shown in Figure 4.16, lowering the evaporator temperature causes an increased condenser thermal energy at any generator-I temperature. As shown in this figure, nearly constant condenser thermal energy was found at an evaporator temperature of 5°C, at all generator-I temperatures. Besides, at evaporator temperature less than 5°C, increasing generator-I temperature decreases the amount of condenser thermal energy. On the other hand, for evaporator temperatures higher than 5°C, increasing generator-I temperature increases the amount of condenser thermal energy.

4.4 Comparison of Single- and Double-Effect Performance

The system COP is a measure used to evaluate the system performance. Usually, the system performs better when it has higher COP. Performance simulation of single- and double-effect ARS is conducted. The COP comparisons of the single- and soluble-effect ARS are shown in Figure 4.17.

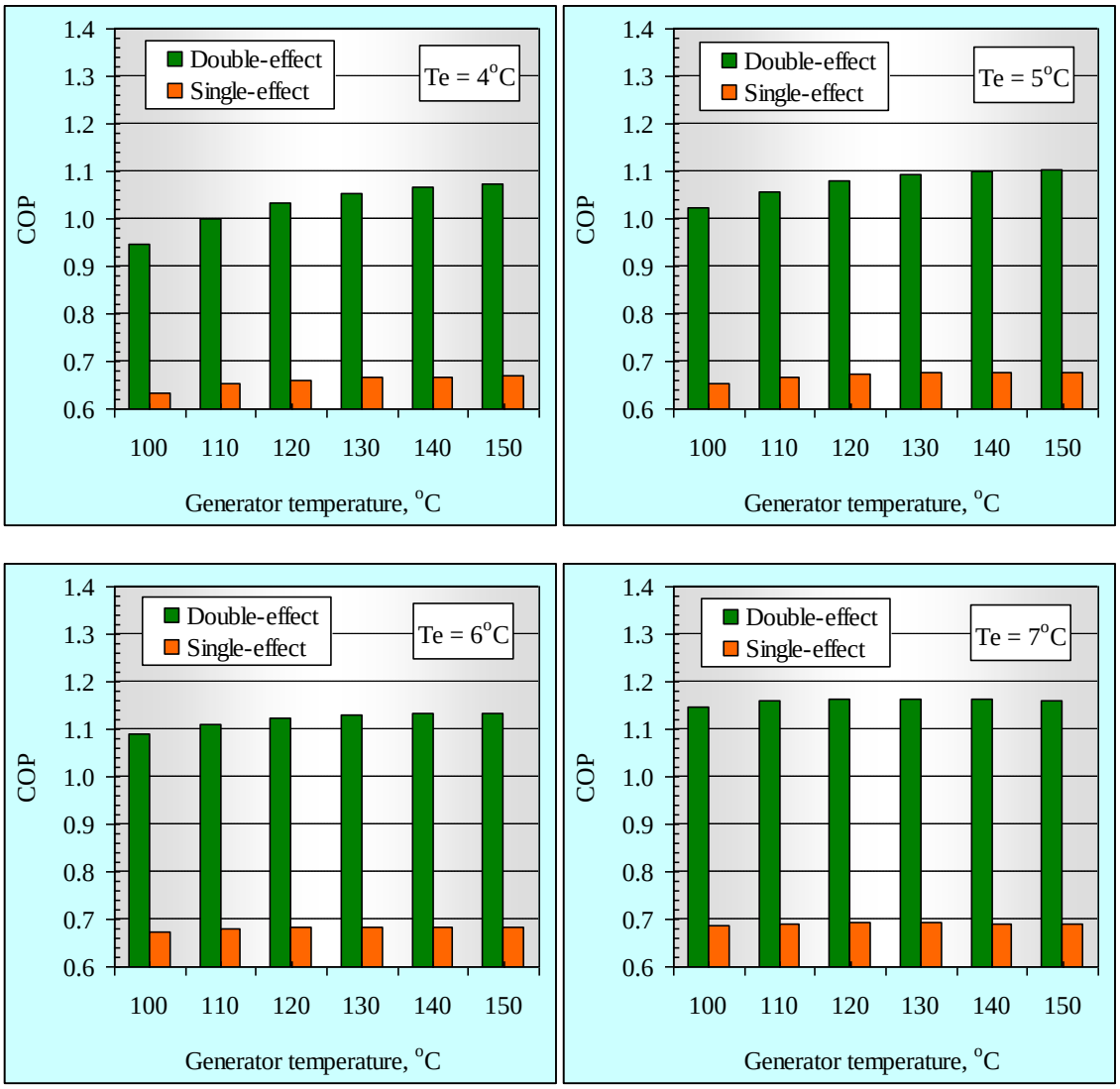

Figure 4.17 COP comparisons of single- and double-effect ARS

As clearly shown in Figure 4.17, the double-effect ARS has higher COP compared with the single-effect ARS, at any evaporator temperature. This can be attributed to the decreased amounts of thermal energy to be supplied to the generator unit of the system, at the same cooling load. The percentage increase of the COP varies from 49.5% (at generator temperature of 100°C and evaporator temperature of 4°C) to 68.6% (at generator temperature of 150°C and evaporator temperature of 7°C).

In addition to the COP, the amount of thermal energy to be supplied to the system (at the generator unit) is the key parameter for the design of this component. Variations of the thermal energy needed for the system operation are shown in Figure 4.18.

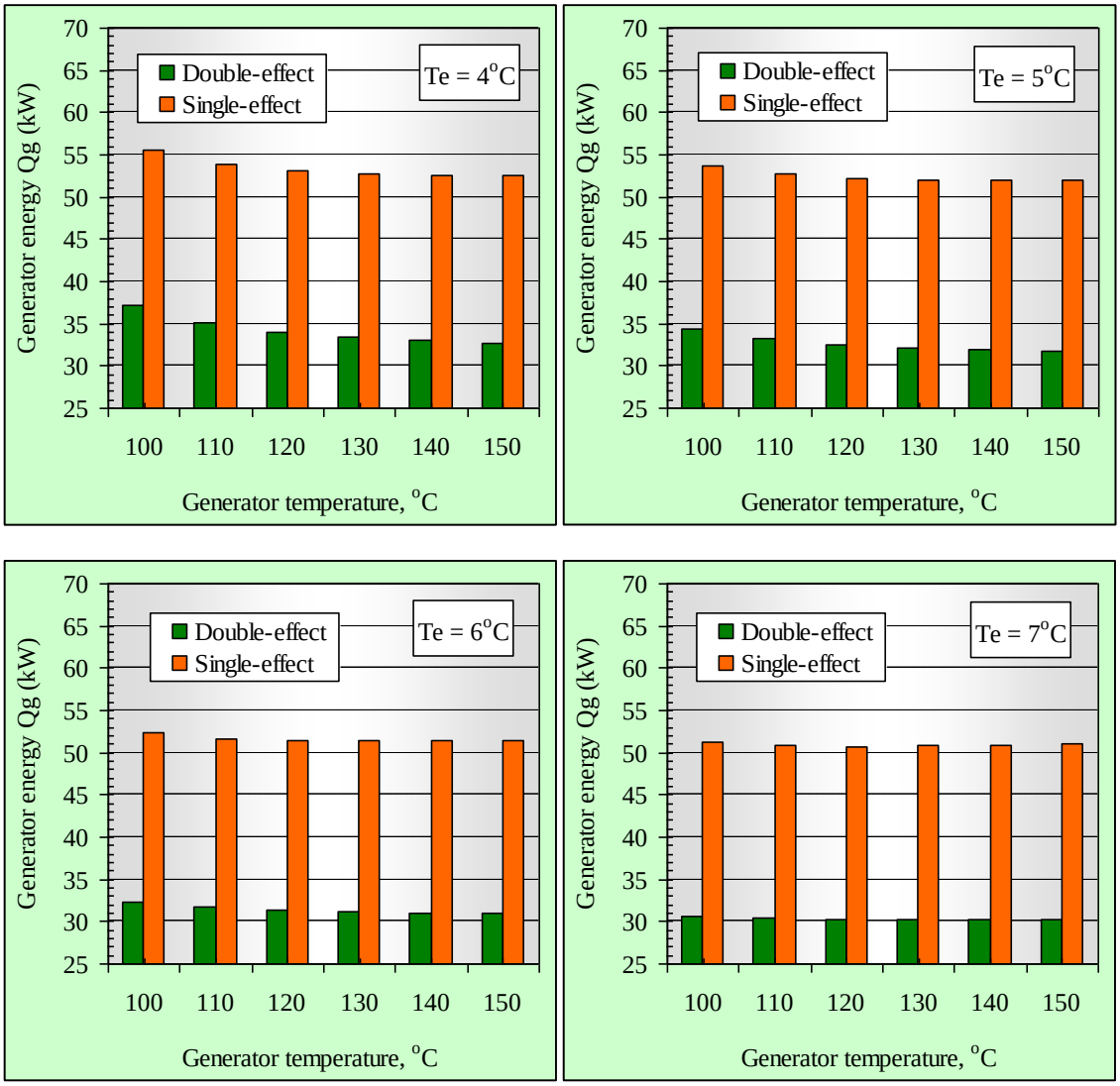

Figure 4.18 Variations of thermal energy needs of the system

As shown in Figure 4.18, the double-effect system requires lower amounts of thermal energy (varies from 33.1 to 40.7%) at the same cooling load. This decreases the size of the generator unit of the system. The reason for this behaviour is the efficient use of the supplied thermal energy so that required total refrigerant mass flow rate can be generated in both generators of the double-effect system while the thermal energy is to be supplied only to generator-I of the system. However, the double-effect system needs more components so that its capital cost will increase. Meanwhile smaller capacity solar system can be utilised effectively with double-effect ARS.

For both systems, cooling facility is required for both absorber and condenser units. The simulation results showed similar amounts of absorber energy for single- and double-effect ARS. Therefore, the control factor for the sizing of the required cooling facility will be the condenser thermal energy. Variations of the condenser thermal energy of both systems are shown in Figure 4.19.

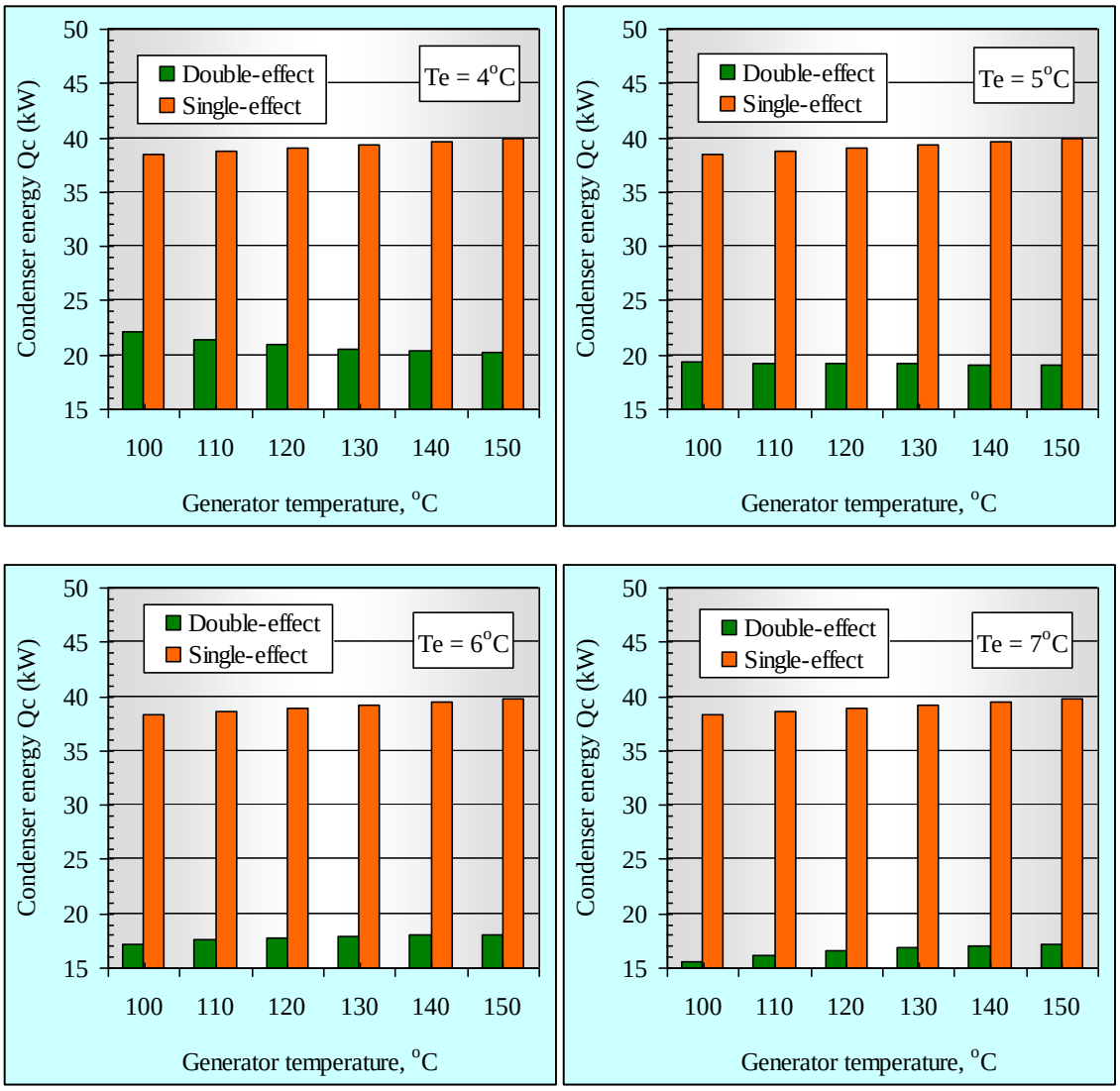

Figure 4.19 Variations of condenser thermal energy of single- and double-effect ARS

As clearly shown in Figure 4.19, the condenser thermal energy of the double-effect system is usually lower than that of the single-effect system. The condenser thermal energy for the double-effect system is 42.4 to 56.7% lower than that of the single-effect system, based on the simulation conditions. This can be attributed to the fact that only part of the refrigerant mass is condensed in the condenser while the other refrigerant mass portion is used to produce more refrigerant mass in the generator-II unit.

4.5 Response of Storage Tank System

4.5.1 Night time operation

The storage tank is used to store thermal energy to be ready to feed the generator unit of the ARS. For efficient operation of the ARS, the storage tank temperature needs to be nearly constant. During the night, the storage tank is fed with the thermal energy by means of electric heaters. The simulation of the system is conducted and the step input response of the open loop considering both the process and the disturbance is shown in Figure 4.20. During this simulation, the back temperature form the generator unit to the storage tank is assumed constant at 100°C.

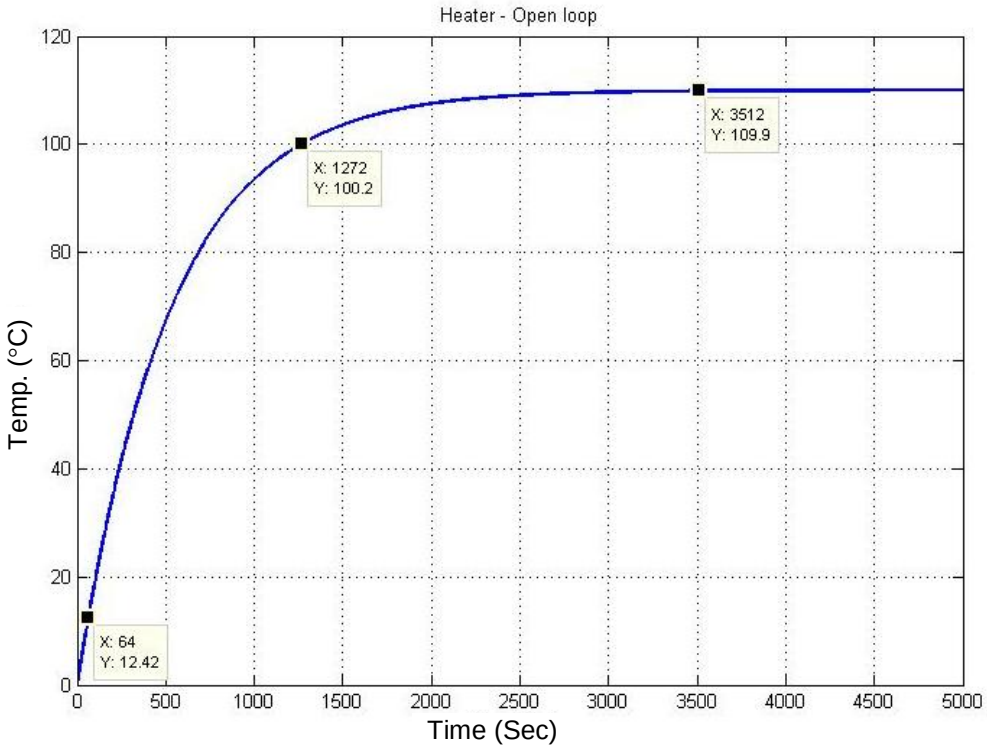

Figure 4.20 Open loop step response

As depicted in Figure 4.20, the steady state temperature due to the using of electric heaters is about 110°C. When the heaters are in operation, the temperature of the tank changed as shown in the figure. The storage tank takes about 60 seconds to reach 10°C (which is about 10% of the required control temperature). Meanwhile, the system needs about 1270 seconds to reach 100°C (which is about 90% of the required control temperature). Therefore, the response of the system can be described by its rise time, which is about 1270 – 60 = 1210 sec. Meanwhile, Figure 4.20 showed that the settling time of the system is about 3512 sec. These demonstrate the considerably slow response

of the system. In order to study the response of the closed loop system, the system is simulated using unity feedback system. Accordingly, the closed loop step response is shown in Figure 4.21.

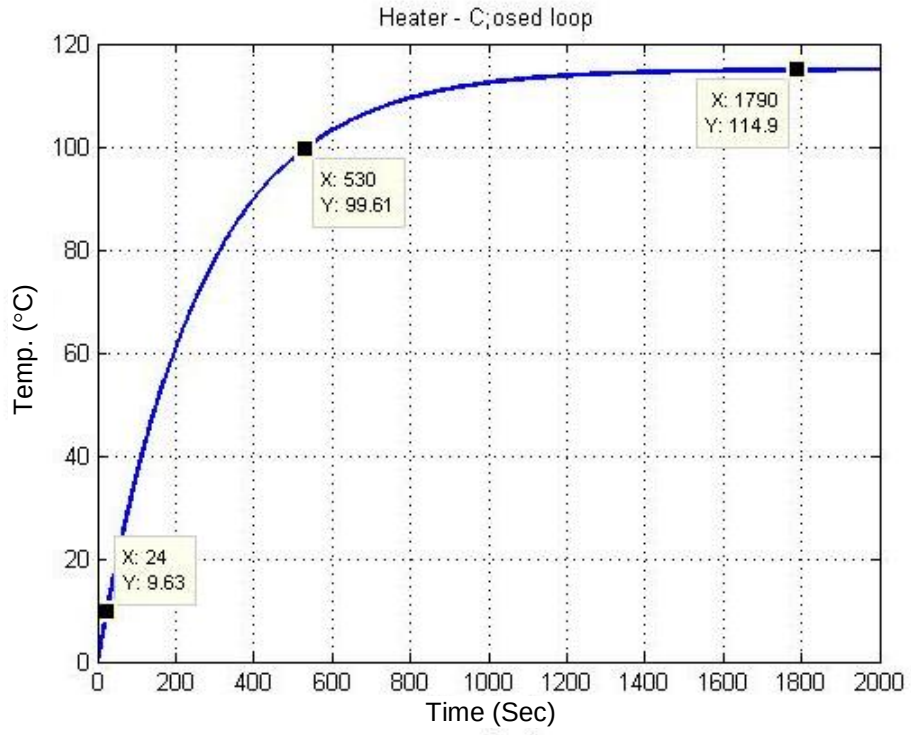

Figure 4.21 Closed loop step response

As depicted in Figure 4.21, the response expressed in terms of rise time and the settling time is improved using the unity feedback. As seen in Figure 4.21, for the closed loop response, the rise time of the system temperature to increase from 10 to 100°C was found to be 530 – 25 = 505 seconds. This means the closed loop response in terms of the rise time is improved because the rise time is decreased from 1210 to 505 seconds (about 41.7% reduction) of the corresponding rise time of the open loop system. Also, the settling time of the system is decreased from 3512 seconds for the open loop system to about 1790 seconds, which is about 51% reduction. Even the closed loop system showed improved performance, but the response of the system still remarkably slow. Therefore, the response of the system needs to be quickened and its steady state error needs improvement. Accordingly, PID compensator is used to improve the system response and steady state error.

First, the PID compensator used to improve the system response and the steady state error can have different components. For simplification, the proportional part of the PID

is considered. The effects of the proportional gain of the PID controller on the step response of the system are investigated and the results are shown in Figure 4.22.

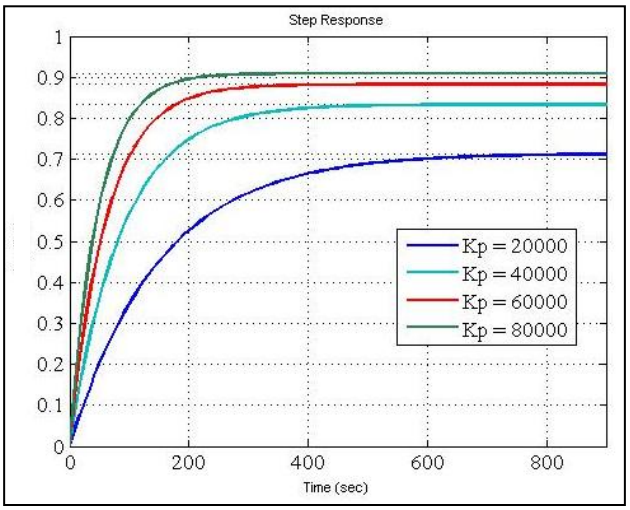

Figure 4.22 Effect of proportional gain on the response of the system

As depicted in Figure 4.22, the increase of the proportional gain of the OID controller improves the system response. Accordingly, higher value of the proportional gain of 80000 is used and the system response using this value is shown in Figure 4.23.

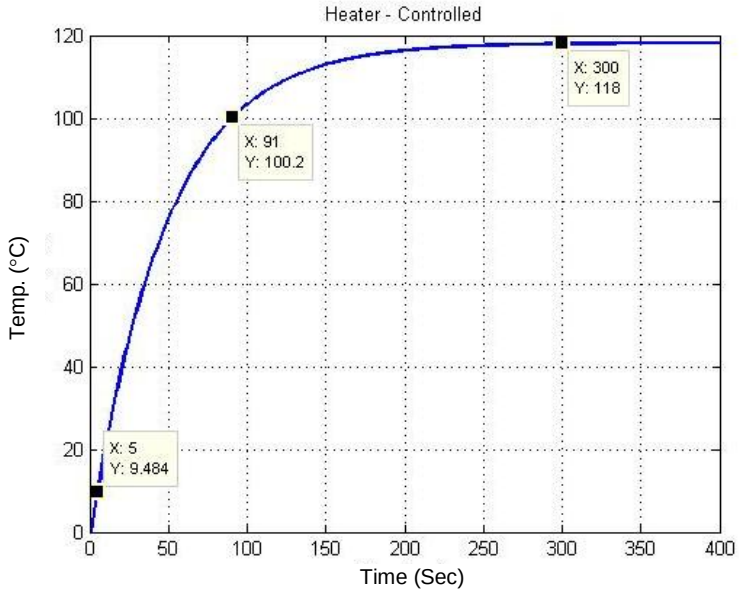

Figure 4.23 Compensated step response of the system

It is shown in Figure 4.24 there are recognised improvements in the system response with the use of the PID controller. The system response becomes faster. The rise time of the system temperature to rise from 10 to 100°C is about 90 - 5 = 85 seconds. This demonstrates that the use of the controller decreased the rise time of the system by to

about 16.8% of the corresponding closed loop rise time and to about 7.0% of the open loop rise time. The settling time of the system decreased as well to 300 seconds, which about 8.5% of the settling time of the corresponding open loop system.

4.5.2 Daytime winter operation

For the daytime operation, the heat supplied to the storage tank comes from solar panels. However, the amount of solar radiation received by the solar panels change with time of the day and with day of the year. The simulation to predict the storage tank temperature response for the daytime operation during the winter season is performed using the solar radiation data for Dubai City on 21st December. The open loop response of the system is shown in Figure 4.24. The lower part of the figure shows short time interval response of the system.

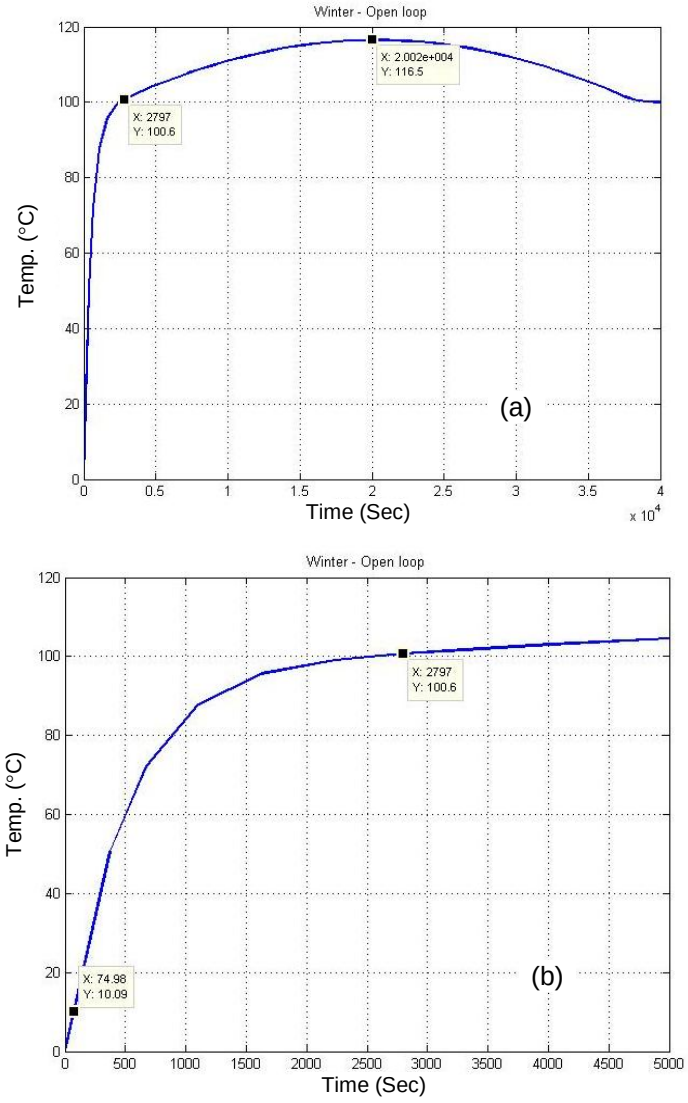

Figure 4.24 Open loop response for daytime winter operation (a) full day (b) part day

As shown in Figure 4.24, the storage tank temperature increases with time to reach maximum of about 116.5°C after about 20000 seconds (5.56 hours). As also shown in this figure, the temperature reached 10°C after 75 seconds and then increased to 100°C after 2790 seconds. Accordingly, the rise time for the system temperature from 10 to 100°C is about 2790 - 75 = 2715 second (about 45 minutes). The closed loop response of the system is shown in Figure 4.25.

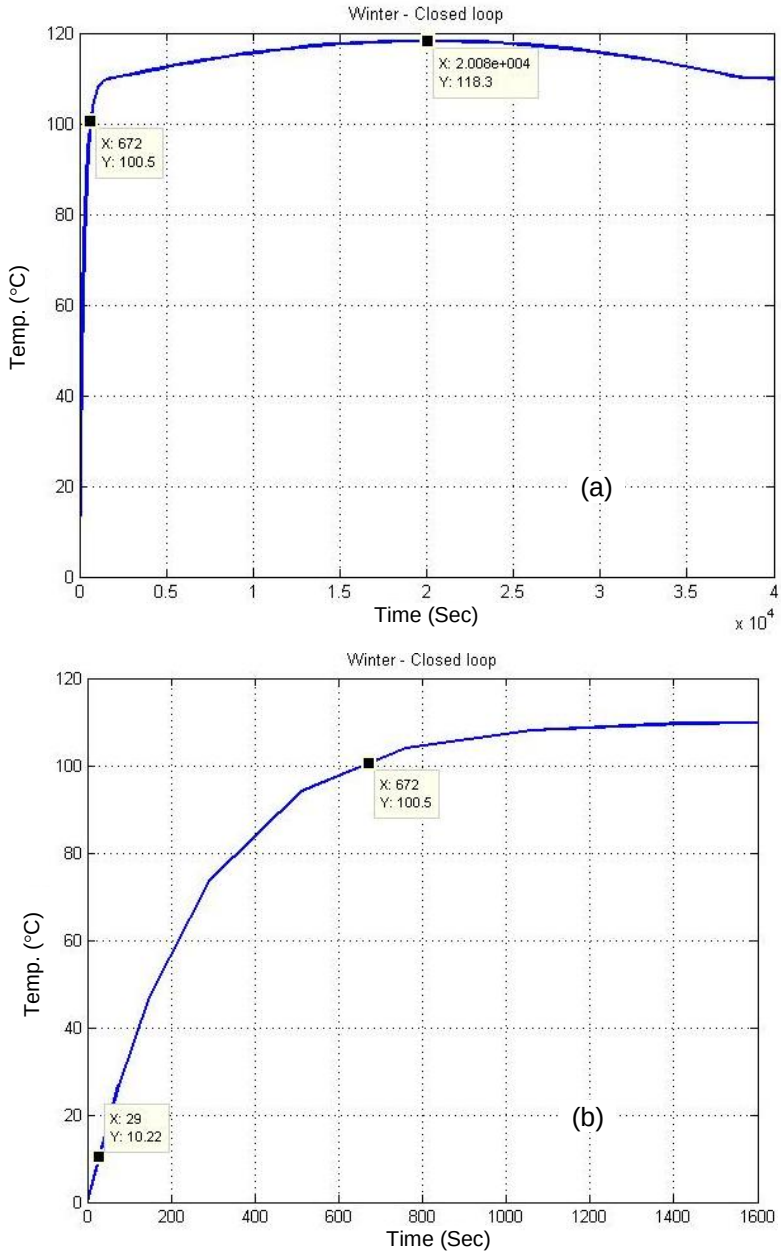

Figure 4.25 Closed loop response for daytime winter operation (a) full day (b) part day

The comparison between the responses of the system open and closed shows the effect of having unity feedback on the system. It is clear that the rise time is considerably decreased with the use of unity feedback. The system temperature reached 10°C after

about 30 seconds and reached 100°C after about 670 seconds. Therefore, the rise time of the system temperature from 10 to 100°C is 670 - 30 = 640 seconds. This rise time of the closed loop system is about 232.6% of the corresponding system response for the open loop system. In general, the system response is considerably slow. The set point of the system is exceeded which requires the use of controller. After using relay as controller, the system response is as shown in Figure 4.26.

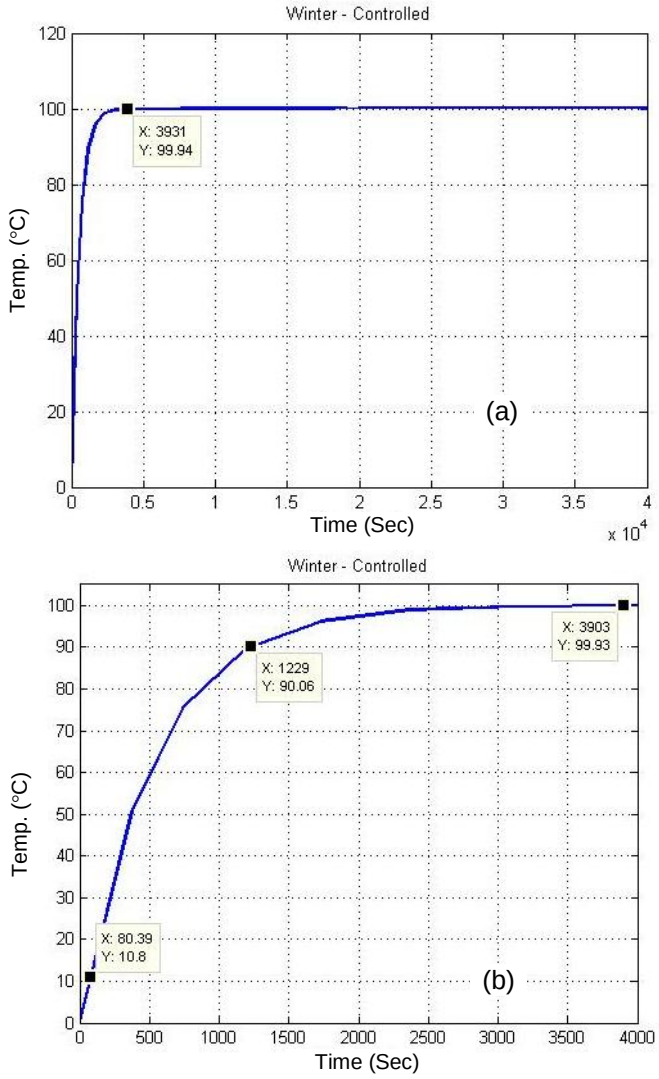

Figure 4.26 Controlled response for daytime winter operation (a) full day (b) part day

As shown in Figure 4.26, the use of controller limits the maximum temperature of the system to the set point of 100°C. However, the settling time of the system is considerably high at about 3900 seconds (65 minutes). The rise time of the system temperature to increase from 10 to 90°C was about 1230 - 80 = 1150 seconds (about 19.2 minutes).

4.5.3 Daytime summer operation

During summer, the intensity of solar radiation on the solar panel is higher in summer compared with winter. Simulation of the system to evaluate the storage tank temperature response during summer season is performed using solar radiation data on Dubai City on 21st June. The open loop response of the system is shown in Figure 4.27.

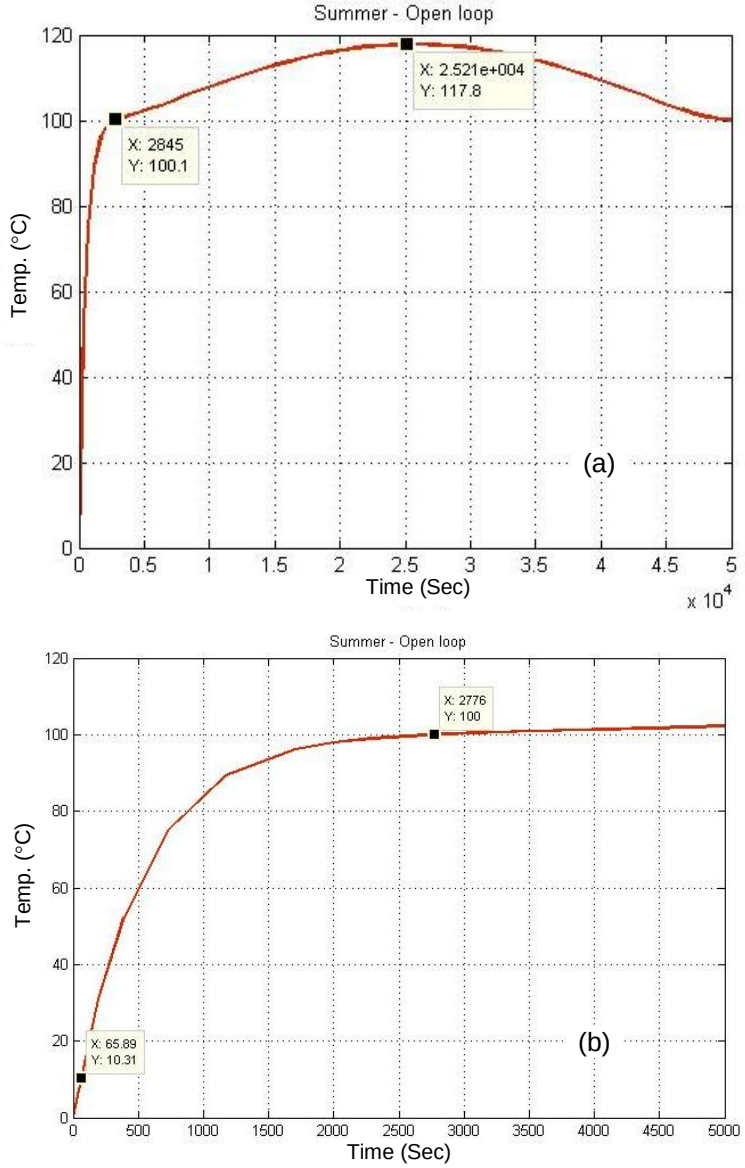

Figure 4.27 Open loop responses for daytime summer (a) full day (b) part day

As shown in Figure 4.27, the storage tank temperature increases with time to reach maximum of about 117.8°C (nearly the same as winter operation) after about 25200 seconds (7 hours). This time is higher than that experienced in winter which is 5.5 hours. As also shown in the figure, the temperature of the storage tank reached 10°C after 65 seconds and then rise to reach 100°C after 2775 seconds. Therefore, the rise

time for the system temperature to rise from 10 to 100°C is about 2775-65 = 2710 second (about 45 minutes). This rise time is nearly the same as the rise time of the open loop system during the winter operation. This demonstrates that no seasonal change was found on the value of the system rise time for the open loop system. The closed loop response is obtained using unity feedback signal to the open loop of the system. The response for the closed loop system is shown in Figure 4.28.

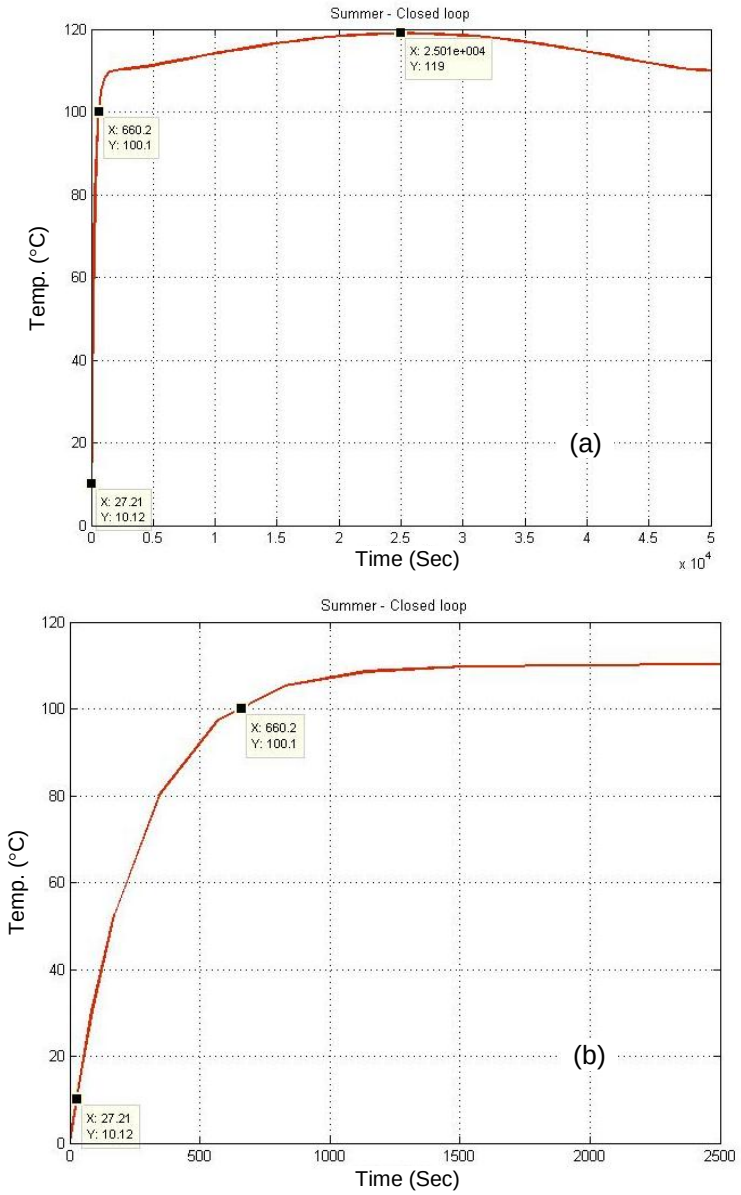

Figure 4.28 Closed loop response for daytime summer (a) full day (b) part day

As shown in Figure 4.28, the system temperature reached 10°C after about 27 seconds and reached 100°C after about 660 seconds. Therefore, the rise time of the system temperature from 10 to 100°C is 660 - 27 = 633 seconds, which is nearly the same as that of the winter operation. The open and closed loop responses show that the set point

temperature of the system is exceeded which requires the use of controller. After using relay controller, the system response is as shown in Figure 4.29.

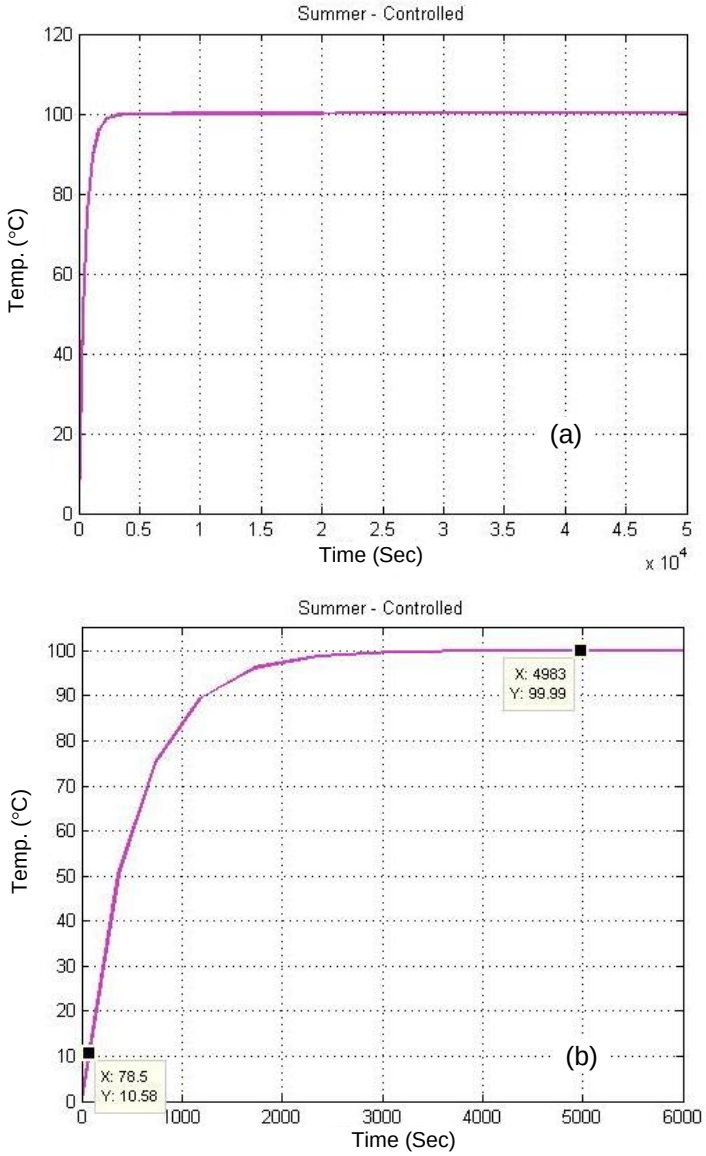

Figure 4.29 Controlled system response for daytime summer (a) full day (b) part day

As shown in Figure 4.29, the use of controller limits the maximum temperature of the system to 100°C. However, the settling time of the system is at about 3000 seconds (50 minutes). The rise time of the system temperature to increase from 10 to 90°C was about 1150 seconds (about 19 minutes), which is nearly the same as that for the winter operation.

Chapter V

Conclusions and Recommendations

5.1 Conclusions

Performance simulation of two design configurations of absorption refrigeration system (ARS) is conducted in this study. These configurations include the single- and double-effect ARS. In order to compare the performance predictions of these configurations, similar assumptions are employed. For the two configurations, same condenser and absorber temperatures are assumed at 40°C. Also, same effectiveness of heat exchanger is assumed at 0.7. For both configurations, the evaporator temperature is varied as 4, 5, 6 and 7°C. The temperature, at which the thermal energy is supplied to the system at the generator, is varied as 100, 110, 120, 130, 140, and 150°C, for both configurations.

The simulation study of the single-effect ARS shows that:

- The increase of generator temperature decreases the generator thermal energy at any evaporator temperatures.
- The increase of generator temperature from 100 to 120°C decreases the required generator thermal energy by 2.7%. Meanwhile, the increase of temperature from 100 to 150°C decreases the generator thermal energy by 3.11%.
- Generator temperature increase enhances the COP, at any evaporator temperature.
- The COP of single-effect ARS was the highest at 0.693, at generator temperature of 120°C and evaporator temperature of 7°C.
- At evaporator temperature 7°C, the increase of generator temperature increases the COP, which reached maximum at 120°C. However, further increase of generator temperature decreases the COP.
- The decrease of evaporator temperature increases the required weak and strong solution mass ratio.
- The increase of generator temperature decreases the piping sizes, materials and cost.
- The increase of generator temperature decreases the absorber thermal energy, at any evaporator temperature.

- Lowering the evaporator temperature requires the use of bigger size absorber unit.
- At evaporator temperature of 4°C, the increase of generator temperature from 100 to 150°C decreases the absorber energy by 5.2%.
- At evaporator temperatures of 5, 6, and 7°C, the percentage reduction of absorber thermal energy with generator temperature are 4.0, 3.1, and 2.4%, respectively.
- The system performance degraded with lowering the evaporator temperature.
- Lowering evaporator temperature decreases the COP, at any generator temperature.
- At constant evaporator temperature, nearly linear relationship is found between the system COP and generator temperature.
- At generator temperature of 110, 130, and 150°C, lowering evaporator temperature from 7 to 4°C decreases the COP by 5.7, 3.8, and 2.9%, respectively.
- Lowering evaporator temperature requires increased strong and weak solution mass flow rates (at nearly constant refrigerant mass flow rate).
- At generator temperature of 110, 130, and 150°C, lowering evaporator temperature from 7 to 4°C increases the required mass flow rate of the strong solution by 40.5, 28.2, and 22.3%, respectively
- Lowering evaporator temperature increases the thermal energy of the absorber.
- The higher generator temperatures decrease the absorber energy to minimum.
- At generator temperatures of 110, 130, and 150°C, lowering evaporator temperature from 7 to 4°C increases the absorber energy by 2.9, 1.8, and 1.3%, respectively.

The simulation study for the double-effect ARS shows that:

- Increasing generator-I temperature decreases generator-I thermal energy at any evaporator temperature.
- Increase generator-I temperature from 100 to 150°C decreases generator-I thermal energy by 7.52%.
- Increasing generator-I temperature increases the system COP, at any evaporator temperature to reach maximum of 1.164 at generator-I temperature of 130°C and evaporator temperature of 7°C.
- Slower rate of COP increase was found, with generator-I temperature, at evaporator temperature of 6°C.

- At evaporator temperature of 7°C, the increase of generator-I temperature increases the COP to reach maximum at 130°C but further generator-I temperature increase decreases the COP.
- At evaporator temperature 5°C, the increase of generator-I temperature increases the refrigerant mass portion produced in generator-I unit whereas the refrigerant mass portion produced in generator-II unit was decreased.
- At evaporator temperature 4°C, the increase of generator-I temperature from 100 to 150°C decreases the condenser energy by 8.8%. At evaporator temperature 5°C, the condenser energy was decreased by 1.24%.
- At evaporator temperatures of 6 and 7°C, the increase of generator-I temperature increases the condenser thermal energy by 5.3, and 11.0%, respectively
- The system performance degraded with lowering the evaporator temperature.
- At generator temperature of 110, 130, and 150°C, lowering the evaporator temperature from 7 to 4°C decreases the COP by 13.6, 9.5, and 7.5%, respectively.
- Lowering evaporator temperature increases the weak, intermediate and strong solution mass flow rates. The increase of mass flow rates increases the required pipe sizes and the system cost
- At generator-I temperatures 110, 130, and 150°C, lowering evaporator temperature from 7 to 4°C increases the weak solution mass flow rate by 36.2, 24.3, and 18.5%, respectively. Also,
- Lowering evaporator temperature increases the condenser thermal energy at any generator-I temperature.
- Constant condenser thermal energy was found at evaporator temperature of 5°C.
- At evaporator temperature less than 5°C, increasing generator-I temperature decreases the condenser thermal energy. For evaporator temperatures higher than 5°C, increasing generator-I temperature increases the condenser thermal energy.

The comparison between single- and double-effect ARS shows that:

- The double-effect ARS has higher COP compared with single-effect ARS, at any evaporator temperature.
- The percentage increase of COP varies from 49.5% (at generator temperature of 100°C and evaporator temperature of 4°C) to 68.6% (at generator temperature of 150°C and evaporator temperature of 7°C).

- The double-effect ARS requires less thermal energy (varies from 33.1 to 40.7%) at the same cooling load, which decreases the generator size.
- The condenser thermal energy of double-effect ARS is usually lower than that of single-effect ARS.
- The condenser thermal energy for double-effect ARS is 42.4 to 56.7% lower than that of single-effect system.

The storage tank temperature response was obtained for the different operating conditions. For the night time operation, electric heater is used for heating purposes. The simulation results using Matlab/Simulink show the slow response of the system. The open loop rise time of the system was 1210 seconds whereas the settling time was about 3512 seconds. For the closed loop system, the rise time decreased to 41.7% to become 505 seconds. Moreover, the settling time decreased by about 51% for the closed loop to reach 1790 seconds. When PID controller of proportional gain 80,000 was used, there were noticeable improvements in the system response as the response becomes faster. The system rise time from 10 to 100°C improved to be 85 seconds, which means reduction of the rise time compared with the open and closed loop. With the controller, the settling time of the system decreased to 300 seconds, which about 8.5% of the settling time of the corresponding open loop system.

For the daytime operation, Solar panels are used to supply the storage tank with the heat. The solar radiation intensity received on the solar panels change with time. Therefore, simulation is conducted twice to predict the system temperature responses during winter and summer. For winter operation, the solar radiation data for Dubai City on 21st December were used whereas the data on 21st June were used for summer simulation. In winter, the temperature of the tank reached maximum of about 116.5°C after 20,000 seconds (5.56 hours). Meanwhile, the open loop rise time was about 2715 second (about 45 minutes). Nearly the same value was found for the summer operation which demonstrates the no-effect of the season on the rise time. In comparison with the open loop, the closed loop response was quick. The rise time has decreased to become about 640 seconds (about 11 minutes). This closed loop rise time is about 232.6% of the corresponding open loop. In general, the system response is considerably slow. The use of relay controller limits the maximum temperature of the system to the set point. However, the settling time of the system is considerably high at about 3900 seconds (65

minutes). The rise time of the system was about1150 seconds (about 19.2 minutes). The system response shows nearly the same results for the summer operation compared with the winter operation.

5.2 Recommendations

Based on the prediction results of the simulation studies in this study, the following are the recommendations for future work:

- Other designs of absorption system can be considered for simulation such as the parallel double-effect configuration and one and half-effect design.
- Simulation at other absorber and condenser temperatures of 30 and 50°C can be performed.
- Studying the effects of using increased strong solution concentrations on the system performance.
- Investigating different control strategies to improve the responses of control system suitable to adjust the generator temperature of the unit.
- Considering the effects of the heat capacity variation of the storage tank material on the system temperature response.
- Investigating the storage tank temperature response if the assumption that the tank is stratified is relaxed.

References

Agarwal, Y., Weng, T. and Gupta, R.K. (2009). *The energy dashboard: improving the visibility of energy consumption at a campus-wide scale*. Report on Embedded Sensing Systems for Energy-Efficiency in Buildings, pp. 55–60, Berkeley.

Alberston, C.E. and Krueger, R.H. (1971). *Heat Transfer Additives for Absorbent Solutions*. US Patent No. 3580759.

Ameel, T.A., Gee, K.G. and W, B.D. (1995). Performance Predictions of Alternative, Low Cost Absorbents for Open-Cycle Absorption Solar Cooling. *Solar Energy*, Vol. 54, No. 2, pp. 65–73.

Anderson, B. (1990a). *Introduction to Solar Building Architecture*. MIT Press, Cambridge, Massachusetts.

Anderson, B. (1990b). *Solar Building Architecture*. MIT Press, Cambridge, Massachusetts

Apte, J., Arasteh, D. and Huang, Y.J. (2003). Future Advanced Windows for Zero-Energy Homes. *ASHRAE Transactions*, Vol. 109, Part 2, pp. 871–882.

Arasteh, D., Selkowitz, S., Apte, J. and LaFrance, M. (2006). *Zero Energy Windows*. Report: Lawrence Berkeley National Laboratory. Berkeley, California, US.

ASHRAE (1981). *ASHRAE Standard 62-81: Ventilation for acceptable indoor air quality*. American Society of Heating and Refrigerating, and Air-Conditioning Engineering, Inc., Atlanta, G.A.

ASHRAE (1989). *ASHRAE Standard 90.1-1989: Ventilation for acceptable indoor air quality*. American Society of Heating and Refrigerating, and Air-Conditioning Engineering, Inc., Atlanta, G.A.

ASHRAE (2002). *Building Sustainability*. Atlanta, Ga: ASHARE, Atlanta.

ASHRAE (2007). *Handbook-2007 HVAC Applications*. American Society of Heating, Refrigerating and Air-Conditioning Engineers, Atlanta, USA.

ASHRAE/IES Standard 90.1-1989 (1989). Energy Efficient Design of New Buildings Except low rise Residential Building. ASHRAE Inc., Atlanta, GA.

Assimakopoulos, M., Tsangrassoulis, A., Guarracino, G. and Santamouris, M. (2004). Integrated energetic approach for a controllable electrochromic device. *Energy & Buildings*, Vol. 36, No. 5, pp. 415–422.

Athienitis, A.K. and Santamouris, M. (2002). *Thermal Analysis and Design of Passive Solar Buildings*. James & James, London, UK.

Athienitis, A.K. and Shou, J.G. (1991). Control of Radiant Heating Based on the Operative Temperature. *ASHRAE Transactions*, Vol. 97, No. 7, pp. 787–794.

Athienitis, A.K.; Stylianou, M. and Shou, J. (1990). A methodology for building thermal dynamics studies and control applications. *ASHRAE Transactions* Vol. 96, Part 2, pp. 839–848.

Ayoub, J., Dignard-Bailey, L. and Filion, A. (2001). *Photovoltaics for Buildings: Opportunities for Canada*. CANMET, Varennes.

Balcomb, J.D. (1992). *Passive Solar Buildings*. MIT Press, Cambridge, Massachusetts.

Bales, C., Hadorn, J.-C., Druck, H. and Streicher, W. (2005). Advanced storage concepts for solar houses and low energy buildings - IEA-SHC Task 32. *Proceedings of the ISES Solar World Congress 2005*.

Bartram, L., Rodgers, J. and Muise, K. (2010). Chasing the Negawatt: Visualization for Sustainable Living. *IEEE Computer Graphics and Applications*, pp. 8–14.

Beggs, C. (2009). *Energy: Management, Supply and Conservation*. 2nd edition, Butterworth-Heinemann, USA.

Belessiotis, V. and Haralabopolos, D. (1993). Testing Solar Water Heating Systems in Athens, Greece. *Solar Energy*, Vol. 50, No. 2, pp. 167–177.

Bereche, R.P., Palomino, R.G. and Nebra, S.A. (2009). Thermoeconomic Analysis of a Single and Double-Effect $LiBr/H_2O$ Absorption Refrigeration System. *International Journal of Thermodynamics*, Vol. 12 (No. 2), pp. 89–96.

Berestneff, A.A. (1949). Absorption Refrigeration. *Mechanical Refrigeration*, Vol. 72, pp. 216–220.

Bessoudo, M. (2008). *Thermal Comfort Conditions near Highly-Glazed Façades: an Experimental and Simulation Study*. MSc Thesis, Concordia University, Montréal, Québec, Canada.

Biaou, A.-L., Bernier, M.A. and Ferron, Y. (2004). Simulation of Net Zero Energy Homes. *Proceedings of eSim2004 - Building Performance Simulation Conference*.

Bonsor, K. (2001). *How Smart Windows Work*. HowStuffWorks website.

Borresen, B. (1981). Thermal room models for control analysis. *ASHRAE Transactions*, Vol. 87, Part 2, pp. 251–261.

Braun, J.E. (1990). Reducing energy costs and peak electrical demand through optimal control of building thermal storage. *ASHRAE Transactions*, Vol. 96, Part 2, pp. 876–888.

Braun, J.E. (2007). Intelligent Building Systems - Past, Present and Future. *In Proceedings of the 2007 American Control Conference*, New York City, USA. July 11-13.

Bushby, S. (1997). BACnet: a Standard Communication Infrastructure for Intelligent Buildings. *Automation in Construction*, Vol. 6, pp. 529–540.

Candanedo, J.A., O'Neill, B., Pantic, S. and Athienitis, A.K. (2007). Studies of control strategies for the Concordia Solar House. *Proceedings of the Joint 2nd Solar Buildings Research Network*, 32nd Solar Energy Society of Canada Inc(SESCI), 2007 Conference.

Candanedo (L.), L.M., Athienitis, A.K.; Candanedo, J., O'Brien, W. and Chen, Y. (2010). Transient and steady state models for open-loop air based BIPV/T systems. *ASHRAE Transactions*, Vol. 116, Part 1, pp. 600–612.

Carmody, J. (2003). *Window Systems for High-performance Buildings*. Norton.

CEC (2006). *Windows of the Future*. California Energy Commission, Consumer Energy Centre website.

Chang, W.C., Marcriss, R.A. and Rush W.F. (1971). *Secondary Alcohol Additives for Lithium Bromide Water Absorption Refrigeration System*. US Patent No. 3609087.

Charron, R. and Athienitis, A.K. (2006). Optimization of the performance of double-façades with integrated photovoltaic panels and motorized blinds. *Solar Energy*, Vol. 80, No. 5, pp. 482–491.

Chiogioji, M.H. and Oura, E.N. (1982). *Energy Conservation in Commercial and Residential Buildings*. Marcel Deker Inc., N.Y.

CMHC. (2006). *Tap the Sun*. Canada Mortgage and Housing Corporation, Ottawa, Ontario

Co., T. (2004). Short Tutorial on Matlab. Available at 25/06/2012, at: http://www.chem.mtu.edu/~tbco/cm416/MatlabTutorialPart4.pdf

Cooperman, A., Dieckmann, J. and Brodrick, J. (2010). Using Weather Data for Predictive Control. *ASHRAE Journal*, pp. 130–132.

Crepinsek, Z., Goricanec, D. and Krope, J. (2009). Comparison of the performances of absorption refrigeration cycles. *WSEAS Transactions on Heat and Mass Transfer*, Vol. 5, No. 3, pp. 65–76.

Cruickshank, C. and Harrison, S. (2006). Analysis of a modular thermal storage for solar heating systems. *Proceedings of the Joint 1st Solar Buildings Research Network - 31st Solar Energy Society of Canada Inc (SESCI), 2006 Conference*.

Daiguji, H., Hihara, E. and Saito, T. (1997). Mechanism of Absorption Enhancement by Surfactants. *International Journal of Heat and Mass Transfer*, Vol. 40, pp. 1743–1752.

Dincer, I. (2002). On thermal energy storage systems and applications in buildings. *Energy & Buildings*, Vol. 34, No. 4, pp. 377–388.

Dincer, I. and Dost, S. (1996). Energy analysis of an ammonia-water absorption refrigeration system. *Energy Sources*, 18, pp. 727–733.

Dincer, I. and Kanoglu, M. (2010). *Refrigeration Systems and Applications*. 2nd Edition, John Wiley & Sons, Ltd., UK.

Dixon, A.E. and Leslie, J.D. (1978). *Solar Energy Conversion: An introductory Course*. Pergamon Press. Toronto.

Dorato, P. and Knudsen, H. (1979). Periodic optimization with applications to solar energy control. *Automatica*, Vol. 15, pp. 673–676.

Dorgan Ch.B., Leight S.P. and Dorgan Ch.E. (1995). *Application Guide for Absorption Cooling/Refrigeration using Recovered Heat*. ASHRAE Atlanta.

Dounis, A.I. and Caraiscos, C. (2009). Advanced control systems engineering for energy and comfort management in a building environment - A review. *Renewable and Sustainable Energy Reviews*, Vol. 13, pp. 1246–1261.

Drees, K. and Braun, J. (1996). Development and evaluation of a rule-based control strategy for ice storage systems. *HVAC & R Research*, Vol. 2, No. 4, pp. 1–8.

Duan, P. and Li, H. (2008). ZigBee Wireless Sensor Network Based Multi-Agent Architecture in Intelligent Inhabited Environments. *IET 4th International Conference on Intelligent Environments*, 1-6, Seattle.

Duffie, J.A. and Beckman, W.A. (1991). *Solar Engineering of Thermal Processes*. John Wiley & Sons, Inc.

Duffie, J.A. and Beckman, W.A. (2006). *Solar Engineering of Thermal Processes*. 3rd edition, John Wiley & Sons, Hoboken, New Jersey.

Dupont, M., Celestine, B. and Beghin, B. (1994a). Desiccant Solar Air Conditioning in Tropical Climates: II- Field Testing In Guadeloupe. *Solar Energy*, Vol. 52, No. 6, pp. 519–524.

Dupont, M., Celestine, B., Nguyen, P.H., Merigoux, J. and Brandon, B. (1994b). Desiccant Solar Air Conditioning in Tropical Climates: 1-Dynarnic Experimental and Numerical Studies of Silicagel and Activated Alumina. *Solar Energy*, Vol. 52, N0.6, pp. 509–517.

Echelon (2009). *Introduction to the LonWorks Platform*. Report: Echelon Corporation.

Egan, D. (2005). The emergence of ZigBee in building automation and industrial control. *Computing and Control Engineering Journal*, Vol. 16, No. 2, pp. 14–19.

Elkassabgi, Y.M. and Perez-Blanco, H. (1991). Experimental Study of the Effects of Alcohol Additives in Lithium Bromide Water pool Absorber. *ASHRAE Transactions*, Vol. 97, pp. 403–405.

Eto, J.H. and Meyer, C. (1988). The HVAC Cost of Fresh Air Ventilation. *ASHRAE Journal*, Issue of month: September.

Florita, A.R. and Henze, G.P. (2009). Comparison of Short-Term Weather Forecasting Models for Model Predictive Control. *HVAC & R Research*, Vol. 15, No. 5, pp. 835–853.

Fraunhofer IAP. (2008). *Thermochromic Polymers*. Fraunhofer Institute for Applied Polymer Research.

Guo, W. and Zhou, M. (2009). An emerging technology for building automation control. *In IEEE International Conference on Systems, Man and Cybernetics*, San Antonio, Texas. October.

Gwerder, M., Lehmann, B., Todtli, J., Dorer, V. and Renggli, F. (2008). Control of Thermally-Activated Building Systems (TABS). *Applied Energy*, Vol. 85, pp. 565–581.

Gwerder, M., Todtli, J., Lehmann, B., Dorer, V., Güntensperger, W. and Renggli, F. (2009). Control of thermally activated building systems (TABS) in intermittent operation with pulse width modulation. *Applied Energy*, pp. 1606–1616.

Gyalistras, D. and OptiControl Team. (2010). *Final Report: Use of Weather and Occupancy Forecasts for Optimal Building Climate Control (OptiControl)*. Report: ETH Zürich. Zürich, Switzerland.

Haggard, K., Bainbridge, D.A. and Aljilani, R. (2010). *Passive Solar Architecture Pocket Reference*. Earthscan, London, UK.

Hauer, A. (2010). *Compact Thermal Energy Storages: Potential and Limitations for Different Applications*, ed. Bayern Z. Presentation at Eurosun 2010, Graz, Austria, Oct. 1st, 2010.

Henze, G.P. (1995). *Evaluation of Optimal Control for Ice Storage Systems*. Ph.D. Thesis. University of Colorado, Boulder, Colorado, US.

Henze, G.P., Dodier, R.H. and Krarti, M. (1997). Development of a predictive optimal controller for thermal energy storage systems. *International Journal of HVAC&R Research*, Vol. 3, No. 3, pp. 233–264.

Henze, G.P., Felsmann, C. and Knabe, G. (2004a). Evaluation of optimal control for active and passive building thermal storage. *International Journal of Thermal Sciences*, Vol. 43, No. 2, pp. 173–183.

Henze, G.P., Kalz, D.E., Felsmann, C. and Knabe, G. (2004b). Impact of forecasting accuracy on predictive optimal control of active and passive building thermal storage inventory. *HVAC & R Research*, Vol. 10, Part 2, pp. 153–178.

Henze, G.P., Kalz, D.E., Liu, S. and Felsmann, C. (2005). Experimental analysis of model-based predictive optimal control for active and passive building thermal storage inventory. *HVAC & R Research*, Vol. 11, No. 2, pp. 189–213.

Henze, G.P. and Krarti, M. (1999). The impact of forecasting uncertainty on the performance of a predictive optimal controller for thermal energy storage systems. *ASHRAE Transactions*, Vol. 105, pp. 10–18.

Henze, G.P., Laguna, M. and Krarti, M. (1995). Heuristics for the optimal control of Thermal Energy Storage. *Proc of the Metaheuristics Int Conf* Kluwer Academic Publishers, Norwell, MA.

Henze, G.P., Pfafferott, J., Herkel, S. and Felsmann, C. (2007). Impact of adaptive comfort criteria and heat waves on optimal building thermal mass control. *Energy and Buildings*, Vol. 39, pp. 221–235.

Herold, K.E., Han, K. and Moran, M. J. (1988). AMMWAT, A Computer Program for calculating the Thermodynamic Propertiesof Ammonia and Water Mixtures using a Gibbs Free Energy Formulation. *ASME Publication of AES*, Vol. 4, pp. 65–75.

Herold K.E., Radermacher R. and Klein S.A. (1996). *Absorption Chillers and Heat Pumps*. Estados Unidos, CRC Press LLC.

Hihara, E. and Saito, T. (1993). Effect of Surfactants on Falling Film Absorption. *International Journal of Refrigeration*, Vol. 16, pp. 339–346.

Hirsch, R.L. (2008). Mitigation of Maximum World Oil Production: Shortage Scenarios. Energy Policy, Vol. 36, pp. 881–889.

Hirsch, R.L., Bezdek, R. and Wendling, R. (2005). *Peaking of World Oil Production: Impacts, Mitigation and Risk Management*. Report: US Department of Energy.

Hoffmann, W. (2006). PV solar electricity industry: Market growth and perspective. *Solar Energy Materials and Solar Cells*, Vol. 90, No. (18-19), pp. 3285–3311.

Holmberg, P. and Berntsson, T. (1990). Alternative Working Fluids in Heat Transformers. *ASHRAE Transactions*, Vol. 96, pp. 1582–1589.

Holmberg, D.G. and Bushby, S.T. (2009). BACnet and the Smart Grid. BACnet Today: *A Supplement to ASHRAE Journal*, B8-B12.

Hudson, G. and Underwood, C.P. (1999). A simple building modelling procedure for MATLAB/Simulink. In *Sixth International IBPSA Conference*, Kyoto, Japan. September 13-15.

Hundy, G. (2008). *Refrigeration and Air-Conditioning*. 4th Edition, Butterworth-Heinemann.

Hutcheon, N.B. and Handegord, G. (1983). *Building Science for a Cold Climate*. Institute for Research in Construction, NRC, Canada.

Hunn, B.D., Grasso, M.M., Jones, J.W. and Hitzfeider, J.D. (1993). Effectiveness of shading devices on Building in Heating-dominated Climate. *ASHRAE Transactions*. Vol. 99, Part 1, pp. 207–222.

IEA (2010). *World Energy Outlook 2010: Executive Summary*. Report: International Energy Agency. Paris.

IPCC (2007). *Climate Change 2007: Synthesis Report*. Report: Intergovernmental Panel on Climate Change. Valencia, Spain.

Jahnig, D., Hausner, R., Wagner, W. and Isaksson, C. (2006). Thermochemical storage for solar space heating in a single family house. *Proceedings of the Tenth International Conference on Thermal Energy Storage*, Ecostock 2006.

Jansen, T.J. (l985). *Solar Engineering Technology*. Prentice-Hall, Inc.

Jeteter, S.M., Moran, J.P. and Teja, A.S. (1992). Properties of Lithium Bromide Water Solutions at High Temperatures and Concentrations-Part III: Specific Heat. *ASHRAE Transactions*, Vol. 98, pp. 134–149.

Johnson, C.A. and Besant, R.W. (1994). Economic Analysis of Daylit and Nondaylit Office Buildings in Canada. *ASHRAE Transactions*, Vo1. 100, Part 2, pp. 571–584.

Joudi, K.A. and Lafta, A.H. (2001). Simulation of a simple absorption refrigeration system. *Energ Convers Manage*, 42, pp. 1575–1605.

Kalogirou, S.A. (2004). Solar thermal collectors and applications. *Progress in Energy and Combustion Science*, Vol. 30, pp. 231–295.

Kampf, J.H. and Robinson, D. (2007). A simplified thermal model to support analysis of urban resource flows. *Energy & Buildings*, Vol. 39, No. 4, pp. 445–453.

Kaynakli, O. and Kilic, M. (2007). Theoretical study on the effect of operating conditions on performance of absorption refrigeration system. *Energy Conversion and Management*, 48, pp. 599–607.

Kaynakli, O. and Yamankaradeniz, R. (2007). Thermodynamic analysis of absorption refrigeration system based on entropy generation. *Current Science*, Vol. 92, No. 4, pp. 472–479.

Kieider, J.F. and Rabl, A. (1994). H*eating and Cooling of Buildings: Design for Efficiency*. McGraw-Hill Inc., N.Y.

Kintner-Meyer, M. and Emery, A. (1995). Optimal control of an HVAC system using cold storage and building thermal capacitance. *Energy & Buildings*, Vol. 23, No. 1, pp. 19–31.

KNX (2011). KNX - The Worldwide Standard for Home and Building Control. http://www.knx.org/

Krarti, M., Henze, G. and Bell, D. (1999). Planning horizon for a predictive optimal controller for thermal energy storage systems. *ASHRAE Annual Meeting*, Seattle, WA (US), 06/18/1999-06/23/1999.

Kuhn, T.E. (2006). Solar control: A general evaluation method for facades with venetian blinds or other solar control systems. *Energy & Buildings*, Vol. 38, No. 6, pp. 648–660.

Kulacki, F., Fellow, A., Davidson, J. H. and Hebert, M. (2007). On the Effectiveness of Baffles in Indirect Solar Storage Systems. *Journal of Solar Energy Engineering*, Vol. 129, pp. 494.

Kummert, M., André, P. and Nicolas, J. (2001). Optimal heating control in a passive solar commercial building. *Solar Energy* 69, 103-116.

Lee, R.J., DiGuilio, R.M., Jeteter, S.M. and Teja, A.S. (1990). Properties of Lithium Bromide Water Solutions at High Temperatures and Concentrations-Part II: Density and Viscosity. *ASHRAE Transactions*, Vol. 96, pp. 709–714.

Lenard, J.L.Y., Jeteter, S.M. and Teja, A.S. (1992). Properties of Lithium Bromide Water Solutions at High Temperatures and Concentrations-Part IV: Vapour Pressure. *ASHRAE Transactions*, Vol. 98, pp. 167–172.

Lewis, J.S., Chaer, I. and Tassou, S.A. (2007). *Reviews of Alternative Refrigeration Technologies*. Centre for Energy and Built Environment Research, School of Engineering and Design, Brunel University. Accessed on 18/06/2012, available at: http://www.grimsby.ac.uk/documents/defra/tech-newrefrigetechs.pdf.

Liao, L., Athienitis, A., Candanedo, L., Park, K.W., Poissant, Y. and Collins, M. (2007). Numerical and experimental study of heat transfer in a BIPV/Thermal system. *Journal of Solar Energy Engineering*, Vol. 129, pp. 423.

Liu, S. (2005). *Analytical and experimental comparison of model-based, model-free and hybrid learning control of active and passive building thermal storage*. MSc Thesis, University of Nebraska - Lincoln, Lincoln, Nebraska, US.

Marcos, J.D., Izquierdo, M. and Palacios, E. (2011). New method for COP optimization in water- and air-cooled single and double effect LiBr-water absorption machines. *International Journal of Refrigeration*, Vol. 34, pp. 1348–1359.

Marcriss, R.A., Gutraj, J.M. and Zawacki, T.S. (1988). *Absorption Fluid Data Survey: Final Report on Worldwide Data*. ORLN/Sub/8447989/3, Ins. Gas Tech.

May-Ostendorp, P., Henze, G.P., Corbin, C.D., Rajagopalan, B. and Felsmann, C. (2011). Model-predictive control of mixed-mode buildings with rule extraction. *Building and Environment*, Vol. 46, pp. 428–437.

McNeely, L.A. (1979). Thermodynamic Properties of Aqueous Solutions of Lithium Bromide. *ASHRAE Transactions*, Vol. 85, pp. 413–434.

McKinley, T.L. and Alleyne, A.G. (2008). Identification of building model parameters and loads using on-site data logs. In *SimBuild 2008: Third National Conference IBPSA-USA*, Berkeley, California. July 30 - August 1.

McQuiston, F.C.; Parker, J.D. and Spitler, J.D. (2005). *Heating, Ventilating, and Air Conditioning: Analysis and Design*. John Wiley & Sons.

Modahl, R.J. and Lynch, P.J. (1971). *Arsenic Trioxide Corrosion Inhibitor for Absorption Refrigeration System*. US Patent No. 3609086.

Morris, F., Braun, J. and Treado, S. (1994). Experimental and simulated performance of optimal control of building thermal storage. *ASHRAE Transactions*, Vol. 100, Part 1, pp. 402–414.

Negron, E. and Hayes, P.H. (2009). System and Method for Appliance Control via a Personal Communication or Entertainment Device. U.S.

Nielsen, K. (2003). *Thermal Energy Storage: A State-of-the-Art*. A report within the research program Smart Energy-Efficient Buildings at NTNU and SINTEF 2002-2006. Report: Department of Geology and Mineral Resources Engineering, Norwegian University of Science and Technology. Trondheim, Norway. Visited 15/06/2012 at: http://www.energy.sintef.no/Prosjekt/Annex29/Publikasjoner/GSHPs_ThermalStorageNO.pdf

NRCan (2006). *Types of Solar Collectors*. Visited on 16/06/2012, available at the website: http://www.canren.gc.ca/tech_appl/index.asp?CaID=5&PgID=282.

Oldewurtel, F., Parisio, A., Jones, C.N., Morari, M., Gyalistras, D., Gwerder, M., Stauch, V., Lehmann, B. and Wirth, K. (2010a). Energy Efficient Building Climate Control using Stochastic Model Predictive Control and Weather Predictions. In *American Control Conference*, Baltimore, Maryland. June 30 - July 2.

Oldewurtel, F., Ulbig, A., Parisio, A., Andersson, G. and Morari, M. (2010b). Reducing Peak Electricity Demand in Building Climate Control using Real-Time Pricing and Model Predictive Control. *49th IEEE Conference on Decision and Control*, Atlanta, Georgia, USA. December 15-17.

Østergaard, S. (2003). *Results from measurements on a roof integrated PV system with preheating of fresh air*. Report: Solar Energy Centre Denmark, Danish Technological Institute. Denmark. apr.

Owen, N.A., Inderwildi, O.R. and King, D.A. (2010). The Status of Conventional World Oil Reserves -Hype or Cause for Concern? *Energy Policy*, Vol. 38, pp. 4743–4749.

Papakostas, K.T., Parageorgiou, N.E. and Sotiropoulos, B.A. (1995). Residential Hot Water Use Patterns in Greece. *Solar Energy*, Vol. 54, No. 6, pp. 369–374.

Park, Y.M. and Sonntag, R.E. (1990). Thermodynamic Properties of Ammonia-Water Mixtures: a Generalised Equation of State Approach. *ASHRAE Transactions*, Vol. 96, pp. 150–159.

Patterson, M.R. and Perez-Blanco, H. (1988). Numerical fits of Properties of Lithium Bromide Water Solutions. *ASHRAE Transactions*, Vol. 94, pp. 2059–2077.

Perez-Blanco, H. (1984). Absorption Heat Pump Performance for Different Types of Solution. *International Journal of Refrigeration*, Vol. 7, pp. 115–122.

Poulin, L., Yu, W. and Hodgson, J. (2006). Renewable energy forecasts for solar powered applications. *First SBRN Conference*, Poster Session.

Puthawala, S., Pal, N. and Shah, P. (2011). *Sustainable Building Technology: Embodied Energy of Building, Energy Conservation in Building, Innovative Construction Techniques*. LAP LAMBERT Academic Publishing, UK.

Rabl, A. and Norford, L. (1991). Peak load reduction by preconditioning buildings at night. *International Journal of Energy Research*, Vol. 15, No. 9, pp. 781–798.

Richardson, T.J., Slack, J.L., Armitage, R.D., Kostecki, R., Farangis, B. and Rubin, M.D. (2001). Switchable mirrors based on nickel-magnesium films. *Applied Physics Letters*, Vol. 78, No. 20, p. 3.

Riederer, P. (2005). MATLAB/SIMULINK for building and HVAC simulation- state of the art. In *Ninth International IBPSA Conference*, Montreal, Canada. August 15-18.

Romero, R.J., Rivera, W. and Best, R. (2000). Comparison of the theoretical performance of a solar air conditioning system operating with water/lithium bromide and an aqueous ternary hydroxide. *Solar Energy Material Solar Cells*, 63, pp.387–399.

Seem, J.E. (2007). Using intelligent data analysis to detect abnormal energy consumption in buildings. *Energy and Buildings*, Vol. 39, pp. 52–58.

Shavit, G. and Richard, W. (1993). Energy Conservation and Control Strategies for Integrated Lighting and HVAC Systems. *ASHRAE Transactions*, Vol.99, Part 2, pp. 785–790.

Sokolov, M. and Hershgal, D. (1993). Optimal Coupling and Feasibility of a Solar-Powered Year-Round Ejector Air Conditioner. *Solar Energy*, Vol. 50, No. 6, pp. 507–516.

Solarbuzz (2011). *Module pricing*. URL: http://solarbuzz.com/facts-and-figures/retail-price-environment/module-prices. Visited on 17/06/2012.

Srikhirin, P., Aphornratana, S. and Chungpaibulpatana, S. (2001). A review of absorption refrigeration technologies. *Renewable and Sustainable Energy Reviews*, Vol. 5, pp. 343–372.

Stauch, V., Hug, C., Schubiger, F. and Steiner, P. (2010). *Weather Forecasts, Observations and Algorithms for Building Simulation and Predictive Control*. Report: MeteoSwiss. Zurich. July 30.

Stein, B. and Reyndds, J.S. (1992). *Mechanical and Electrical Equipment for Buildings*. 8th edition, John Willy & Sons Inc., N.Y.

Stene, J. (2005). Residential CO_2 heat pump system for combined space heating and hot water heating. *International Journal of Refrigeration* 28(8), 1259-1265.

SunEarth Inc. (2005).

Sun, D.W. (1997). Computer simulation and optimization of ammonia-water absorption refrigeration systems. *Energy Sources*, 19, pp. 677–690.

Tonkoski, R., Lopes, L.A.C. and El-Fouly, T.H.M. (2011). Coordinated active power curtailment of grid connected PV inverters for overvoltage prevention. *IEEE Transactions on Sustainable Energy* 2(2), 139-147.

Torcellini, P., Deru, M., Griffith, B., Long, N., Pless, S. and Judkoff, R. (2004). Lessons Learned from Field Evaluation of Six High-Performance Buildings. *ACEEE Summer Study*, Pacific Grove, California.

Tzempelikos, A. (2005). *A Methodology for Integrated Daylighting and Thermal Analysis of Buildings*. MSc Thesis, Concordia University, Montréal, Canada.

Tzempelikos, A. and Athienitis, A.K. (2003). Simulation for fa\ccade options and impact on HVAC system design. *Proceedings of the Eighth IBPSA Conference*, pp. 1301–1308.

Underwood, C.P. (1999). *HVAC Control Systems: Modeling Analysis and Design*. Taylor & Francis, London.

Underwood, C.P. and Yik, F.W.H. (2004). *Modelling Methods for Energy in Buildings*. Blackwell Publishing.

van Schijndel, A.W.M.J. and Hensen, J. (2005). Integrated heat, air and moisture modeling toolkit in MATLAB. In *Ninth International IBPSA Conference*, Montreal, Canada. August 15-18.

Verma, S.K., Mekhjian, M.S., Sandor, G.R. and Nakada, N. (1999). Corrosion Inhibitor in Lithium Bromide Absorption Fluid for Advanced and Current Absorption Cycle Machines. *ASHRAE Transactions*, Vol. 105, pp. 813–815.

Wang, S. and Ma, Z. (2008). Supervisory and Optimal Control of Building HVAC Systems: A Review. *HVAC & R Research*, Vol. 14, No. 1, pp. 3–32.

Waters, J.R. (2003). *Energy Conservation in Buildings: A Guide to Part L of the Building Regulations*. Wiley-Blackwell, UK.

Wenham, S., Green, M., Watt, M. and Corkish, R. (2006). *Applied Photovoltaics*. UNSW Centre for Photovoltaic Engineering, Sydney, Australia

Wilson, B., Hagenstrom, H. and Dvorjetski, P. (2002). The Optical Properties of Gasochromic Glazing. *Proceedings of the 4th International Conference on Coatings on Glass*, pp. 649–657.

Wong, J.K.W.; Li, H. and Wang, S.W. (2005). Intelligent Building Research: a Review. *Automation in Construction* 14, 143-159.

WordNet. (2008). Definition of Sorption. Retrieved on 15/06/2012 at: http://wordnet.princeton.edu/perl/webwn?s=sorption.

Yoon, J-I. and Kwon, O-K. (1999). Cycle analysis of air-cooled absorption chiller using a new working solution. *Energy*, 24, pp. 795–809.

Yu, Z. and Dexter, A. (2009). Simulation based predictive control of low-energy building systems. In *Eleventh International IBPSA Conference*, Glasgow, Scotland. July 27-30.

Yvette, S. (1988). Photovoltaic applications in rural areas of developing countries: a survey of evidence. *International Journal of Global Energy Issues*, Vol. 2, No. 1, pp. 50–62.

Ziegler, B. and Trepp, C. (1984). Equation of State for Ammonia-Water Mixtures. *International Journal of Refrigeration*, Vol. 7, pp. 101–106.

Zhou, G., Krarti, M. and Henze, G.P. (2005). Parametric analysis of active and passive building thermal storage utilization. *Journal of Solar Energy Engineering*, Vol. 127, pp. 37.

Appendix (A)

Sample of Simulation Results

A.1 Single-Effect ARS

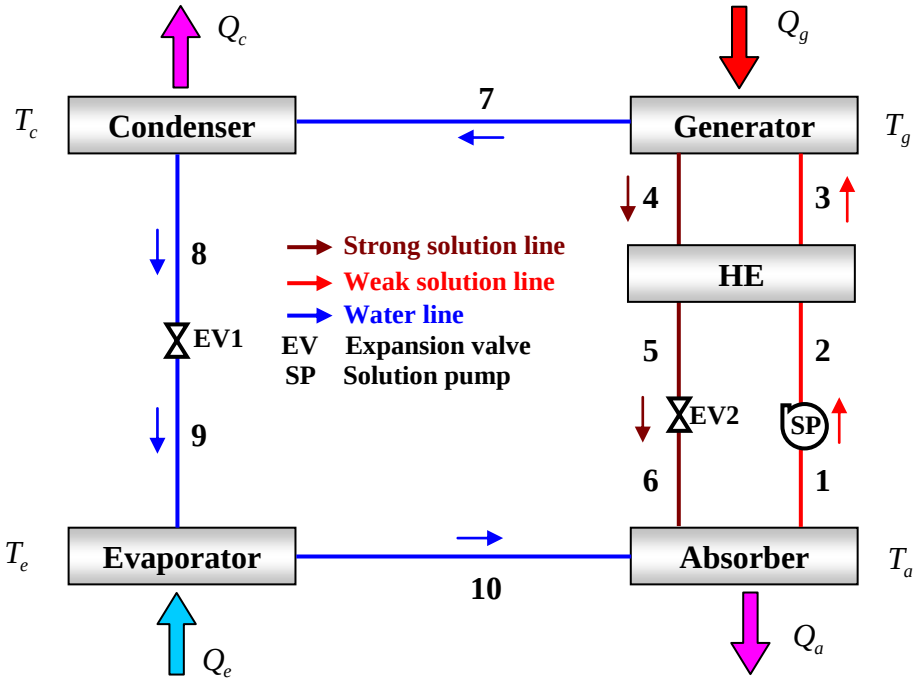

Figure A.1 Single-effect ARS

Assumptions of the design parameters

Condenser temperature (T_c) = 40°C — Absorber temperature (T_a) = 40°C

Evaporator temperature (T_e) = 5°C — Generator temperature (T_g) = 150°C

Heat exchanger effectiveness = 0.7. — Cooling capacity = 35.17 kW

Solution temperature after cooling = T_5=50°C.

Mass flow rate at each point

$\dot{m}_1 = \dot{m}_2 = \dot{m}_3 = m_I$ — Weak solution

$\dot{m}_4 = \dot{m}_5 = \dot{m}_6 = m_{II}$ — Strong solution

$\dot{m}_7 = \dot{m}_8 = \dot{m}_9 = \dot{m}_{10} = m_{III}$ — Water and vapour

Temperature at each point

By ignoring the pump work:

$T_1 = T_2 = T_8 = 40\,°C$ (Condenser and absorber temperatures)

$T_9 = T_{10} = 5\,°C$ (Evaporator temperature)

$T_4 = T_7 = 150\,°C$ (Generator temperature)

Concentration of each point

For the absorber outlet, the weak solution temperature equals the absorber temperature and the pressure is corresponding to the saturation temperature of the evaporator unit. Therefore the minimum concentration level of the system is evaluated, using Equation 3.8, as follows:

At $T_a = 40\,°C$ and $T_e = 5\,°C$, $x_I = 57.84\%$

This value remains constant with the variation of the generator temperature. It only varies with the evaporator temperature.

For the generator outlet, the solution temperature is the generator temperature and the pressure is the condenser pressure corresponding to the condenser temperature. The concentration of the solution coming out of the generator is the maximum concentration of the system. For comparison purposes, the maximum concentration values evaluated for the double-effect ARS will be used.

Then use $x_{II} = 68.039\%$

For the water and vapour branch, $x_{III} = 0.0$

Therefore:

$x_1 = x_2 = x_3 = x_I = 57.84\%$	Weak solution
$x_4 = x_5 = x_6 = x_{II} = 68.039\%$	Strong solution
$x_7 = x_8 = x_9 = x_{10} = x_{III} = 0$	Water and vapour (no LiBr)

Enthalpy of each point

Water and vapour enthalpies

In the condenser, there is condensation process at temperature of 40°C. From the steam tables, the corresponding condenser pressure is 0.0738 bar (7.38 kPa), which is the maximum pressure of the system inside the condenser and the generator units. The water vapour (refrigerant) coming out of the generator unit, condition (7), is superheated

vapour at temperature 150°C and condenser pressure. The condenser outlet condition (8) is saturated liquid at condenser pressure. Therefore:

h_7 = 2783.2 kJ/kg

h_8 = 167.54 kJ/kg

The throttling process through expansion valves takes place at constant enthalpy, then:

$h_9 = h_8$ = 167.54 kJ/kg

Inside the evaporator, evaporation process takes place at 5°C. So, the corresponding condenser pressure is 0.0087 bar (0.87 kPa), which is the minimum pressure of the system i inside the evaporator and absorber units. The evaporator exit condition (10) is saturated vapour at 5°C, so:

h_{10} = 2510 kJ/kg

The enthalpy of the remaining conditions can be obtained by studying the balance equations at each system component.

Solution points enthalpies

The enthalpy of the weak solution, condition (1), is obtained using Equation (3.9). So, it is evaluated using concentration $x_I = 57.84\%$ and solution temperature of the absorber (40°C), so:

h_1 = 104.98 kJ/kg

By ignoring the pump work:

$h_2 = h_1$ = 104.98 kJ/kg

The enthalpy of generator outlet solution condition (4) can be obtained at the highest concentration $x_{II} = 68.039\%$ and the solution temperature equals to that of the generator (150°C). Therefore:

h_4 = 363.50 kJ/kg

The enthalpy of the strong solution at the heat exchanger outlet (condition (5)) can be obtained at concentration $x_{II} = 68.039\%$ and solution temperature of (50°C). Therefore,

h_5 = 195.17 kJ/kg

Balance Equations of Each Component

Balance equations of the evaporator

Energy balance

$$Q_e + \dot{m}_9\ h_9 = \dot{m}_{10}\ h_{10}$$

$$Q_e + m_{III}\ h_9 = m_{III}\ h_{10}$$

The cooling capacity is Q_e 35.17 kW

$$Q_e = m_{III}\ (h_{10} - h_9)$$

$$35.17 = m_{III}\ (2510 - 167.5)$$

$$m_{III} = 0.01524 \text{ kg/s}$$

$$m_{III} = 0.01524 \text{ kg/s} \qquad \text{(A.1)}$$

Balance equations of the condenser

Energy balance

$$Q_c + \dot{m}_8\ h_8 = \dot{m}_7\ h_7$$

$$Q_c + m_{III}\ h_8 = m_{III}\ h_7$$

$$Q_c = m_{III}\ (h_7 - h_8)$$

$$Q_c = (0.01524)(2783.2 - 167.54)$$

$$Q_c = 39.87 \text{ kW} \qquad \text{(A.2)}$$

Balance equations of the generator

Mass balance

$$\dot{m}_3 = \dot{m}_4 + \dot{m}_7$$

$$m_I = m_{II} + m_{III}$$

$$m_I = m_{II} + 0.01524 \qquad \text{(A.3)}$$

Partial mass balance

$$\dot{m}_3\ x_3 = \dot{m}_4\ x_4 + \dot{m}_7\ x_7$$

$$m_I\ x_I = m_{II}\ x_{II} + m_{III}\ x_{III}$$

But $x_{III} = 0.0$. Then:

$$m_I\ x_I = m_{II}\ x_{II}$$

$$m_I = m_{II}\ \frac{x_{II}}{x_I} = m_{II}\left(\frac{68.039}{57.84}\right)$$

$$m_I = (1.176)\, m_{II} \qquad \text{(A.5)}$$

The solution of the equations A.4 and A.5 yields:

$$m_I = m_{II} + 0.01524$$

$$1.176\, m_{II} = m_{II} + 0.01524$$

$$m_{II} = 0.0865 \text{ kg/s} \qquad \text{(A.6)}$$

From Equation (A.5):

$$m_I = 0.01017 \text{ kg/s} \qquad \text{(A.7)}$$

Energy balance equation of the heat exchanger

The heat exchanger effectiveness is 0.7

$$\varepsilon = \frac{m_I\ (h_3 - h_2)}{m_{II}\ (h_4 - h_5)}$$

$$h_3 = 207.32 \text{ kJ/kg}$$

Energy balance of the generator

$$Q_g + \dot{m}_3\ h_3 = \dot{m}_4\ h_4 + \dot{m}_7\ h_7$$

$$Q_g + m_I\ h_3 = m_{II}\ h_4 + m_{III}\ h_7$$

$$Q_g = m_{II}\ h_4 + m_{III}\ h_7 - m_I\ h_3$$

$$Q_g = 52.03 \text{ kW} \qquad \text{(A.8)}$$

Balance equations of the absorber

Energy balance

$$Q_a + \dot{m}_1\ h_1 = \dot{m}_6\ h_6 + \dot{m}_{10}\ h_{10}$$

$$Q_a + m_I\ h_1 = m_{II}\ h_6 + m_{III}\ h_{10}$$

$$Q_a = m_{II}\ h_6 + m_{III}\ h_{10} - m_I\ h_1$$

$$Q_a = 43.41 \text{ kW} \qquad \text{(A.9)}$$

Performance Evaluation

The coefficient of performance (COP) is:

$$COP = \frac{Q_e}{Q_g}$$

$$COP = \frac{35.17}{52.03} = 0.676 \qquad \text{(A.10)}$$

The weak solution to the refrigerant mass ratio:

$$R_{ws} = \frac{m_I}{m_{III}} \qquad R_{ws} = 6.67 \qquad \text{(A.11)}$$

The strong solution to the refrigerant mass ratio:

$$R_{ss} = \frac{m_{II}}{m_{III}} \qquad R_{ss} = 5.67 \qquad \text{(A.12)}$$

A.2 Series Double-Effect ARS

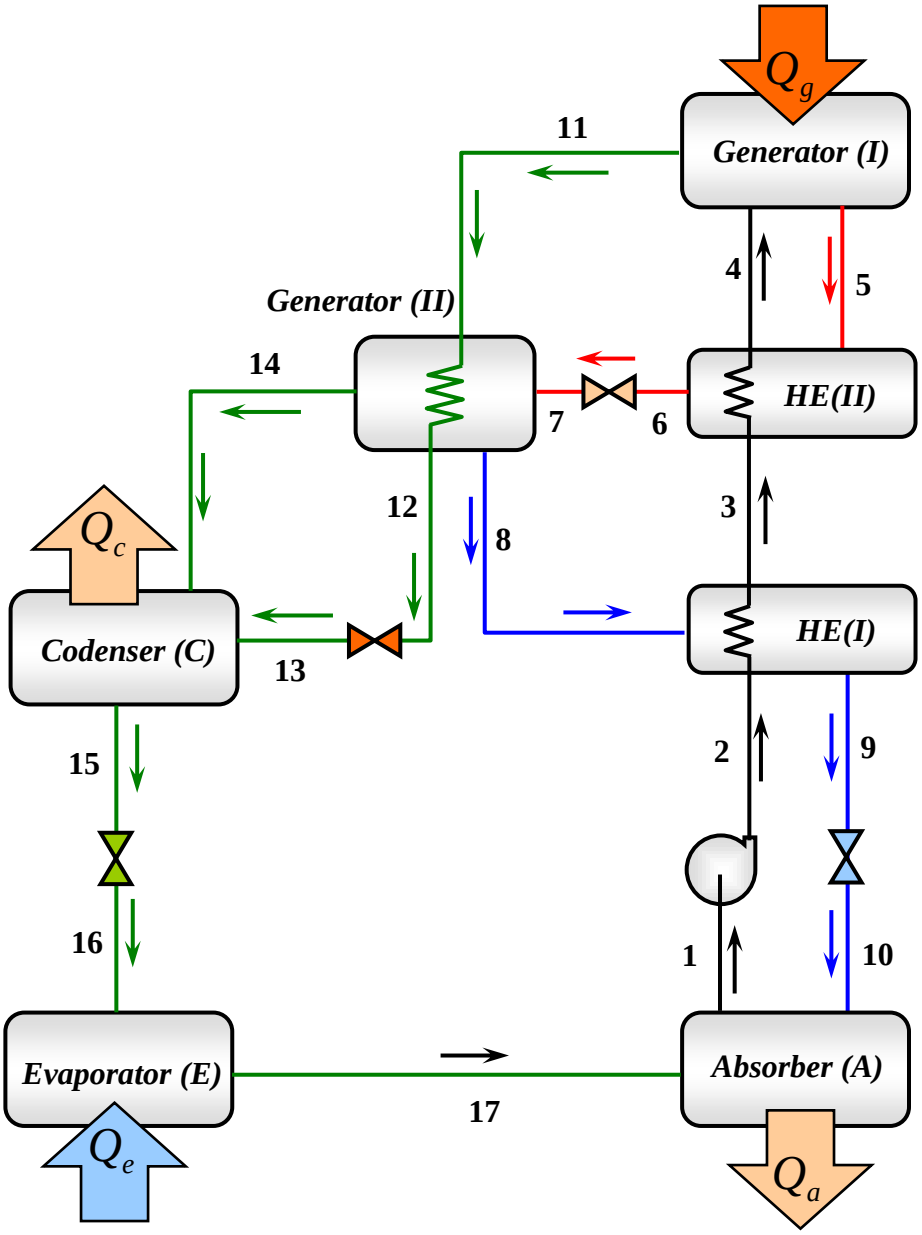

Figure A.2 Schematic diagram of series double-effect ARS

Assumptions of design parameters

Condenser temperature (T_c) = 40°C

Absorber temperature (T_a) = 40°C

Evaporator temperature (T_e) = 5°C

Generator (I) temperature (T_g) = 150°C

Heat exchanger effectiveness = 0.7

The cooling capacity is 35.17 kW

The solution temperature after cooling = T_9=50°C

High pressure level (P_H) = 120.9 kPa

Mass flow rate at each branch

$\dot{m}_1 = \dot{m}_2 = \dot{m}_3 = \dot{m}_4 = m_I$ Weak solution

$\dot{m}_5 = \dot{m}_6 = \dot{m}_7 = m_A$ Intermediate solution

$\dot{m}_8 = \dot{m}_9 = \dot{m}_{10} = m_{II}$ Strong solution

$\dot{m}_{11} = \dot{m}_{12} = \dot{m}_{13} = m_B$ Refrigerant line I

$\dot{m}_{15} = \dot{m}_{16} = \dot{m}_{17} = m_{III}$ Refrigerant line

Temperature at each point

By ignoring the pump work:

$T_1 = T_2 = T_{15} = 40\,°\text{C}$ (Condenser and absorber temperatures)

$T_{16} = T_{17} = 5\,°\text{C}$ (Evaporator temperature)

$T_4 = T_7 = T_5 = T_g$ (Generator (I) temperature) = 150°C

Concentration of each point

For the weak solution outlet of the absorber, the minimum concentration of the system is evaluated as:

At $T_a = 40\,°\text{C}$ and $T_e = 5\,°\text{C}$, $x_1 = x_I = 57.84\%$

For the strong solution outlet of the generator (II), the solution temperature is the saturation temperature at the higher system pressure, which is 105°C. The refrigerant branch is at pressure equals the condenser pressure i.e. the corresponding temperature is 40°C. Therefore, the maximum concentration of the system is evaluated as:

At $T_{sol} = 105\,°\text{C}$ and $T_{ref} = 40\,°\text{C}$, $x_8 = x_{II} = 68.039\%$

The concentration of the intermediate solution can be evaluated as follows:

$$x_A = x_I + \left(\frac{x_{II} - x_I}{2}\right) = x_I + \left(\frac{\Delta x}{2}\right), \qquad x_5 = x_A = 62.94\%$$

For the water and vapour, $x_{III} = 0.0$

In summary:

$x_1 = x_2 = x_3 = x_4 = x_I = 57.84\%$ Weak solution

$x_5 = x_6 = x_7 = x_A = 62.94\%$ Intermediate solution

$x_8 = x_9 = x_{10} = x_{II} = 68.039\%$ Strong solution

$x_{11} = x_{12} = x_{13} = x_{14} = x_{15} = x_{16} = x_{17} = x_{III} = 0$

Enthalpy of each point

Water and vapour enthalpies

In the generator (I), state (11) is superheated refrigerant vapour at temperature of 150°C and pressure 120.9 kPa. Therefore:

h_{11} = 2775.06kJ/kg

In the generator (II), there superheated vapour (11) will be condensed at the higher system pressure 120.9 kPa. Therefore, state (12) is saturated water at 120.9 kPa.

h_{12} = 440.21 kJ/kg

$h_{13} = h_{12} = 440.21$ kJ/kg

In the generator (II), there is further refrigerant evaporation process taking place at the condenser temperature of 40°C. Therefore, state (14) is saturated vapour at condenser temperature of 40°C. Then:

h_{14} = 2573.5 kJ/kg

In the condenser, refrigerant condensation process takes place at condenser temperature of 40°C. So, state (15) is saturated water at condenser temperature of 40°C. Then:

h_{15} = 167.5 kJ/kg

$h_{16} = h_{15} = 167.5$ kJ/kg

In the evaporator, refrigerant evaporation process takes place at evaporator temperature of 5°C. Therefore, state (17) is saturated vapour at evaporator temperature of 5°C. So:

h_{17} = 2510 kJ/kg

Solution points enthalpies

The enthalpy of weak solution at absorber outlet, condition (1), is obtained using Equation (3.9) at concentration $x_I = 57.84\%$ and solution temperature of the absorber (40°C). Therefore,

h_1 = 104.98 kJ/kg

By ignoring the pump work:

$h_2 = h_1$ = 104.98 kJ/kg

The enthalpy of the intermediate solution at generator (I) outlet, condition (5), can be obtained at concentration $x_A = 62.94\%$ and solution temperature of (150°C), which equals the generator temperature. Therefore,

h_5 = 335.88 kJ/kg

The enthalpy of strong solution at generator (II) outlet, condition (8), can be obtained at concentration $x_{II} = 68.093\%$ and solution temperature of (105°C), which is the saturation temperature at the maximum pressure of the system. Therefore,

h_8 = 277.55 kJ/kg

The enthalpy of the strong solution at heat exchanger (I) outlet, condition (9), can be obtained at concentration $x_{II} = 68.093\%$ and solution temperature of (50°C). Therefore,

h_9 = 182.96 kJ/kg

$h_{10} = h_9 = 182.96$ kJ/kg

Balance Equations of Each Component

Energy balance of the evaporator

$$Q_e + \dot{m}_{16}\, h_{16} = \dot{m}_{17}\, h_{17}$$

$$Q_e + m_{III}\, h_{16} = m_{III}\, h_{17}$$

The cooling capacity is Q_e = 35.17 kW

$$Q_e = m_{III}\,(h_{17} - h_{16})$$

$$m_{III} = 0.01524 \text{ kg/s} \qquad \text{(A.13)}$$

Mass and partial mass balance of the absorber

Mass balance

$m_I = m_{II} + m_{III}$

$$m_I = m_{II} + 0.01524 \quad \text{(A.14)}$$

Partial mass balance

$m_I \; x_I = m_{II} \; x_{II} + m_{III} \; x_{III}$

But $x_{III} = 0.0$. Then:

$m_I \; x_I = m_{II} \; x_{II}$

$m_I = m_{II} \; \dfrac{x_{II}}{x_I} = m_{II} \left(\dfrac{68.093}{57.84} \right)$, then:

$$m_I = (1.176)\, m_{II} \quad \text{(A.15)}$$

The solution of the equations A.14 and A.15 yields:

$m_I = m_{II} + 0.01524$

$1.176\, m_{II} = m_{II} + 0.01524$

$$m_{II} = 0.0856 \text{ kg/s} \quad \text{(A.16)}$$

$m_I = 1.176 \times 0.1543 = 0.1695$ kg/s

$$m_I = 0.1017 \text{ kg/s} \quad \text{(A.17)}$$

Mass and partial mass balance of the control volume

The control volume includes generator (II), HE (I) and HE (II)

Mass balance

$m_A = m_{II} + m_{14}$

$$m_A = 0.0856 + m_{14} \quad \text{(A.18)}$$

Partial mass balance

$m_A x_A = m_{II} x_{II}$

$m_A = m_{II} \; \dfrac{x_{II}}{x_A} = m_{II} \left(\dfrac{68.093}{62.94} \right)$, then:

$m_A = (1.0810) \times 0.0856$

$$m_A = 0.0935 \text{ kg/s} \quad \text{(A.19)}$$

The solution of the equations A.18 and A.19 yields:

$$m_{14} = m_A - 0.0856$$

$$m_{14} = 0.007 \text{ kg/s} \quad \text{(A.20)}$$

This mass represents the first portion of the total mass of the refrigerant, which is generated in generator-II.

Mass balance of generator (I)

Mass balance

$$m_I = m_A + m_B$$

$$0.1017 = 0.007 + m_B$$

$$m_B = 0.0082 \text{ kg/s} \quad \text{(A.21)}$$

This mass represents the second portion of the total mass of the refrigerant, which is generated in generator-I.

To check the results:

$m_{14} + m_B = 0.007 + 0082 = 0.0152$ kg/s, which equals the refrigerant total mass.

Energy balance of generator (II)

$$m_A\ h_7 + m_B\ h_{11} = m_{II}\ h_8 + m_B\ h_{12} + m_{14}\ h_{14}$$

$$m_A\ h_7 = m_{II}\ h_8 + m_B\ (h_{12} - h_{11}) + m_{14}\ h_{14}$$

$h_7 = 243.77$ kJ/kg $\qquad$ $h_6 = h_7 = 243.77$ kJ/kg

Energy balance of heat exchanger (I)

$$h_3 = \left[(\varepsilon) \frac{m_{II}}{m_I} (h_8 - h_9) \right] + h_2$$

$h_3 = 161.26$ kJ/kg

Energy balance of heat exchanger (II)

$$h_4 = \left[(\varepsilon) \frac{m_A}{m_I} (h_5 - h_6) \right] + h_3$$

$h_4 = 220.51$ kJ/kg

Energy balance of the condenser

$$Q_c + m_{III}\ h_{15} = m_B\ h_{13} + m_{14}\ h_{14}$$

$$Q_c = 19.1 \text{ kW} \tag{A.22}$$

Energy balance of the absorber

$$Q_a + m_I \; h_1 = m_{II} \; h_{10} + m_{III} \; h_{17}$$

$$Q_a = 43.4 \text{ kW} \tag{A.23}$$

Energy balance of generator (I)

$$Q_g + m_I \; h_4 = m_A \; h_5 + m_B \; h_7$$

$$Q_g = 31.83 \text{ kW} \tag{A.24}$$

Performance Evaluation

The coefficient of performance:

$$COP = \frac{Q_e}{Q_g} \qquad COP = \frac{35.17}{31.83} = 1.105 \tag{A.25}$$

The weak solution mass ratio:

$$R_{ws} = \frac{m_I}{m_{III}} \qquad R_{ws} = 6.67 \tag{A.26}$$

The strong solution mass ratio:

$$R_{ss} = \frac{m_{II}}{m_{III}} \qquad R_{ss} = 5.67 \tag{A.27}$$

The intermediate solution mass ratio:

$$R_{is} = \frac{m_A}{m_{III}} \qquad R_{is} = 6.13 \tag{A.28}$$

The percentage of refrigerant mass to be generated in generator-I is:

$$R_{gi} = \frac{m_{14}}{m_{III}} \times 100 \qquad R_{gi} = 45.9\% \tag{A.29}$$

The percentage of refrigerant mass to be generated in generator-II is:

$$R_{gii} = \frac{m_{14}}{m_{III}} \times 100 \qquad R_{gii} = 54.1\% \tag{A.30}$$